Fall 2018

Engineering polymeric hollow fiber membrane reactors for sustainable chemical transformation reactions

Yingxin He

Department: Chemical and Biochemical Engineering

ENGINEERING POLYMERIC HOLLOW FIBER MEMBRANE REACTORS FOR SUSTAINABLE CHEMICAL TRANSFORMATION REACTIONS

by

YINGXIN HE

A DISSERTATION

Presented to the Faculty of the Graduate School of the

MISSOURI UNIVERSITY OF SCIENCE AND TECHNOLOGY

In Partial Fulfillment of the Requirements for the Degree

DOCTOR OF PHILOSOPHY

in

CHEMICAL ENGINEERING

2018

Approved by:

Dr. Ali Rownaghi, Advisor
Dr. Xinhua Liang
Dr. Fateme Rezaei
Dr. Joseph Smith
Dr. Shubhender Kapila

PUBLICATION DISSERTATION OPTION

This dissertation consists of the following four articles that have been published or submitted for publication:

Paper I, Pages 15-57, "Direct Aldol and Nitroaldol Condensation in an Aminosilane-Grafted Si/Zr/Ti Composite Hollow Fiber as a Heterogeneous Catalyst and Continuous Flow Reactor" has been published in ***Journal of Catalysis*** 341: 149-159, 2016.

Paper II, Pages 58-93, "Engineering Porous Polymer Hollow Fiber Microfluidic Reactors for Sustainable C-H Functionalization" has been published in ***ACS applied materials & interfaces*** 9(19): 16288-16295, 2017.

Paper III, Pages 94-131, "Aminosilane-grafted SiO_2-ZrO_2 Polymer Hollow Fibers as Bifunctional Microfluidic Reactor for Tandem Reaction of Glucose and Fructose to 5-Hydroxymethylfurfural" was accepted by ***ACS Sustainable Chemistry & Engineering***, 2018 inpress DOI: 10.1021/acssuschemeng.8b04555.

Paper IV, Pages 132-157, "A Pd-immobilized aminosilane-grafted SiO_2/SiO_2-TiO_2 composite hollow fiber as a heterogeneous catalyst and continuous flow reaction in the degradation of 4-nitrophenol" was submitted to ***Reaction Chemistry and Engineering*** in 2018.

ABSTRACT

Over the past decade, laboratory-scale continuous-flow processes have witnessed explosive developments and have attracted a great deal of interest with respect to the significance of the economic and environmentally-sustainable production of pharmaceuticals, fine chemicals, and agrochemicals, as well as upgrading of biomass feedstocks. Immobilization of organocatalysts and metal nanoparticles on continuous-flow microreactors offers an efficient catalytic system that exploits and enhances the advantages of both nanocatalysis and flow chemistry, the so-called flow nanocatalysis approach. Various approaches have been developed for the development of continuous-flow reactions including immobilization and subsequent anchoring of organocatalysts and metal nanoparticles within microfluidic reactors. However, many applications of microfluidic reactor-supported catalysts are still hampered by catalysts decomposition and their subsequent leaching from the microfluidic reactor to the product stream. This dissertation focuses on the investigation of structure/property/performance relations of a new catalytic membrane reactor platform for conducting catalytic reactions in a continuous-flow fashion. More specifically, it focuses on permanent immobilization/impregnation of organic or metal nanoparticle catalysts by covalent bonding within highly swelling-resistant asymmetric polymeric hollow fiber surfaces for non-leaching catalysis. This novel hollow fiber membrane reactor was used as a heterogeneous catalyst and continuous-flow reactor for various reactions including aldol and nitroaldol condensation, Heck coupling, tandem reaction of glucose and fructose to 5-hydroxymethylfurfural, and nitrophenol reduction reactions.

ACKNOWLEDGMENTS

The author would like to express her sincere appreciation to her advisor, Dr. Ali Rownaghi for his help, patient, unconditional support, and knowledge education throughout her Ph.D. study in Chemical Engineering Department, Missouri University of Science and Technology (MST). The author would want to express her thanks to Dr. Fateme Rezaei for her kindly help, research discussion and education. The author also acknowledges Dr. Shubhender Kapila for giving her access to his analytical facilities. Meanwhile, appreciations also being shown to all her committee members namely, Dr. Liang and Dr. Smith.

The author acknowledges Professor William J. Koros from the School of Chemical and Biomolecular Engineering at Georgia Institute of Technology for giving her access to his fiber-spinning facilities.

Besides, the author also wants to acknowledge all the generous help from Dr. Xin Li, Dr. Harshul Thakkar, and all the lab mates. Without their help, this noble dissertation could not be finished within the four and half years of research. Meanwhile, the author want to express her gratitude to Dr. Seemamahannop Rachadaporn for her generosity help in her study of all analytical instrument. The author also wants to takes this opportunity to thank Ms. Huang Ming for her generous help on the NMR analyzation.

Last but not least, the author also wants to show the sincerest and greatest appreciation to her parents in China for their endless love, encouragement, and support during the years for her Ph.D. studies. Thank you very much!

TABLE OF CONTENTS

LIST OF ILLUSTRATIONS

PAPER II

PAPER III

PAPER IV

LIST OF TABLES

PAPER IV

1. INTRODUCTION

1.1. SUSTAINABLE CHEMICAL TRANSFORMATION REACTION

People established numbers of industries and companies to meet the requirement of rapid speed of economic development in the last decades, without regard of the impact on the human health, environment, and society, such as the serious air pollution caused by the industries in Beijing, China [1–3]. Nowadays, in order to have a sustainable development of the manufacture synthesis without impairing the service's ability of the next generation in the future, conducting sustainable processes is an important task that needs to be achieved for the current and future chemical engineering[4,5]. Sustainable processes include sustainable resource management, environmentally friendly processes, and the application of sustainable chemical[6–8]. Sustainable chemicals, with using less dangerous substances, and causing a less adverse impact on the environment, as well as society, show high advancement in the protection of workers, consumers, and the environment[8,9]. Since the environmental protection and sustainable economic development are attracting more and more concern of the people those working in various areas, such as the petrochemical industries, pharmaceutical companies, and fine chemicals manufacture, numbers of catalysts and reaction systems were being generated and investigated for the sustainable chemical transformation reactions[10–13]. In recent years, the development of the flow chemistry and microreactor technology demonstrate the amazing expanding speed of the sustainable process because of its excellent catalytic efficiency and contribution on the sustainable chemical synthesis[14–16]. However, it is still a big challenge to develop the ideal catalysts and laboratory-scale continuous-flow reactor system perform excellent in the sustainable synthesis process.

In this dissertation, the novel polymeric hollow fibers (HFs) membrane reactors assembled within a novel laboratory-scale continues-flow reactor system were developed for the investigation of a series of sustainable chemical transformation reactions, such as the aldol and nitroaldol condensation reaction[17], Heck coupling reaction[18], fructose/glucose to HMF reaction and the 4-nitrophenol reduction reaction.

1.2. CATALYSTS APPLIED IN THE INVESTIGATION OF SUSTAINABLE CHEMICAL TRANSFORMATION REACTION

To develop a laboratory-scale continuous-flow reactor system, except for the reactor design, the most important part is the catalyst development. Here in this dissertation, a novel composite hollow fiber membrane reactor was being developed and applied to various sustainable chemical formation process. The concept of membrane reactor, by combining with the separation through the membrane and the catalytic reaction process into the same single unit reactor, were first being utilized by Godini et la. in 2009[19]. Generally, the membrane reactor can remove a product or reactant by the selective separation process and shift the equilibrium to carry out the reaction in lower catalytic requirement. Meanwhile, with the stronger chemical bonding, the membrane reactor could be operated under both high and mild temperature in the catalystic reactions. In this thesis, a hollow fiber membrane reactor were engineered by immobilized the catalytic efficiency composition on the membrane layer with a strong chemical bonding interaction. Catalytic reaction process occurred during the diffusion of the reactants to get into the catalytic zone, and reaction mixture were being separated with the catalytic efficiency composition after they diffuse out from the catalytic membrane layer. The separation process between reaction mixture and catalysts could be simplify by this step also.

The composite hollow fibers (shown as “HFs” in below thesis) were synthesized by the commercially available polyamide-imide (PAI, also called Torlon), which appear to have a thermostable and swelling resistivity characteristic, via the template-free, “dry-jet, wet-quench spinning” method[19,20] , as the schematic diagram shown in Figure 1.1. With high porosity[19,20] and surface area[22,23] the HFs could be functionalized by the various inorganic, organic, and metal nanoparticles catalytic efficiency composite. This hollow fiber material has been applied in various gas separation processes successfully, such as working excellent in the CO_2 capture done by Brennan et al.[21] but having being worked as catalysts in the organic reactions. This HFs membrane reactor was the first time being investigated and developed into the laboratory-scale continuous-flow reactor system for various sustainable chemical formation reactions.

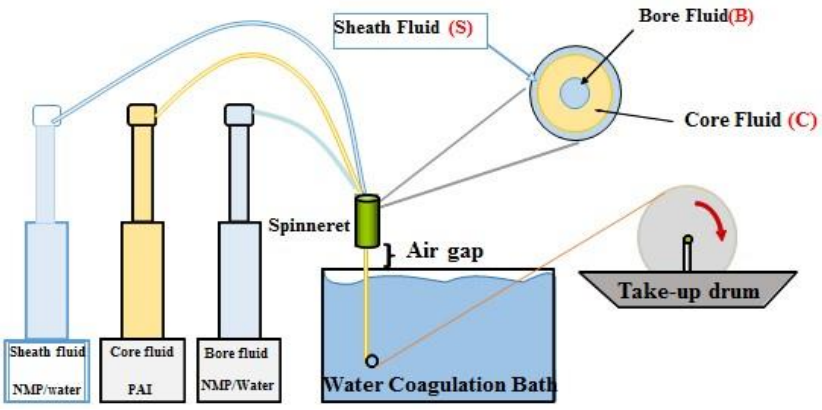

Figure 1.1. Schematic diagram of fiber spinning apparatus.

These HFs membrane reactor catalysts were pseudo-monolithic materials comprising a porous bare polymer matrix with doping of various metal oxide nanoparticles, such as silica, zirconia, titania, to improve the mechanical strength, and a membrane layer with doping or immobilized with a catalytic efficient composition formed onto the matrix materials by various surface modification methods [17].

1.3. SURFACE MODIFICATION

There were mainly two different kinds of HFs catalysts being discussed and investigated the catalytic performance in different sustainable chemical transformation reaction in this dissertation, they are the bifunctional[17] and the metal nanoparticles (MNPs)-immobilized membrane hollow fiber microfluidic reactor[18].

1.3.1. Bifunctional Hollow Fiber Microfluidic Reactor Catalysts. Compared to the homogeneous catalysts, the heterogeneous catalyst appears to be more stable with higher economic efficiency[24–27], as well as easy to separate from the reactor system for recycling with a longer lifetime. However, unlike the homogeneous catalysts showing high catalytic performance owing to the high degree of interaction[27,28] with the reactant, to improve the catalytic efficiency is an important task needed to solve for the heterogeneous catalysts design. The concept of bifunctional catalysts was generated to improve the catalytic performance problem of the heterogeneous catalysts[29,30].

By the studying of the functioning mechanism of the homogeneous catalysts[31], more strong heterogeneous catalysts were generated with the integration of two different catalytic efficiency site into a single supporting material. To meet the target of the economic efficiency, the inexpensive elements and materials are always employed as a primary raw material applied in the formation of bifunctional catalysts system[32,33]. The functional

catalysts, also called Dual-function catalysts[34], possess two distinct functional groups to bring about new reactivity, the general bifunctional catalysts refer to the single catalysts with both two separately activated nucleophile and electrophile discrete functional groups, as Figure 1.2.-a shown[35]. The most popular bifunctional catalysts that being study, shown as Figure 1.2.-b is the one with Lewis or Brønsted basic functionality and a hydrogen-bond donor group suitably positioned over a chiral scaffold catalysts system, which is also the catalytic mechanism concept[35] that being applied in the bifunctional hollow fiber microfluidic catalysts reactor system for this dissertation paper.

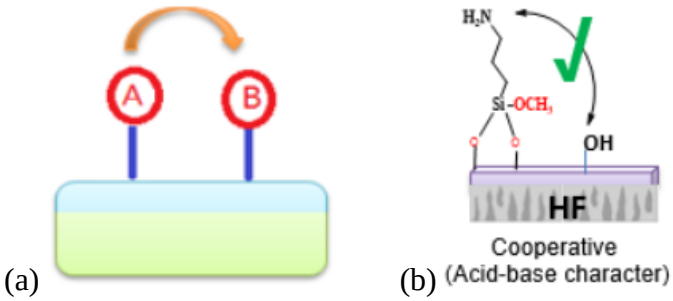

* A: Nucleophile site; B: Electrophile site.

Figure 1.2. (a) General bifunctional catalysts; (b) Acid-Base cooperated structure.

The polymeric hollow fiber was treated by the surface modification process to functionalized with 3-aminopropyltrimethoxy silane (APS)[17,19,21]. This step can graft the amino group as the APS layer on the inner wall of the hollow fiber and providing the weakly basic characteristic. Meanwhile, the combination with the silanol acidic functional group which provided by the hollow fiber, a silanol group neighboring with the amine

functional group provided thee cooperated acid-base characteristic. This bifunctional polymeric hollow fiber microfluidic reactor was being successfully applied to the aldol and nitroaldol condensation reaction, as well as the glucose/fructose to 5-hydroxymethylfurfural (5-HMF) reaction.

1.3.2. Metal Nanoparticles (MNPs)-Immobilized Hollow Fiber Membrane Catalysts. The metal nanoparticles as catalysis have been a highlight topic for numbers of leading experts to work on [13, 36–39]. During these decades, hundreds of applications have been investigated by different research groups[40–42], such as the synthesis of organic transformation and pharmaceutical product[16,43,44], the water treatment[13,36], and the catalytic of various novel organic chemicals[45,46].

To increase the economic efficiency and meet the green chemistry principle, the immobilization of the metal nanoparticles (MNPs) on to the surface of heterogeneous catalysts become a popular research area[18,47]. To immobilize the MNPs on solid supports, such as the various oxides[38,48,49] and a different polymer[38,48–51], is the most comment method to synthesize the MNPs heterogeneous catalysts[28,51]. In this dissertation, the novel metal nanoparticles (MNPs)-immobilized membrane reactor were being synthesized.

As shown in Scheme 1., the MNPs immobilization step was based on the APS-grafted HFs, after the APS-grafted step, the HFs were being post-modification to reacted with the salicylic aldehyde, to provide the Pd-immobilized platform. After to react with the $PdCl_2(CH_3CN)_2$, the Pd-immobilized membrane layer was formed of the surface of the polymeric hollow fiber, and the palladium could convert from Pd(II) to Pd(0) via reducing by the $NaBH_4$[18].

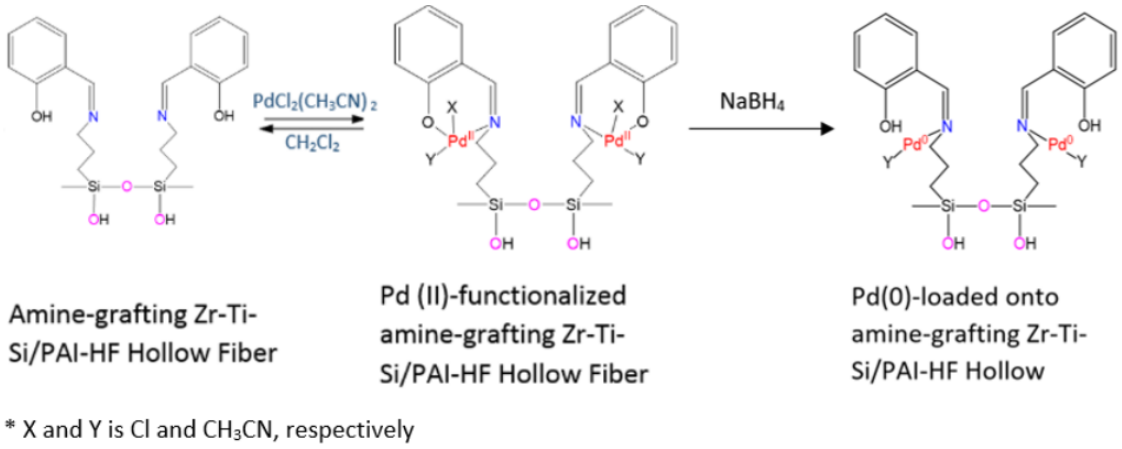

Scheme 1. Proposed reaction mechanism from APS-grafted HFs to the Pd-MNPs immobilized HFs.

The Pd-immobilized polymeric hollow fiber membrane microfluidic catalysts reactor has been successfully proving to be applied in the Heck coupling and the 4-nitrophenol reduction reaction and being discussed in this dissertation.

1.4. THE NEED FOR CONTINUOUS-FLOW REACTOR SYSTEM

In organic synthesis, which organic and inorganic molecules catalyze single or multiple organic reactions have been investigated into a wide range of research area over these decades, the selection of the catalysts, the reactor system, and reaction condition play significant roles in enhancing the consistent results of the outcome of the reaction.

Therefore, when the investigation of an organic reaction, the reactor system always comes as one of the important considerations. Basically, the comment reactor system being used were mainly included the batch reactor system and continuous-flow reactor system[52–54]. The most popular reactor selected in the laboratory research field is the batch reactor system[54,55], owing to its convenience and efficiency for the small-scale synthesis. While

considering to develop a scale-up reactor system, the continuous-flow reactor system appeared to be more safety and controllable to the reaction outcome[24,47,56,57].

1.4.1. Comment Reactor System. To have a better insight view of the need of a continuous-flow reactor system, further study of various reactor system is needed. There were several typical reactor systems which have been widely studying and used in academic and research areas, such as the batch reactor[56,58,59], continuous stirred-tank reactor (CSTR)[60,61], plug flow reactor (PFR), and semi-batch reactor.

Batch, as mentioned above, is the most comment reactor system being used in the small-scale research, as well as the reaction related to the biochemistry due to its simple design and operation. The reactant mixture and catalysts can be mixed completely and increasing the interaction time between the catalysts with the reactant mixture[14, 62]. However, when employed the batch reactor into the scale-up reactor system, it will become a change to control the reaction conditions, such as the reaction temperature, pressure, and volume. Especially, when facing a serious complicated reaction, it is impossible to control the selectivity of the target product by controlling the reactor parameter, as in the batch reactor system, it is a start till end process, which is difficult for you to control the various selectivity of a specific product in different purposes[28,63]. Therefore, to meet the safety requirement, the batch reaction will not be the first choice to work as the scale-up reactor.

The continuous stirred tank reactor (CSTR) is the development of the batch reactor system which is suitable for the series steps of continuous reaction, which is suitable for the fluidic reactant mixture in series step introduce into the tank reactor, is easier to control the reaction outcome compare to the single batch reactor system and much suitable for the homogeneous reactor system[64–66]. However, similar to the batch reactor system, the CSTR

system is facing the safety problems when employed into the large scale-up system also, as it is difficult to control the reaction conditions, like the reaction temperature and pressure.

Since the CSTR is more focus on the homogeneous reaction, the semi-batch reactor was being developed to solve the heterogeneous scale up reaction problems, which is operated in the continuous as well as batch input and output[67–69]. The semi-batch reactor is more suitable for the reaction with one of the reactants to add into the system slowly or the product phase change situation to separate from the reactor system so that improve the catalytic performance. As the definition mentioned above, both CSTR and the semi-batch reactor system is based on and developed from the traditional batch reactor system to meet the large scale-up manufacture requirement[55,70,71]. Therefore, both CSTR and semi-batch reactor are all facing the drawback that the traditional batch reactor system facing, like the uncontrollable reaction parameter and overall lower process efficiency.

Plug flow reactor (PFR), also referred to the continuous tubular reactor (CTR), is the reactant was pumped through the pipe or tube[4,72,73], and reaction occurred during the reactant mixture pass through the PFR. The PFR system is much more controllable compared to the CSTR and semi-batch reactor. Reaction rate could be changed dealing with the gradient generated by the change of concentration of the reactant, also in the case of the using the heterogeneous catalysts, the interaction and resident time could be changed by the flow rate controlled by the pump inlet flow rate[8,74–77]. And the continuous-flow reactor system being studied in this dissertation mainly based on the plug flow reaction model combined with the heterogeneous catalysts. Since the continuous-flow system has the significance of economic and environmentally friendly sustainable production of

pharmaceuticals[28,78], fine chemicals[4,8], and agrochemicals companies[79], continuous-flow synthesis processes become a popular research topic in these decades.

1.4.2. Laboratory-scale Continuous-flow Reactor System. In the continuous-flow heterogeneous catalytic reactor system, the commercial flow reactor is available from numerous vendors to offer advantages over the batch reactor[61,78,80]. Compare to the batch reactor system, the continuous-flow system appear to be more safety for the handling of toxic and explosive materials[4,68], able to operate in higher temperature and pressure, as well as improve the heat and mass transfer. Depend on the forms of incorporate and immobilize of the catalytic efficiency composite, applied in the continuous-flow reactor system, the most comment continuous-flow reactors are the pack-bed reactor[81–83] and the monolith flow-thought reactor[79,84–86]. For the powder and particles catalyst, the most comment reactor being used is the pack-bed reactor, as it is much easier to pack the catalysts into the reactor system.

The pack-bed system can increase the concentration of the catalysts as well as increasing the turnover number of the reactant. However, because the higher concentration of the catalysts, great pressure drop also generate and caused it much difficult to control the reaction, which leads the overall low process efficiency of the reactor. Therefore, later on, the concept of monolith flow-through reactor was developed, which could overcome most of the drawbacks of the pack-bed reactor because of the structural design of the monolith, and providing the ideal supporting platform for loading the catalytic efficiency composite. However, since the most comment raw material to form the monolith is the polymer, in during the reaction the polymer swelling problem would be generated to block the monolith channel. Besides, the monolith mainly obtained by the commercial monolith

and the newly developed technology-3-D printing [21,87–90]. The commercial monolith is pretty expensive and also fragile owing into to the swelling situation, while the 3-D printing monolith[87] can help to improve the economic efficiency of the monolith. However, the fragile of the monolith is still a huge challenge facing nowadays.

Here in this dissertation, a novel continuous-flow hollow fiber membrane reactor system has been developed and investigated for the sustainable transformation organic synthesis reaction. The polymeric HFs were being synthesis by the Torlon material and its mechanical strength can be improved by doping various metal oxide practical, like silica, titania, and zirconia. As shown in Figure 1.3., three to five HFs catalysts were in assembling into the hollow fiber reaction module and the reactant was being introduced by the syringe pump into the reaction module. The efficient catalytic composition was being embedded on the inner wall of the hollow fiber shell, and reaction occurred during the reactant mixture pass through the shell wall of the HFs microfluidic reactor. Separation with catalysts process could be also finished the reactant mixture traveled to the bore channel. Since the highly polymeric characteristic of the HFs structure, the HFs could provide a higher surface area to volume ratio, and the reaction condition could be easier to control by adjusting the flow-rate. Owing to the high mechanical strength of the HFs membrane reactor, the polymeric HFs membrane reactor applied into the laboratory-scale continuous-flow reactor system appeared to be an ideal concept to scale up for the sustainable chemical transformation reactor system with economic efficiency[17,18].

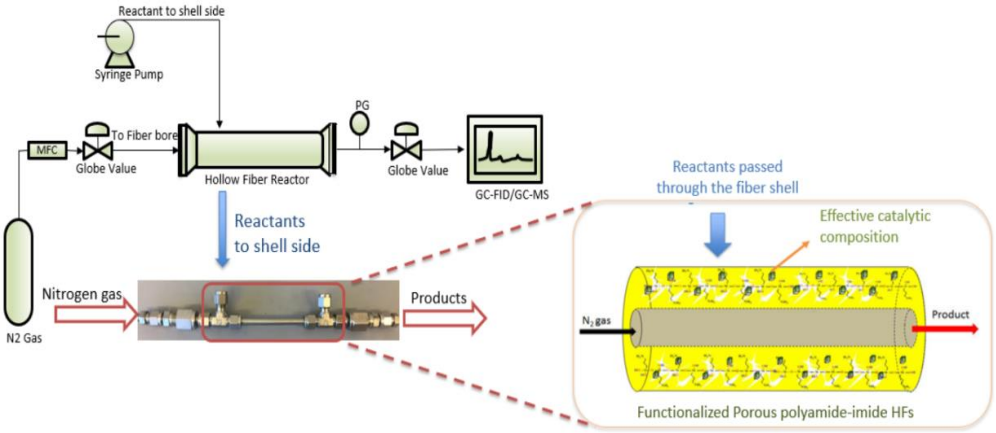

Figure 1.3. Scheme of the laboratory-scale continuous-flow hollow fiber reactor.

Hence, the continuous-flow reactor system plays a much important role in the scale-up manufacture industry. And the novel laboratory-scale continuous-flow hollow fiber microfluidic reactor is an ideal system for the scale-up organic synthesis.

1.5. DISSERTATION SUMMARY

There were four papers included in the paper part. The novel hollow fiber is an ideal platform for further surface modification to synthesis heterogeneous catalysts which suitable for sustainable organic chemical transformation reaction. There were mainly two kinds surface modification methods that applied in the novel hollow fiber catalysts during the whole Ph.D. study, which the aminosilane(APS)-grafted bifunctional catalysts and metal nanoparticles (MNPs) immobilized membrane catalysts. Four different organic synthesis reaction was being investigated by applying these novel surface modification hollow fiber catalysts and all successfully being conducted in the laboratory-scale continuous-flow reactor system.

In Paper I, the novel APS-grafted bifunctional catalysts were first introduced as heterogeneous catalysts in the organic synthesis reaction. The surface modification step of APS-grafted has introduced the Lewis and Brønsted acid sites on the novel hollow fiber. Since the novel heterogeneous catalysts with the Lewis and Brønsted acid sites can provide the different functionality of an efficient catalytic site, which is suitable for some two steps or complex reactions.

In Paper II, the bifunctional catalysts which reported in the Paper I was being improved by post-modification to provide a better platform for metal nanoparticle (MNPs) immobilization. The post-modification step can form the membrane layer on the surface of the hollow fiber,

In Paper III, depend on the bifunctional HFs catalysts published in the Paper I, the bifunctional catalysts with the support of the Lewis and Brønsted acid sites can be successfully applied in the condensation reaction between two chemicals, therefore, further investigation of the catalytic test were being conducted in other complexity reaction, such as the Tandem reaction, which was combined the isomerization and dehydration reaction among glucose, fructose, and 5-hydroxymethylfurfural. This two steps of reactions were successfully being catalytic by the bifunctional HFs catalysts.

In Paper IV, the Pd MNPs immobilization reaction, which has been successfully motivated the heck coupling reaction and achieved the palladium cycle in Paper II, has been successfully applied in the 4-nitrophenol reduction reaction which also being proved of it the multi-function catalytic ability and the stability for cycling reaction in the 4-nitrophenol self-reduction reaction. Meanwhile, the high conversion and selectivity also proving in the continuous-flow reactor system at room temperature.

After the presentation of the four paper, summarization of all the finding was conducted depend on this dissertation, and the future study directions were also being discussed in the final section.

PAPER

I. DIRECT ALDOL AND NITROALDOL CONDENSATION IN AN AMINOSILANE-GRAFTED Si/Zr/Ti COMPOSITE HOLLOW FIBER AS A HETEROGENEOUS CATALYST AND CONTINUOUS FLOW REACTOR

Yingxin He, Abbas Jawad, Xin Li, Marktus Atanga, Fateme Rezaei, Ali A. Rownaghi*

Department of Chemical & Biochemical Engineering, Missouri University of Science and Technology, Rolla, MO 65409-1230, USA

E-mail: rownaghia@mst.edu; ali.rownaghi@gmail.com

ABSTRACT

A proof of concept study for a new type of continuous flow reactor based on porous aminosilane-grafted Si-Zr-Ti/Torlon composite hollow fibers was considered for aldol and nitroaldol condensations of aromatic aldehydes with acetone and nitromethane. These novel hollow fiber reactors consist of bifunctional groups in fiber wall which render them as bifunctional catalysts for cooperative interactions (*i.e.*, acid-base catalysis). In this study, the effects of reactants flowrate, reaction time and temperature, electron-donating, and electron-withdrawing groups of para-substituted benzaldehyde derivatives on the catalytic activity of aldol and nitroaldol condensation reactions were systematically investigated. The yield of products was found to be dependent on the cooperative interactions of the acid-base pair, para-substituted benzaldehyde, and the reaction conditions such as temperature and contact time. Moreover, the relatively high yields of *ca.* 100% were obtained at higher flow rates for primary aldol and nitroalcohol products, while

benzylideneacetone and nitrostyrene yields were higher at longer contact times. The obtained results indicate that the aminosilane-grafted Si-Zr-Ti/Torlon composite hollow fibers provide a new platform as flow reactors for heterogeneously catalyzed reactions that may facilitate the ultimate scale-up of practical fiber catalysts for the synthesis of complex organic compounds.

Keywords: Cooperative catalysis; bifunctional acid-base catalysts; aminosilane-grafted Si-Zr-Ti/Torlon composite hollow fibers; aldol and nitroaldol condensations; continuous flow reactor

1. INTRODUCTION

The aldol and nitroaldol condensation reactions are essential steps in C-C bond formation for organic synthesis, production of complex molecules in the fine chemical and pharmaceutical industries, and development of biomass conversion schemes [1–4]. Aldol and nitroaldol condensation reactions are industrially catalyzed by homogeneous catalysts that typically have a short lifetime and require further separation from reaction mixture [5–8]. The short catalyst lifetime and relatively high energy requirement for recycling are drawbacks of homogeneous catalysts which limit their use in industrial applications. Fortunately, insights from homogeneous catalysts can be applied to the development of more robust heterogeneous catalysts that integrate acid-base sites into a single support material. The design of bifunctional catalysts that combine basic sites together with other acidic sites usually relies on incorporating inexpensive elements into chemically

functionalizable materials to enable simultaneous activation of both electrophilic and nucleophilic reaction partners [2,5,6,9]. Bifunctional catalysts that contain two distinct catalytic sites can act as cooperative catalysts for achieving a higher reaction rate than that achieved by using either of the catalytic species independently [9–11].

The incorporation of silanol groups (weak acid sites) next to amine sites (base sites) was previously shown to increase the overall rate of reaction in aldol condensation and other important C-C coupling reactions such as Knoevenagel [12,13], Claisen-Schmidt [14,15], Michael addition, and Henry (nitroaldol) condensations [5,6]. The use of amine-functionalized mesoporous silica (*e.g.,* SBA-15 and MCM-41), zirconia (ZrO_2) and titania (TiO_2) have been studied in aldol condensation by several research groups [5,9,11,14,16–20]. These materials exhibited improved activity as bifunctional catalysts for aldol condensation [2,5,6,9]. An alternative method is to engineer the surface silanol groups by introducing new types of hydroxyl species such as titanols [21] or Brønsted acid sites (like unsaturated Zr^{4+} species) that are stronger than the silanols or Lewis acidic sites [11,22]. Higher activity and selectivity could be obtained on catalysts having two or more functionalities on the surface. Vermoortele *et al.*[23] showed that amine-functionalized UiO-66-NH_2 metal-organic frameworks (MOFs) with Lewis acid Zr-sites and Brønsted base -NH_2 sites are more active and selective than bare UiO-66 for cross-aldol condensation reaction of heptanal with benzaldehyde to form jasminaldehyde. It has been shown that primary, secondary, and tertiary amines with various alkyl linker lengths exhibit totally different catalytic activities in the aldol condensation reaction due in part to significant differences in the ability to form imine species, as key intermediates for this

reaction, and partly due to difference in the degree of amine sites deactivation which dramatically affects catalyst activity [5,24,25].

Waste reduction and catalyst recycling have attracted intense research interest in recent years due to economic concerns for sustainable production of chemicals and pharmaceuticals [26]. The continuous-flow approach is a rapidly emerging technology that offers an interesting alternative to inherently less efficient batch processes. Homogeneous catalysis performed in a flow system has demonstrated successful examples inefficient mixing and heat control, however, the current flow systems suffer from some limitations including the multistep transformation of unstable intermediates, and low potential for catalyst recycling. [27,28]. Heterogeneous bifunctional catalysis, on the other hand, offers options for catalyst separation and recycling and integration into a flow system. In contrast to homogeneous catalysts, however, the performance of heterogeneous catalysts in a continuous-flow reactor system has been less explored as a result of lower catalytic efficiency and stereoselectivity as compared with their homogeneous counterparts [28,29]. Shibasaki *et al.* [28] prepared a series of Nd/Na heterogeneous catalysts by self-assembly of an amide-based chiral ligand and a multi-walled carbon nanotube and evaluated them for nitroaldol reaction with high stereoselectivity to nitroalcohol in a continuous-flow system. In another study, Kobayashi *et al.*[30] synthesized β-nitrostyrene derivatives in two-step continuous-flow reactor using heterogeneous catalysts. Asefa *et al.*[31] reported a facile method for continuous nitroaldol reaction in a fixed-bed reactor packed with primary and secondary amine-functionalized MCM-41 materials. These previous studies have primarily focused on the evaluation of physical properties of support (mainly silica) or modification of organic constituent for tuning the amine-silanol cooperative interactions

in a flow system to promote condensation reaction. Packing heteroatom bifunctional catalysts into an appropriate contactor such as hollow fiber appears to be a promising approach for scaling up the continuous-flow process to practical sizes. Such novel configurations could function as a flow reactor while catalyzing the aldol condensation reaction at the same time. The composite hollow fiber flow system not only confers advantages at the laboratory scale but also offers an excellent potential for large-scale production of valuable chemicals. This proposed system can potentially offer lower operational, maintenance and capital costs, ease of installation, and smaller footprint. Amine-functionalized polymeric hollow fibers composed of metal oxide particles embedded into a polymer matrix have recently been used for gas separations, namely separation, and purification of CO_2 [32,33]. Such contractors offer advantages over traditional pellets or beads, due to the high surface area to volume ratio, avoidance of particle attrition and low-pressure drop, enhanced flow pattern reliability for scale-up, and the ability to control mass transfer resistances [32,34]. Off the advantages offered by hollow fiber-based continuous-flow technology, process intensification is a key feature as composite hollow fiber-flow reactors can facilitate effective reactants interactions and mixing within the porous structure of the polymer matrix, the transformation of unstable intermediates, and functionalization with various agents, while expanding the window of reaction conditions for a specific transformation.

Aldol condensation [35,36] and other reactions such as nitroaldol [28], Michael [26], Mannich [36,37], and Mizoroki-Heck [38] reactions have been previously investigated using flow platforms to promote these reactions [27,35,39–41]. However, to the best of our knowledge, no catalytic investigations on the use of amine-functionalized

composite hollow fiber reactors for these condensation reactions have been reported so far. In the present contribution, we demonstrate the applicability of aminopropyltriethoxysilane (APS)-grafted polyamide-imide (Torlon) hollow fibers (APS-grafted Zr-Ti-Si/PAI-HF) as a bifunctional heterogeneous catalyst in the cross-aldol and nitroaldol condensation of aromatic aldehydes with acetone or nitromethane under mild reaction conditions in a continuous flow reactor.

2. THEORY AND BACKGROUND

Hybrid organic-inorganic functional groups can be easily immobilized into high surface area supports for applications in various gas separation and reaction processes [10,42]. Recent advances have led to the development of polymeric hollow fibers that comprise various inorganic fillers with different functional groups that can provide cooperative catalysis by controlling their spatial arrangements [32,43]. These hollow fiber catalysts are in fact pseudo-monolithic materials comprised of a porous polymer matrix with catalyst nanoparticles such as silica, zirconia, titania, zeolites, and MOFs embedded into the matrix. In this effort, we engineer hybrid organic-inorganic catalysts by tethering organic functional groups onto inorganic surfaces that can act together to provide catalytic activity and selectivity superior to what can be obtained from either monofunctional materials or homogeneous catalysts. The silica, zirconia and titania support surfaces grafted with aminosilanes provide a continuous range of weakly acidic and basic bifunctional catalyst sites that play a significant role in the outcome of an acid-base catalyzed reaction. Herein, we report that these hollow fiber catalysts can also be used in continuous flow reactions for the production of large quantities of selective aldol or nitroaldol reaction

products (Figure 1). As schematically shown, in a hollow fiber reactor, the catalyst is immobilized and resides within the porous wall while the reagents are passed through the fiber shell and products are collected from the bore side, so in principle, no separation of the product from the catalyst is required. Also, by operating under optimum conditions to achieve high conversion, minimal separation of unreacted products are required. Furthermore, through this configuration, the hollow fiber catalysts can be easily regenerated and reused. These advantages render the hollow fiber catalyst system as the most convenient configuration to perform a reaction under continuous flow conditions. It is anticipated that this catalytic hollow fiber reactor becomes an industrially viable substitute to the current commercial homogeneous catalytic systems for the aldol and nitroaldol condensation reactions involving soluble bases such as NEt_3, KH_2PO_4, Na_2CO_3, KOH, and NaOH [44,45].

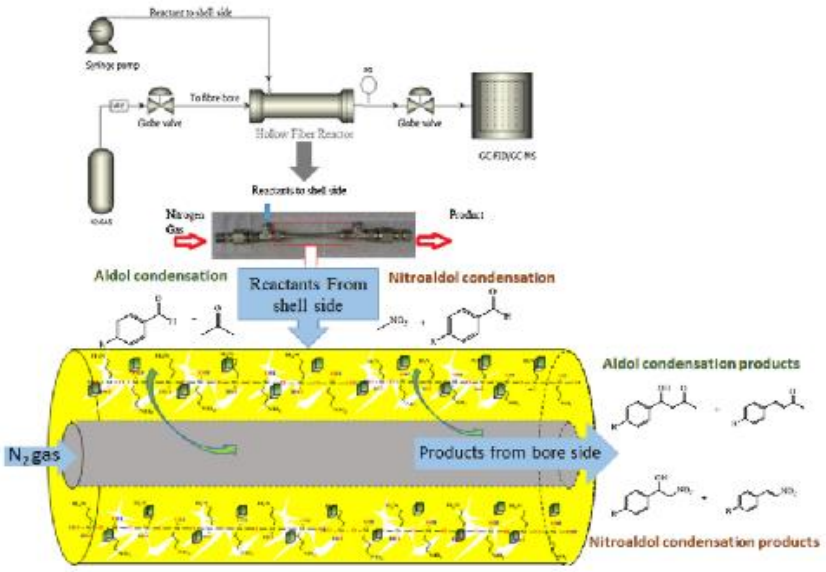

Figure 1. Schematic diagram of an aminosilane-grafted Si-Zr-Ti/PAI-HF reactor for the continuous aldol and nitroaldol condensation reactions.

3. EXPERIMENTAL

3.1. CHEMICAL AND MATERIALS

Zirconia, titania, and silica (average particle size 100 nm, Sigma Aldrich), Torlon 4000T-HV, a commercially available polyamide-imide (PAI) (Solvay Advanced Polymers, Alpharetta, GA), poly(vinylpyrrolidone) (PVP) (average Mw≈ 1300 K, Sigma Aldrich), N-Methyl-2-pyrrolidone (NMP) and Methanol (ACS Reagent, >98.5%, VWR) were used for polymer dope preparation and formation of the composite hollow fiber catalysts. The 3-Aminopropyltrimethoxysilane (APS) (95%) was purchased from Gelest and used as the agent for grafting zirconia, titania, and silica-Torlon hollow fiber catalysts. Benzaldehyde (98%), 4-bromobenzaldehyde (99%), 4-nitrobenzaldehyde (99%), 4-methoxybenzaldehyde (98%), 4-hydroxybenzaldehyde (97%), acetone (98%) and nitromethane (99%) were purchased from Sigma-Aldrich. Inert UHP nitrogen gas was purchased from Airgas.

3.2. ZIRCONIA-, TITANIA- AND SILICA-TORLON HOLLOW FIBERS REACTOR FORMATION AND AMINOSILANE GRAFTING

The polymer dope composition was determined by the cloud-point technique [67] and fibers were produced via co-extrusion of the polymer dope and a bore fluid solution through a spinneret using an important variation of the well-known nonsolvent phase inversion technique commonly referred to as “dry-jet, wet quench spinning”. The polymer dope composition and zirconia-titania-silica hollow fiber formation approach taken in this work has been already described in our previous works in detail [32,43] (see Section S2, Table S1, and Figure S6, Supporting Information).

Silica, zirconia, and titania were chosen on the basis of previous studies[31,68-70], as noted above, demonstrating that more effective amine-stabilizing sites can be created

upon zirconia/titania/silica addition. The post-infusion grafting of hollow fibers was carried out under nitrogen pressure at 80 °C for 2 h (see Section S3 and Figure S7, Supporting Information for details). The amine grafting was performed in a mixture of toluene and water. The water content of the mixture was kept within the range of 0.01-2.00 wt%. Hollow fibers were then washed, filtered with 100 mL each of toluene and ethanol, and dried under vacuum at 80 °C for 4 h. The hollow fiber reactors contain three different types of catalysts for aldol and nitroaldol condensations: (i) only weakly acidic silanol catalysts (bare Si-Zr-Ti/Torlon composite hollow fiber), (ii) only amine base catalysts (amine/Torlon composite hollow fiber), and (iii) cooperative acid-base catalysts (APS-grafted Si-Zr-Ti/Torlon composite hollow fiber).

3.3. FIBER CATALYST CHARACTERIZATION

A high-resolution scanning electron microscope (Hitachi S-4700 FE-SEM) was used to assess the morphology of the hollow fibers before and after grafting. The cross-section and surface of the fiber catalysts were examined. Aminosilane grafting within the Torlon fiber catalyst and onto zirconia, titania and silica nanoparticles was confirmed by Fourier transform infrared spectroscopy (FTIR) at room temperature over a scanning range of 400-4000 cm^{-1} with a resolution of 4.0 cm^{-1}, using Bruker Tenser spectrophotometer. Bulk elemental analysis (EA) was performed to determine amine loading and zirconia, titania and silica nanoparticles content of the hollow fiber. The corresponding results are given in Table 1. Nitrogen physisorption isotherms were measured using a Micromeritics 3Flex Surface Characterization Analyzer apparatus at 77 K. Amine-grafted titania, zirconia and silica-hollow fiber sorbents were degassed at 110 °C under vacuum for 24 h prior to analysis. Surface area and pore volume were calculated from the isotherm data using the

Brunauer-Emmett-Teller (BET) and Barrett-Joyner-Halenda (BJH) methods, respectively. Pyridine IR experiments were conducted on a Bruker Tensor 27 FTIR spectrometer to collect IR-Py spectra. About 20-30 mg of the sample was pretreated at 120 °C for 1 h in an in-situ cell. After being cooled down to 50 °C under 50 STP mL/min He, a background spectrum was recorded. Pyridine adsorption took place at 50 °C through a bubbler for 5-10 min while He flowed at 10 STP mL/min. A pyridine purge took place at 50 °C under a He flow of 50 STP mL/min for 30 min. Spectra were taken during absorption to ensure pyridine saturation and were recorded every 5 min. Spectra were recorded at 50 °C after 30 min of He purging to remove physisorbed pyridine. The total amount of acid sites for each catalyst was calculated using the integrated peak areas and molar extinction coefficients for Brønsted acid sites and Lewis acid sites from the literature [60]. The products were analyzed by Gas Chromatography (GC) using a Varian 3800 equipped with a flame ionization detector (GC-FID) and a capillary column (DB-5) and mass spectrometry (GC-MS). In addition, ^{1}H NMR spectra were recorded at room temperature using a Bruker-DRX 500 MHz spectrometer.

Table 1. Textural properties, N2 permeance, and amine and metal oxide loading of the bare and the resulting aminosilica bifunctional catalysts.

Catalyst	S_{BET} (m^2/g)[a]	V_{pore} (cm^3/g)[a]	Permeance (GPU)[b]	Amine loading (mmol N/g-fiber)[c]	Metal oxide loading (wt.%)[b]		
					SiO_2	TiO_2	ZrO_2
Bare Si/PAI-HFs	40	014	102,000	0	19.5	-	-
APS-grafted Si/PAI-HFs	15	0.08	36,000	5.82	-	-	-
Bare Si-Zr/PAI-HFs	45	0.19	112,500	0	11.0	-	8.5

Table 1. Textural properties, N2 permeance, and amine and metal oxide loading of the bare and the resulting aminosilica bifunctional catalysts. (cont.)

APS-grated Si-Zr/PAI-HFs	27	0.12	41,000	5.73	-	-	-
Bare Si-Ti/PAI-HFs	41	0.16	103,500	0	11.0	9.0	-
APS-grafted Si-Ti/PAI-HFs	14	0.07	34,500	5.7	-	-	-
Bare Si-Zr-Ti/PAI-HFs	57	0.25	113,000	0	7.0	7.1	6.2
APS-grafted Si-Zr-Ti/PAI-HFs	28	0.12	53,000	6.17	-	-	-

[a] Determined by nitrogen physisorption experiments at 77 K.
[b] GPU refers to 1×10^{6} cc (STP)/(cm^2 s cmHg).
[C] Amine and metal oxide loadings determined by elemental analysis.

3.4. GENERAL PROCEDURE FOR ALDOL AND NITROALDOL CONDENSATION REACTION

3.4.1. Batch Condensation Reactions. About 20 mol% of hollow fiber catalyst (by amine loading), 4 mL of reaction mixture containing 0.05 M benzaldehyde as a reactant and 0.05 M 1,4-dimethoxybenzene as an internal standard in acetone or nitromethane were added to a 25 mL two-neck flask with a magnetic stir bar. The reactions were run in an oil bath at 50 °C under reflux with an atmosphere of nitrogen for 4 h. Reactant conversions for benzaldehyde and aldol and nitroaldol condensations were determined by a VARIAN gas chromatography CP-3800 equipped with a flame ionization detector (FID) and a DB-5 GC column (30 m, 0.25 mm inner diameter, 0.25 μm film thickness). For each reaction,

1,4-dimethoxybenzene was used as an internal standard to determine the reactant conversion.

3.4.2. Continuous Flow Condensation Reactions. To test the bifunctional catalytic activity of hollow fibers in a continuous flow system, we carried out a set of proof-of-concept studies. The reaction was conducted in a stainless steel module containing five hollow fibers (with the inner diameter of 0.1 μm, length of 15 cm, and the total volume of 10 mL) at 50 and 90 °C. The PAI hollow fiber reactor was coiled in a heating jacked to adjust the temperature. Cooperative catalysis with acid-base bifunctional APS-grafted Si-Zr-Ti/PAI-HF (weak Brønsted acid-Lewis base) was investigated systematically. The reactants were then continuously run through the hollow fiber reactor at various flow rates (0.02-0.1 cm^3min^{-1}) and temperatures (50-90 °C). A syringe pump equipped with two syringes was used to feed the hollow fiber reactor with the reagents through a T-junction. To start the reaction, in one syringe the benzaldehyde and internal standard were charged, while in a second syringe, acetone or nitromethane was loaded. A 0.05 M solution of aldehyde in acetone or nitromethane was introduced at one inlet (hollow fiber shell side) at a flow rate of 0.02-0.1 cm^3/min, while pure nitrogen was introduced from the other inlet (bore side) at 25 cm^3/min flowrates. Total outlet flow was 4.8-24 cm^3/min (various residence time). The schematic diagram of the system is illustrated in Figure 1. The product was then cooled and collected from the bore side of the hollow fiber reactor. Pure nitrogen gas was passed through hollow fiber bores for preventing pore blockage and also pushing product out of the bore.

4. RESULTS AND DISCUSSION

4.1 PHYSICAL AND CHEMICAL CHARACTERIZATION OF APS-GRAFTED ZIRCONIA/TITANIA/SILICA/PAI-HF CATALYSTS

The APS-grafted hollow fiber catalysts consisting of a series of heteroatoms (i.e., Si, Ti, and Zr) were successfully formed. To further assess the impact of metal oxide nanoparticles and amine post-infusion on fiber structure and performance, N_2 permeation and sorption measurements were carried out on both bare and post-infused hollow fiber catalysts. Nitrogen permeance through fiber catalysts was measured at 35 °C and 30 psig, and the corresponding data are presented in Table 1. It is apparent from these data that the fiber catalysts permeability was significantly influenced upon grafting (as a result of the partial collapse of the pores), however, the pore network remained open, indicating that the fiber catalysts retained sufficient porosity for effective catalytic performance.

Figure 2 shows N_2 adsorption-desorption isotherms of fiber catalysts before and after aminosilane grafting. The isotherms are of type IV (IUPAC classification) with hysteresis between the adsorption and the desorption branches for both fibers [46]. Although the amount of N_2 adsorbed on aminosilane functionalized fiber catalysts were significantly smaller than that on the bare fiber catalysts, the shape of the isotherms was found to be almost identical. Table 1 also presents a brief summary of the textural properties (BET surface area and pore volumes) of the bare and amine-grafted hollow fiber catalysts. Both surface area and pore volume decreased after aminosilane grafting. This could be related to filling of the smaller pores of the corrugated fiber substructure and surface with the deposition of the aminosilane molecules during the grafting process. Among all mixed metal oxides hollow fiber catalysts, the ternary Si-Zr-Ti/PAI-HF catalyst showed higher surface area and porosity before and after aminosilane grafting than the

binary catalysts (Si-Zr- or Si-Ti/PAI-HF). The BET surface area for the Si-Zr-Ti/PAI-HF fiber catalyst was calculated to be 57 m^2/g while pore volume (at $P/P_0 = 0.99$) was found to be 0.25 cm^3/g in comparison to aminosilane-grafted Si-Zr-Ti/PAI-HF catalysts with 28 m^2/g BET surface area and 0.12 cm^3/g pore volume. The reduction in both surface area and pore volume implies that amine groups were indeed anchored onto zirconia-titania-silica surface and pore walls of the bare fiber catalyst. The APS-grafted binary Si-Zr- and Si-T-/PAI-HF catalysts exhibited similar nitrogen physisorption isotherms.

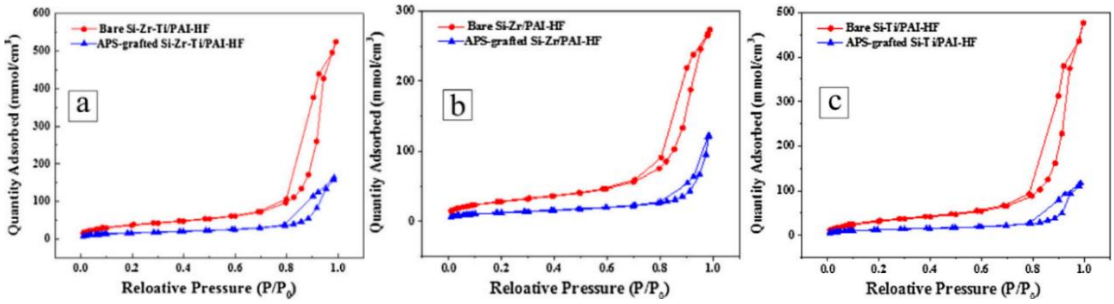

Figure 2. Nitrogen adsorption/desorption isotherms for bare and aminosilane-grafted (a) Si-Zr-Ti-, (b) Si-Zr-, and (c) Si-Ti/hollow fibers.

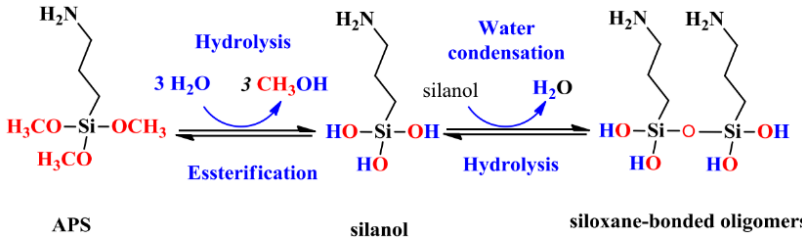

Scheme 1. The proposed mechanism of reaction between Si-Zr-Ti/PAI-fiber catalysts and primary aminosilanes during amine grafting.

Previous studies [32,33,43] showed that the aminosilane can be activated and polymerized with itself in the presence of water in toluene solvent. In addition, heat treatment step leads to multilayer formation of aminosilane on Si-, Zr and Ti-composite hollow fibers surfaces [47]. Hydrolysis occurs by the nucleophilic attack of the oxygen contained in water and is facilitated in the presence of a non-polar solvent such as toluene which is especially beneficial in promoting the hydrolysis of silanes [48]. The activated aminosilane undergoes condensation reaction between Si-OH groups of the silanol and OH groups of zirconia, titania and silica nanoparticles or co-existing methanol that formed in the fiber pores from aminosilane hydrolysis in the first step, as shown in Scheme 1. As noted above, transient silanol groups may condense with other silanols leading to high -NH_2 group loading. This condensation is dramatically influenced by the content and density of reactive aminosilane moieties at the substrate surface and number of Lewis acid sites. With grafting of aminosilane on the fiber catalyst surface, Lewis acid density can be further increased in the presence of zirconia, titania and silica nanoparticles, however, as noticed from N_2 physisorption and permeation tests, the porous polymer matrix can become partially collapsed, thereby increasing mass transport resistance in the hollow fiber catalyst as indicated by decrease in surface area, pore volume, and permeability.

The Si, Zr and Ti contents of PAI-HF composites were determined by elemental analysis and the results are summarized in Table 1. Furthermore, to determine if amine grafting was successful, elemental analysis was carried out on the fiber catalysts before and after fiber post-treatment. The results are presented in Table 1. The nitrogen loading of the grafted fiber catalyst depends on several factors including the degree of APS grafting on zirconia, titania and silica surfaces and the hydrolysis of methoxy group of APS. The

amount of amine loading on hollow fiber catalysts was systematically optimized with respect to grafting time and temperature, and amine concentration (see Supporting Information). In addition, the total amount of titania, zirconia and silica loading determined by elemental analysis were found to be about 20 wt% of fiber weight (~7 wt% each oxide). After amine grafting, the hollow fiber catalysts with 20 wt% zirconia, titania, and silica were demonstrated to have a nitrogen loading of 6.17 mmol N/g-fiber. Previous studies [5,6,11,49] have shown that the free electron pairs of the amine are necessary for the catalytic aldol or nitroaldol condensation cycle. Several research groups have also pointed out that the maximum activity in aldol condensation reactions could be achieved when amine with surface weak acid sites (e.g., silanols[32], titanol[50] and hydrous zirconia [51]) create an acid-base cooperative catalyst [5,6,49].

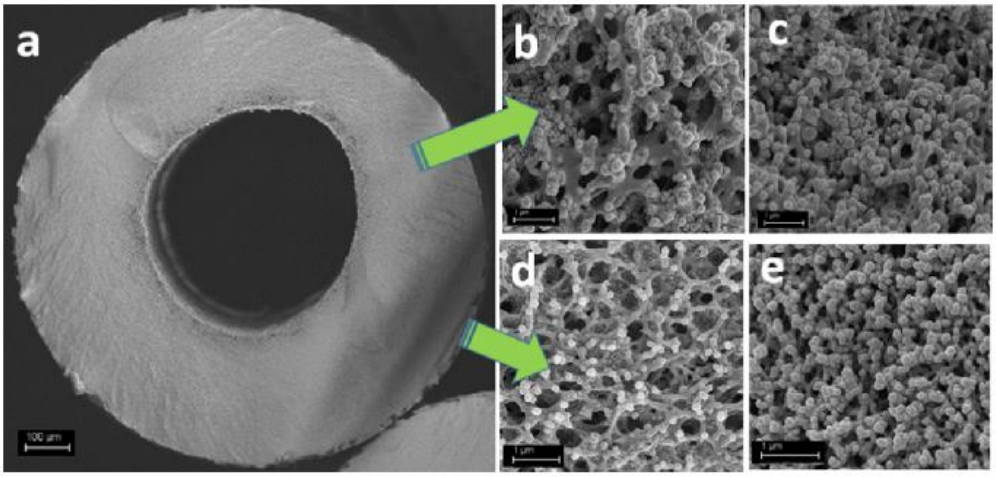

Figure 3. SEM images of (a) the cross-section of a single-layer bare Si-Zr-Ti/PAI hollow fiber catalyst, (b) the cross-section of bare Si-Zr-Ti/PAI-HF, (c) the cross-section of APS-grafted Si-Zr-Ti/PAI-HF, (d) the outer surface of bare Si-Zr-Ti/PAI-HF, and (e) the outer surface of APS-grafted Si-Zr-Ti/PAI-HF.

The detailed morphology of hollow fiber catalysts was analyzed by SEM images of the outer surface of the fiber structure. As can be seen from SEM images in Figure 3, an extremely porous layer was formed on the surface and across the Si-Zr-Ti/PAI-HF catalysts for both bare and amine-grafted fibers. Furthermore, Figure 3 reveals the presence of well-dispersed metal oxide nanoparticles with an average diameter of ~100 nm within the polymer matrix. These SEM images clearly show that the fiber structure is highly porous and spongy as a result of surface engineering by incorporation of ZrO_2, TiO_2, and SiO_2 nanoparticles in the polymer dope even after amine-grafting. Such morphology is indeed highly desirable for preventing pressure drop along the fiber length and also for facilitating reactants/products diffusion through the fiber matrix. Additionally, the SEM images of the APS-grafted Si-Zr- or Si-Ti/PAI-HF catalysts are presented in Figure S1 (Supporting Information). Figure S2 (Supporting Information) also displays the SEM images of metal oxides nanoparticles.

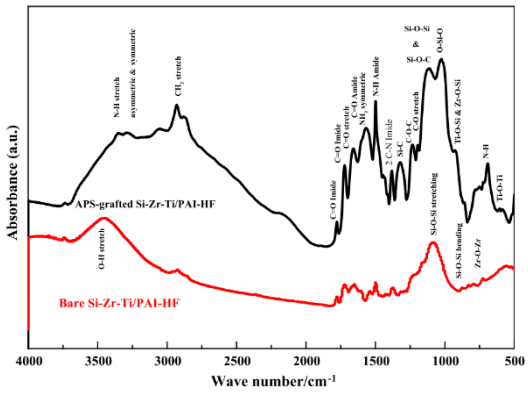

Figure 4. IR spectra of bare and APS-grafted Si-Zr-Ti/PAI-HF catalysts.

The successful APS-grafting of hollow fiber catalysts were confirmed by comparing the FTIR spectra of fiber catalysts before and after amine-grafting. The FTIR spectra in the range of 4000-500 cm^{-1} of Si-Zr-Ti/PAI-HF fiber catalysts before and after amine-grafting are shown in Figure 4. Also, the corresponding FTIR spectra of the bare and aminosilane-grafted Zr-Si and Ti-Si/PAI-HF catalysts are presented in Figure S3 (Supporting Information). As shown in Figure 4 and Figure S3, the Si-O-Si [52,53] Zr-O-Zr [52,54], Si-O-Zr [55] and Si-O-Ti [52,56] stretching vibrations appear at **ca.** 1100, 984, 926-919, and 750, 665 cm^{-1}, respectively, which confirm that zirconia, titania, and silica were well-dispersed in hollow fiber catalysts. In addition, the peaks at 820 and 763 cm^{-l} are believed to be due to Ti-O-Ti bonds [52,55,56]. Both bare and APS-grafted Si-Zr-Ti/PAI-HF catalysts exhibit C-O-C stretch at 1243 cm^{-1}, imide C-N stretch at 1360 cm^{-1}, amide N-C=O stretch at 1510 cm^{-1}, N-H stretch at 1515-1570 cm^{-1}, amide carbonyl (C=O stretch) absorbance at 1650 cm^{-1}, imide symmetrical carbonyl (C=O) absorbance at 1719 cm^{-1}, and imide asymmetrical carbonyl (C=O) absorbance at 1778 cm^{-1}. Comparing the IR spectra of bare and amine-functionalized fibers revealed that the intensity of vibrational bands located in the vicinity of ~1000-1026 cm^{-1}, 1618 cm^{-1}, and 1489 cm^{-1} (which were attributed to Si-O-Si, O-Si-O, and N-H bending vibrations, respectively) increase by aminosilane grafting, indicating that the condensation of APS went to completion to form Si-O-Si bond framework. Additionally, absorption peaks at 850 cm^{-1} and 1270 cm^{-1} wavelengths may be assigned to Si-O and Si-CH_3 stretching vibrations, respectively [53,57,58]. The absence of NH_2 symmetric bending vibration at 1532 cm^{-1} and N-H bending vibration at 690 cm^{-1} for bare Si-Zr-Ti/PAI-HF catalysts, presence in APS-grafted

Si-Zr-Ti/PAI-HF catalysts, exhibits the successful grafting of the aminosilane onto the surface [59].

The amount of Brønsted and Lewis acid sites on each of the hollow fiber catalysts determined by IR spectroscopy measurements (Figure S4) are listed in Table 2. All mixed metal oxides had higher amounts of Lewis acid sites than Brønsted acid sites. Notably, APS-grafted Si/PAI-HFs displayed a peak near 1600 cm^{-1}, corresponding to weakly physisorbed (hydrogen-bond) pyridine [60]. The IR spectra revealed that APS-grafted Si-Zr/PAI-HFs contains a large amount of both types of acid sites. Peaks at 1650, 1620, and 1541 cm^{-1} correspond to Brønsted acid sites while peaks at 1443, 1590, and 1615 cm^{-1} correspond to Lewis acid sites [60]. The APS-grafted Si-Ti/PAI-HFs displayed peaks at 1447 and 1600 cm^{-1}, corresponding to Lewis acid sites which are in the Lewis acid sites region of the IR spectra [60]. No measurable Brønsted acid sites were observed since the strengths of these acid sites were likely not significant enough to measure. Peaks, characteristic of both Brønsted acid sites and Lewis acid sites, were observed on APS-grafted Si-Zr-Ti/PAI-HFs IR spectrum. The pyridine IR results suggest that the ratio, chemical, and physical properties of the mixed metal oxides contributed to the strengths and amounts of the Brønsted and Lewis acid sites present in each hollow fiber catalyst.

Table 2. Total numbers of Brønsted and Lewis acid sites for the Si-, Si-Ti-, Si-Zr-, and Si-Zr-Ti/ PAI-HFs as determined via pyridine IR experiments at 50 °C.

Materials	**Brønsted acid sites** (μmol/g-fiber)	**Lewis acid sites** (μmol/g-fiber)
APS-grafted Si/PAI-HF	0	0
APS-grafted Si-Zr/PAI-HF	11	24
APS-grafted Si-Ti/PAI-HF	0	7
APS-grafted Si-Zr-Ti/PAI-HF	5	9

4.2. CATALYTIC ACTIVITY OF AMINE-GRAFTED ZIRCONIA/TITANIA/ SILICA/PAI-HF CATALYSTS

4.2.1. Initial Assessment of Catalytic Activity in Batch Reaction. The initial study was focused mainly on ascertaining if aminosilane-grafted Si-, Zr-, Ti/PAI-HF materials are active for aldol and nitroaldol condensations. To prove that, the fibers were utilized in batch condensation reactions. The catalytic performance of bare and APS-grafted Si-, Zr-, Ti/PAI-HF/Torlon HF were assessed for condensation of acetone and nitromethane with para-substituted benzaldehyde towards the primary aldol (A) and nitroaldol (C) products, as represented in Scheme 2. The secondary aldol (B) and nitroaldol (D) products are obtained by dehydration of the primary product in the continuous flow reactor using continuous hollow fiber module packed with cooperative solid-base catalysts, as illustrated in Scheme 2.

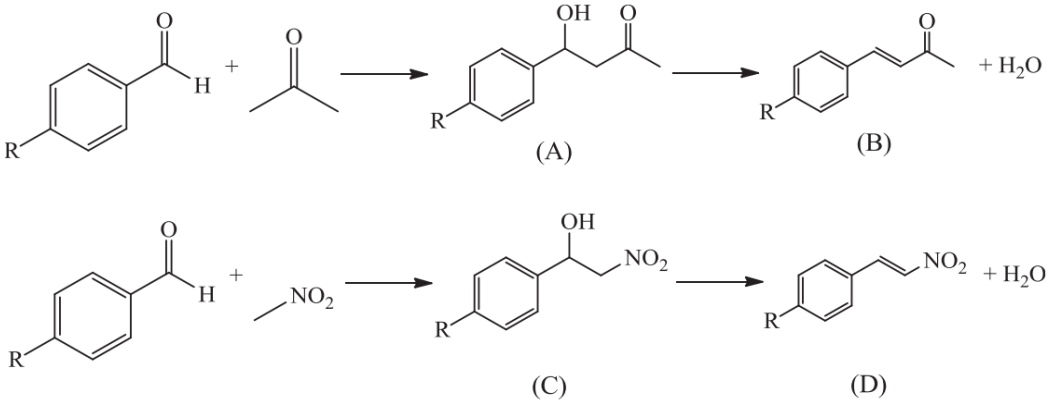

R: -H; -OH; -OCH_3; -Br; -NO_2
A: primary aldol product (4-hydroxy-4-phenyl-2-butanone)
B: Benzylideneacetone
C: primary nitroaldol product (nitroalcohol)
D: Nitrostyrene

Scheme 2. Aldol and nitroaldol condensation of acetone and nitromethane with para-substituted benzaldehyde.

Table 3. Effect of heteroatom content in bare and APS-grafted hollow fiber catalysts on aldol condensation (batch reaction at 50 °C).

Entry	Hollow fiber catalyst	TOF (h^{-1})	Conversion (%)	Selectivity (%)	
				A	B
1	Bare Si/PAI-HFs	1	0	-	-
2	APS-grafted Si/PAI-HFs	1.8	75	68	32
3	Bare Si-Zr/PAI-HFs	-	0	-	-
4	APS-grated Si-Zr/PAI-HFs	1.4	69	26	74
5	Bare Si-Ti/PAI-HFs	-	0	-	-
6	APS-grafted Si-Ti/PAI-HFs	1.5	72	13	87
7	Bare Si-Zr-Ti/PAI-HFs	-	0	-	-
8	APS-grafted Si-Zr-Ti/PAI-HFs	2.0	82	17	83

Notes: A: 4-hydroxy-4-phenyl-2-butanone; B: benzylideneacetone. Reaction conditions: 0.1 M benzaldehyde in acetone; reaction time 4 h. Conversion and selectivity are calculated by GC-FID. Entries 1, 3, 5, 7: 2 g bare SiO_2, SiO_2-ZrO_2, SiO_2-TiO_2, SiO_2-TiO_2-ZrO_2 mixed oxide PAI-HF catalyst. Entries 2, 4, 6, 8: 2 g APS-grafted SiO_2, SiO_2-ZrO_2, SiO_2-TiO_2, SiO_2-TiO_2-ZrO_2 mixed oxide PAI-HF catalyst (~20 mol.% of the catalyst by amine loading).

Both bare and APS-grafted Si-, Si-Zr-, Si-Ti-, and Si-Zr-Ti/PAI-HF materials were evaluated as catalysts in aldol reactions. The conversion and selectivity results which were calculated from the GC-FID analysis are shown in Table 3. The initial turnover frequencies (TOFs) are reported for all materials as well. The pyridine IR results for APS-grafted Si-Zr/PAI-HF indicate that this catalyst has the largest number of Lewis acid sites and the largest number of strong acid sites of all the APS-grafted hollow fiber catalysts, which explains why the other Lewis-acidic catalysts such as APS-grafted Si-Ti/PAI-HF and APS-grafted Si-Zr-Ti/PAI-HF are more active than APS-grafted Si-Zr/PAI-HF in the aldol condensation. Titanols in Si-Ti/PAI-HFs provides stronger Brønsted acidity than silanols, which explains the decreased activity of APS-grafted Si-Ti/PAI-HF compared to the

Si/PAI-HF for the aldol condensation, though the pyridine IR results for both of these materials indicated very weak Brønsted acidity.

Trukhan et al.[21] prepared a series of Ti-substituted silicates and reported differences in acid strength for the materials depending on the nature of the synthetic conditions and Ti dispersion in the silica framework. In addition, they concluded via FTIR spectra of adsorbed CD_3CN that the addition of Ti to the silica materials increased the strength of the surface Brønsted acid sites (titanols) [21]. In this study, the APS-grafted Si-Zr-Ti/PAI-HF materials had weaker Brønsted and Lewis acidities compared to APS-grafted Si-Zr/PAI-HF and APS-grafted Si-Ti/PAI-HF materials, respectively. This observation is consistent with published reports using heteroatom-substituted aminosilane materials [11,24].

Furthermore, Table 3 shows the product selectivity after 4 h for all hollow fiber catalysts in the aldol condensation reaction. The APS-grafted Si/PAI-HF materials with fewer total acid sites were selective toward the 4-hydroxy-4-phenyl-2-butanone (A) while the other mixed metal oxides materials with more total acid sites (e.g. Si-Zr, Si- Ti and Si-Zr-Ti) were selective toward the unsaturated dehydration (B, benzylideneacetone) product. These results suggest that APS could be used with Zr-, Ti- and silica to create catalysts that favor the formation of benzylideneacetone at higher conversion. The enhancing the amount of Lewis acid sites did appear to affect slightly on the selectivity of the 4-hydroxy-4-phenyl-2-butanone, given that APS-grafted Si-Zr/PAI-HF had the higher selectivity than APS-grafted Si-Ti/PAI-HF and APS-grafted Si-Zr-Ti/PAI-HF, which does have a higher amount of Lewis acid sites. Additionally, the large difference in total acid sites between APS-grafted Si-Zr/PAI-HF and APS-grafted Si-Zr-Ti/PAI-HF further supports the notion

that the number of acid sites did affect the selectivity. The reaction data shown here for the aldol condensation is consistent with the previous studies that multiple Lewis acid sites are involved in the reaction [11,24]. The APS-grafted Si/PAI-HF catalysts favored formation of the aldol product (A, 68% selectivity) compared to the unsaturated dehydration product (B, 32% selectivity). This finding is in agreement with previous reports for an aminosilica catalyst with no heteroatom content [11,24,61,62].

Table 4. Effect of para-substituted benzaldehyde on aldol condensation in bare and APS-functionalized Si-Zr-Ti/PAI-HF catalyst (batch reaction at 50 °C).

Entry	Para-substituted	Conversion (%)	Selectivity (%)	
			A	B
1	H	0	-	-
2	H	75	68	32
3	H	0	-	-
4	OH	69	26	74
5	CH_3	0	-	-
6	Br	72	13	87
7	NO_2	0	-	-

Entries 3–7: 2 g APS-grafted Si-Zr-Ti/PAI-HFs (20 mol.% of the catalyst by amine loading).

Compared with the binary hollow fiber catalysts, the APS-grafted Si-Zr-Ti/PAI-HF catalysts exhibit the highest surface area, permeation, and activity in aldol condensation. Thus, in this work, we have decided to continue further catalytic evaluation of APS-grafted Si-Zr-Ti/PAI-HF materials for aldol and nitroaldol reactions. Both bare and APS-grafted Zr-Ti-Si-/PAI-HF materials were evaluated as catalysts in these reactions and the corresponding conversion and selectivity results obtained by GC-FID are shown in Tables

4 and 5, respectively. The bifunctional acid-base cooperativity in heterogeneous catalytic aldol and nitroaldol condensation reactions is well-documented in the literature [2,31,42,63]. Prior to reaction, the fibers used were heated for 1 h at 100 °C under vacuum to remove adsorbed moisture. This step is particularly important as the activity strongly depends on the catalyst pretreatment. Entry 1 with only weakly acidic silanol groups on the surface of zirconia, titania and silica and entry 2 with only weakly basic functional groups (i.e., $-NH_2$) serve as control experiments to exemplify the improvement in catalyst activity by immobilizing aminosilanes that have the ability to behave in a cooperative manner.

As can be seen from Table 4, the bare Si-Zr-Ti/PAI-HF gave rise to no conversion compared to the same material grafted with aminosilane (entries 1 vs. 3). The combination of silanol with amines (entries 3-7, Table 1) gives rise to ~93% conversion to aldol products (A and B), clearly illustrating the cooperative catalysis between these functional groups. These results further confirm that multifunctional groups can act together to undergo cooperative catalysis, which is not possible with only one monofunctional catalyst.

Table 5 shows the nitroaldol condensation results at 4 h for the same para-substituted benzaldehyde described for aldol condensation. As can be observed from these data, all experiments show remarkable catalytic activity, with the conversion significantly increased upon amine grafting. The control reaction performed with the bare Si-Zr-Ti/PAI-HF (i.e., no amines grafted) and amine grafted pure Torlon hollow fibers led to no observable nitroaldol products. Interestingly, in the absence of substituents at the para position, the reaction gave a mixture with a 1:6 molar ratio of nitroaldol to nitrostyrene products, with significant selectivity toward nitrostyrene product.

Table 5. Effect of para-substituted benzaldehyde on nitroaldol condensation in bare and APS- functionalized Si-Zr-Ti/PAI-HF catalysts (batch reaction at 50 °C).

Entry	Para-substituted	Conversion (%)	Selectivity (%)	
			A	B
1	H	0	-	-
2	H	0	-	-
3	H	80	13	87
4	OH	96	7	93
5	CH_3	88	2	98
6	Br	92	31	69
7	NO_2	97	23	77

Notes: C: nitroalcohol; D: nitrostyrene. Reaction conditions: 0.1 M benzaldehyde in acetone; reaction time 4 h. Conversion and selectivity are calculated by GC-FID. Entry 1: 2 g bare Si-Zr-Ti/PAI-HFs. Entry 2: 2 g amine-grafted pure PAI-HFs. Entries 3–7: 2 g APS-grafted Si-Zr-Ti/PAI-HFs (20 mol.% of the catalyst by amine loading).

Previous studies by Asefa [4,31,49] and Jones [2,11] research groups showed that electron-withdrawing groups (EWGs) at para-substituted sites facilitate the ion-pair mechanism, favoring the 4-hydroxy-4-phenyl-2-butanone product, while electron-donating groups (EDGs) at the para-substituted benzaldehyde stabilize the imine intermediate and favor the formation of the benzylideneacetone product [49]. Although aldol condensation reaction over both EDGs and EWGs of para-substituted benzaldehyde has been extensively studied before [2,49], however, such investigations in the context of APS-grafted Si-Zr-Ti/PAI-HFs, as a selective catalyst toward para-substituted benzaldehyde reactants and as a continuous flow reactor, are reported herein for the first time. The electron-withdrawing strength of the substituents slightly affected the catalyst's selectivity towards the primary product. However, for both condensations, EDG substituents did not affect the reaction's selectivity towards the product. Having the cooperative interaction between acid and base sites on the surface not only produces more

effective acidic sites for the aldol reaction but also makes the synthesis less costly and safer. It has been well documented that weak acidity of the silanol groups together with amine cooperative interactions (acid-base catalysis) give higher catalytic activity and favor less dehydration of the alcohol products into benzylideneacetone during aldol condensation reaction [1,2,4,64].

The productive synergistic effect between SiO_2 and ZrO_2/TiO_2 and grafted amines for CO_2 capture demonstrated previously by our research group [43] may also open new opportunities for developing high-performance heterogeneous catalysts in continuous flow process for carbene insertion. We investigated the effect of para-substituted benzaldehyde on the activity and selectivity of the aldol and nitroaldol reactions toward specific products. Table 4 and 5 display the percent conversion and selectivity toward primary and secondary condensations of acetone and nitromethane with various para-substituted benzaldehyde. A significant difference in the reaction conversion was observed over various para-substituted benzaldehydes. Regardless of the electron-donating and electron-withdrawing groups of para-substituted benzaldehyde, the APS-grafted Si-Zr-Ti/PAI-HFs catalyst yielded exclusively the benzylideneacetone (B) and nitrostyrene (D) derivatives. By using the aforementioned primary APS-grafted PAI-HFs, we show that the selectivity toward benzylideneacetone and nitrostyrene products depends exclusively on the type of substituents on the para-substituted benzaldehyde. On the basis of our findings, we can conclude that EDGs such as -OH and $-CH_3$ selectively give rise to benzylideneacetone (B) during aldol condensation and nitrostyrene (D) during nitroaldol condensation as the major products, whereas EWGs such as $-NO_2$ and -Br produce 4-hydroxy-4-phenyl-2-butanone (A) and nitroalcohol (C) exclusively (Table 4 and 5). In other words, the electron-donating

or -withdrawing nature of the substituent at the para-substituted benzaldehyde controls the outcome of the aldol and nitroaldol reactions when it is catalyzed by APS-grafted PAI-HF catalysts.

4.2.2. Catalytic Activity in Continuous Flow Aminosilane-Grafted Si-Zr-Ti/PAI-HF Reactor. During aldol and nitroaldol homogeneous reactions, catalyst deactivation occurs which necessitates frequent catalyst regeneration. Another shortcoming is that in conventional flow systems, the reagents and homogeneous catalyst flow through the reactor together. Thus, separation of the product from the catalyst and possible byproducts is required at the end. The improvement of catalyst lifetime is one of the key challenges in homogeneous catalyst development. The new catalytic methodologies that offer simpler and more cost-effective approaches are essential for the development of sustainable and efficient chemicals and pharmaceutical processes. Heterogeneous catalytic aldol and nitroaldol condensations under continuous flow conditions in hollow fibers offer the opportunity to eliminate the tedious and costly separation and recycling step [27,40,41].

Here we report the first example of bifunctional heterogeneous catalysts for aldol and nitroaldol reactions conducted in a new type of continuous-flow reactor for comparison to the above data example. The aldol condensation reaction was carried out over both bare and aminosilane-grafted Si-Zr-Ti/PAI-HF catalysts in the module as a continuous-flow reactor system. As stated earlier, fiber catalyst morphology and structure offer advantages over fixed-bed [31], plug-flow [28], and multistep continuous flow reactors [30] by providing a high surface area to volume ratio, avoidance of particle attrition and quenching operation, and the ability to minimize mass transfer resistances. In particular, as a result of

tunable oxide particle size and porosity in hollow fiber structures and amine loading, the reaction capabilities of certain composite hollow fiber catalysts are shown in this section to meet or exceed those achievable by amine-grafted silica reported previously [2,11]. In our experiments, we used a hollow fiber reactor with a total volume of 10 mL to demonstrate the compatibility of the bifunctional catalyst in a continuous flow system.

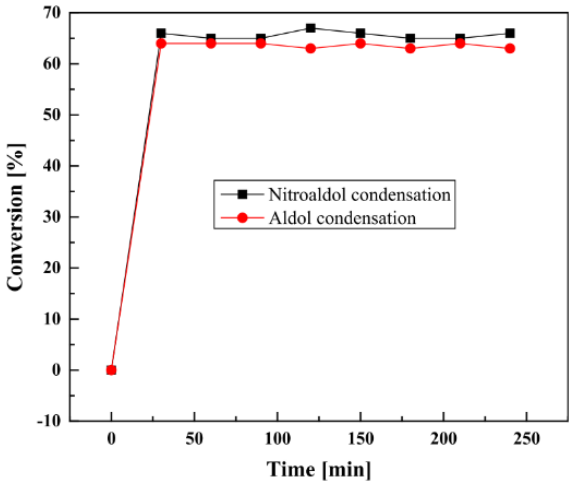

Figure 5. Continuous aldol and nitroaldol reactions over APS-grafted Si-Zr-Ti/PAI-HFs in a hollow fiber module (flow rate 0.02 cm3/min; reaction temperature 50 °C).

After demonstrating the efficiency of APS-grafted Si-Zr-Ti/PAI-HFs in aldol and nitroaldol condensation reaction in the batch reactor, the performance of the bifunctional hollow fiber catalysts was further evaluated in a continuous-flow platform. The hollow fiber module was formed using five APS-grafted Si-Zr-Ti/PAI fibers. The performance of the hollow fiber module for the continuous reaction was investigated under the same conditions as the batch reactor (i.e., catalyst loading, reaction time, and temperature). The

experiments were carried out by feeding the reactants into the reactor for 4 h and then analyzing the products every 30 min. As shown in Figure 1, a syringe pump was used to continuously introduce reactants at different flow rates onto the shell side of hollow fiber reactor at 50 °C. The benzaldehyde with acetone (aldol condensation) or nitromethane (nitroaldol condensation) along with an internal standard (see section 5.4) was used for each reaction. As shown in Figure 5, after 30 min reaction, the conversion of benzaldehyde reached 64 and 66% for aldol and nitroaldol condensations, respectively. Asefa et al.[31] reported that shorter contact times results in lower aldehyde conversion and high selectivity to the nitrostyrene (D) while higher conversion and dinitroalkane (side product) were obtained at higher reaction temperatures. Also as evident from this figure, the catalyst retained its activity after 240 min. These findings demonstrate that bifunctional catalysts developed here give almost the same conversion and selectivity while being resistant to deactivation.

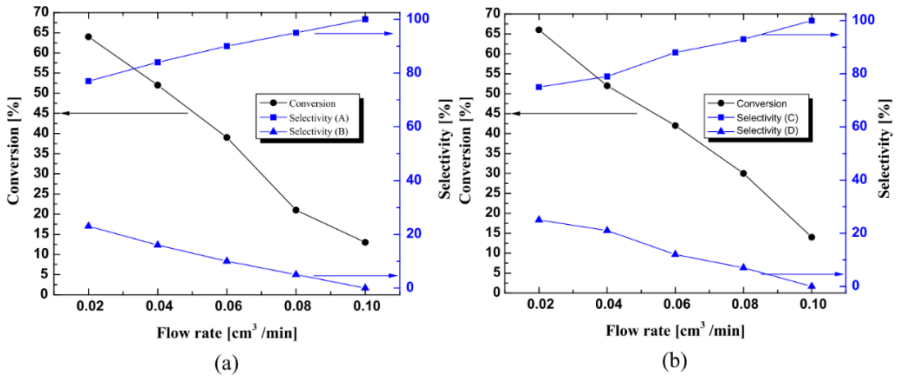

Figure 6. Effect of flow rate on the catalyst conversion and selectivity in aldol (a) and nitroaldol (b) condensation reactions in an APS-grafted Si-Zr-Ti/PAI-HFs continuous-flow reactor (15 cm hollow fiber module, five fibers; 0.05 M benzaldehyde in acetone; reaction temperature 50 °C). A: 4-hydroxy-4-phenyl-2-butanone; B: benzylideneacetone; C: nitroalcohol; D: nitrostyreneß.

Figure 6 shows the relationship between catalyst performance (product selectivity and conversion of benzaldehyde) and flowrate in a continuous hollow fiber module for aldol (a) and nitroaldol (b) reactions. As shown in Figure 6, depending on the flow rate, the reaction yields the primary condensation products, (A and C) or the secondary ketone products (B and D), or a mixture of the two products with different ratios in a continuous flow system. As can be seen from Figure 6a, the highest conversion value of 65% and lowest selectivity value of 52% toward the primary product (A) were achieved at the lowest flow rate (0.02 cm^3/min) whereas, by increasing the flow rate to 0.1 cm^3/min, conversion dropped drastically to 13% while selectivity toward A reached 100% for aldol condensation. Although by increasing reactants flowrate, the reaction conversion decreased the 4-hydroxy-4-phenyl-2-butanone was still the primary aldol product. When the contact time was increased (lower flow rate), the primary product (4-hydroxy-4-phenyl-2-butanone) underwent the dehydration reaction resulting in the formation of benzylideneacetone (B) product. The same trends were observed for the nitroaldol condensation as evident from Figure 6b. A significant amount of nitrostyrene (D) and nitroalcohol (C) mixture with ratios of nitroalcohol to nitrostyrene (75:25) was produced at lower flow rates. By raising the reactant flowrate up to 0.1 cm^3/min, 100% selectivity toward nitroalcohol was obtained at 14% conversion. On the basis of these catalytic results, it can be inferred that the APS-grafted Si-Zr-Ti/PAI-HF catalysts are excellent candidates for continuous reactions without losing their catalytic activity (high stability), as far as flow rate and temperature in the hollow fiber module are maintained.

It is also worth noting that APS-grafted Si-Zr-Ti/PAI-HFs catalysts were more selective toward alcohol products (A and C) than the dehydrated products (B and D)

compared to those reported for batch reaction (Table 4 and 5). This finding further confirms that our APS-grafted Si-Ti-Zr/PAI-HFs continuous flow reactor is not only an efficient reactor for continuous aldol condensation but also is more selective for producing a higher primary alcohol/secondary ketone ratio. This may be due to the fact that both condensations go to almost complete within 30 min in a continuous system (see Figure 5). Also, the tendency of alcohol products to undergo dehydration over this relatively shorter time period is less than that over 4 h reaction time employed in the batch reaction. Contrary to the batch reaction in which the majority of products were dehydrated (B and D), continuous flow reactor gave exclusively (or in a major proportion) the alcohol (A and C) products, regardless of the identity of the substituents on the benzaldehyde. The implications of this work include the possible synthesis of these two important chemical precursors (the 4-hydroxy-4-phenyl-2-butanone and the benzylideneacetone) in pure form and in high yield. The crude reaction mixtures of the aldol and nitroaldol condensations were examined by ^{1}H NMR spectroscopy to determine the selectivity. No dinitroalkane products were observed in the crude nitroaldol condensation mixtures with is in agreement with a previous report [2,29] (see Figure S5, Supporting Information).

According to Arrhenius theory, the internal energy and reaction rate of the reactant molecules can be enhanced by increasing the reaction temperature. Therefore, the effect of reaction temperature on catalyst activity of nitroaldol condensation reaction was evaluated at different temperatures from 50 to 90 °C. Upon raising reaction temperature, the benzaldehyde conversion and dehydration products formation were found to increase for benzaldehyde and nitromethane condensations in APS-grafted Si-Zr-Ti/PAI-HF reactor (Figure 7). For instance, at 50 °C and 0.02 cm^3/min, the reaction gave only 66% reactant

conversion but exclusively (~25%) nitrostyrene product. However, increasing the temperature to 50 °C at the same flow rate of 0.02 cm^3/min benzaldehyde led to significantly higher (~100%) reactant conversion with 55% nitrostyrene product yield which is in good agreement with those in the literature [31,65,66]. Interestingly, both the nitroalcohol and nitrostyrene were formed upon using unsubstituted benzaldehyde, indicating that the origin of the reaction conversion and selectivity are strongly dictated by the reaction temperature, reaction contact time and the nature of the substituent at the para position. The hollow fiber catalyst reactor system is especially promising because it works under conditions in which many aldol and nitroaldol condensation catalysts are widely used in the batch process and lose their activity for reuse. Future study needs to focus on other condensation reactions and a systematic comparison of the catalytic activity of cooperative acid-base catalysts with various polymeric hollow fibers that contain metal oxides should be performed.

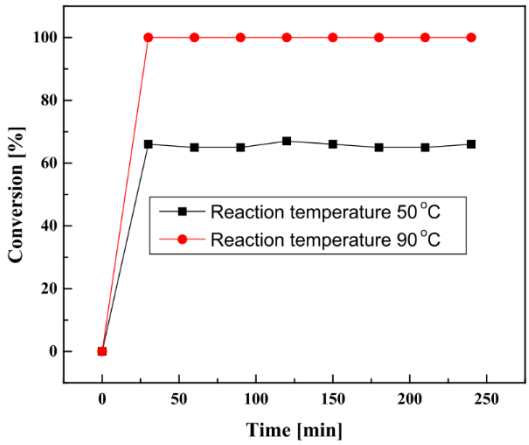

Figure 7. Effect of the reaction temperature on nitroaldol condensation in an APS- grafted Si-Zr-Ti/PAI-HFs continuous-flow reactor (15 cm hollow fiber module, five fibers; 0.05 M benzaldehyde in acetone; reaction temperatures 50 and 90 °C).

As a sustainable alternative for conventional batch-based synthetic techniques, the concept of hollow fiber catalysts for continuous-flow processing has emerged in the synthesis of fine chemicals. In particular, as a result of tunable metal oxide particle size and porosity in hollow fiber structures and amine loading, the reaction capabilities of hollow fiber-based bifunctional catalysts were shown to meet or exceed those achievable by homogeneous catalysts. The aldol and nitromethane condensation of aromatic aldehydes with acetone and nitromethane were carried out in continuous flow hollow fiber-based bifunctional catalysts resulted in shorter reaction times compared to batch process. In addition, slightly higher yields and selectivities toward alcohol were obtained in the continuous process compared to reactions in a batch reactor.

The fiber synthesis allows for a variety of supported catalysts to be embedded in the walls of the fibers, thus leading to a diverse set of reactions that can be catalyzed inflow. Additionally, the fiber synthesis is scalable (e.g. several reactor beds containing many fibers in a module may be used) and thus could potentially be used for the large-scale production of organic compounds. The resulting self-supported catalysts are stable and well-behaved under catalytic conditions, demonstrating outstanding reactivity and selectivity, comparable to or even better than their analogous homogeneous counterparts. Incorporating acid-base bifunctional heterogeneous catalysts in the walls of the fibers presents an alternative to a traditional packed-bed reactor. A continuous flow reaction system is an ideal platform for the aldol and nitroaldol reaction because the reaction proceeds through proton transfer between reactants, thereby affording the desired products by simply controlling contact time and reaction temperature.

5. CONCLUSION

This article describes experimental studies focusing on the assessment of aminosilane-grafted ternary oxide zirconia, titania and silica/Torlon hollow fiber composites as a bifunctional heterogeneous catalyst and a continues-flow reactor for aldol and nitroaldol condensation reactions. The benefits of the Si-Zr-Ti/PAI-HF grafted with aminosilanes are (i) providing bifunctional acid-base character and catalyst activity, and (ii) good distribution and accessibility of both amine and weakly acidic silanols sites, and (iii) adequate porosity retained within the fibers to facilitate the rapid mass transfer and reaction kinetics. In summary, we have prepared a catalytic system capable of providing excellent conversion in the aldol reaction that is rationalized by the proper pairing of weaker acid groups with amine moieties. Amine-grafted Si-Zr-Ti/PAI-HF (cooperative acid-base catalyst) serves as an efficient catalyst in a continuous flow-reactor system and is capable of near-quantitative conversion in the aldol and nitroaldol condensations with long-term stability. The good catalytic potency and excellent stability at different reaction temperatures of amine-grafted Si-Zr-Ti/PAI-HF render this new continuous reaction system more suitable for preparation of either primary (alcohol) or secondary dehydrated products at large scale than reported methodologies.

ACKNOWLEDGMENT

The authors would like to acknowledge Prof. William J. Koros from School of Chemical & Biomolecular Engineering at Georgia Institute of Technology for giving access to his fiber spinning facilities.

REFERENCE

1. J.D. Lewis, S. Van De Vyver, Y. Román-Leshkov, Angew. Chemie - Int. Ed. 54 (2015) 9835–9838.

2. V.E. Collier, N.C. Ellebracht, G.I. Lindy, E.G. Moschetta, C.W. Jones, ACS Catal. 6 (2016) 460–468.

3. R. Tan, C. Li, J. Luo, Y. Kong, W. Zheng, D. Yin, J. Catal. 298 (2013) 138–147.

4. Y. Xie, K.K. Sharma, A. Anan, G. Wang, A. V. Biradar, T. Asefa, J. Catal. 265 (2009) 131–140.

5. J. Lauwaert, E. De Canck, D. Esquivel, P. Van Der Voort, J.W. Thybaut, G.B. Marin, Catal. Today 246 (2015) 35–45.

6. J. Lauwaert, E.G. Moschetta, P. Van Der Voort, J.W. Thybaut, C.W. Jones, G.B. Marin, J. Catal. 325 (2015) 19–25.

7. C. Lucarelli, A. Vaccari, Green Chem. 13 (2011) 1941.

8. K. Tanabe, W.F. Hölderich, Appl. Catal. A Gen. 181 (1999) 399–434.

9. L. Marcoux, J. Florek, F. Kleitz, Appl. Catal. A Gen. 504 (2014) 493–503.

10. E.L. Margelefsky, R.K. Zeidan, M.E. Davis, Chem. Soc. Rev. 37 (2008) 1118–1126.

11. E.G. Moschetta, N. a. Brunelli, C.W. Jones, Appl. Catal. A Gen. 504 (2015) 429–439.

12. T. Yokoi, H. Yoshitake, T. Yamada, Y. Kubota, T. Tatsumi, J. Mater. Chem. 16 (2006) 1125.

13. Y. Xia, R. Mokaya, Angew. Chemie - Int. Ed. 42 (2003) 2639–2644.

14. X. Wang, K.S.K. Lin, J.C.C. Chan, S. Cheng, J. Phys. Chem. B 109 (2005) 1763–1769.

15. X. Wang, Y.H. Tseng, J.C.C. Chan, S. Cheng, J. Catal. 233 (2005) 266–275.

16. J.E. Rekoske, M.A. Barteau, Ind. Eng. Chem. Res. 50 (2011) 41–51.

17. M. Zamora, T. López, M. Asomoza, R. Meléndrez, R. Gómez, Catal. Today 116 (2006) 234–238.

18. C. Petrucci, M. Cappelletti, O. Piermatti, M. Nocchetti, M. Pica, F. Pizzo, L. Vaccaro, J. Mol. Catal. A Chem. 401 (2015) 27–34.

19. S. Calogero, D. Lanari, M. Orr??, O. Piermatti, F. Pizzo, L. Vaccaro, J. Catal. 282 (2011) 112–119.

20. D. Lanari, F. Montanari, F. Marmottini, O. Piermatti, M. Orr, L. Vaccaro, J. Catal. 277 (2011) 80–87.

21. N.N. Trukhan, A.A. Panchenko, E. Roduner, M.S. Mel'gunov, O.A. Kholdeeva, J. Mrowiec-Białoń, A.B. Jarzębski, Langmuir 21 (2005) 10545–10554.

22. D.J. Jones, J. Jiménez-Jiménez, a. Jiménez-López, P. Maireles-Torres, P. Olivera-Pastor, E. Rodriguez-Castellón, J. Rozière, Chem. Commun. 2 (1997) 431–432.

23. F. Vermoortele, R. Ameloot, A. Vimont, C. Serre, D. De Vos, Chem. Commun. (Camb). 47 (2011) 1521–3.

24. N. a. Brunelli, C.W. Jones, J. Catal. 308 (2013) 60–72.

25. K. Kandel, S.M. Althaus, C. Peeraphatdit, T. Kobayashi, B.G. Trewyn, M. Pruski, I.I. Slowing, J. Catal. 291 (2012) 63–68.

26. J. Izquierdo, C. Ayats, A.H. Henseler, M.A. Pericàs, Org. Biomol. Chem. 13 (2015) 4204–4209.

27. D. Zhao, K. Ding, ACS Catal. 3 (2013) 928–944.

28. K. Hashimoto, N. Kumagai, M. Shibasaki, Org. Lett. 16 (2014) 3496–3499.

29. T. Tsubogo, T. Ishiwata, S. Kobayashi, Angew. Chemie - Int. Ed. 52 (2013) 6590–6604.

30. H. Ishitani, Y. Saito, T. Tsubogo, S. Kobayashi, Org. Lett. (2016) acs.orglett.6b00282.

31. A. V. Biradar, K.K. Sharma, T. Asefa, Appl. Catal. A Gen. 389 (2010) 19–26.

32. A.A. Rownaghi, F. Rezaei, Y. Labreche, P.J. Brennan, J.R. Johnson, S. Li, W.J. Koros, ChemSusChem 8 (2015) 3439–3450.

33. F. Rezaei, R. Lively, Y. Labreche, G. Chen, Y. Fan, W.J. Koros, C.W. Jones, ACS Appl. Mater. Interfaces 5 (2013) 3921–3931.

34. F.S. Li, W. Qiu, R.P. Lively, J.S. Lee, A.A. Rownaghi, W.J. Koros, ChemSusChem 6 (2013) 1216–1223.

35. S.B. Ötvös, I.M. Mándity, F. Fülöp, J. Catal. 295 (2012) 179–185.

36. A. Odedra, P.H. Seeberger, Angew. Chemie - Int. Ed. 48 (2009) 2699–2702.

37. C. Ayats, A.H. Henseler, E. Dibello, M.A. Peric??s, ACS Catal. 4 (2014) 3027–3033.

38. M. Viviano, T.N. Glasnov, B. Reichart, G. Tekautz, C.O. Kappe, Org. Process Res. Dev. 15 (2011) 858–870.

39. F.G. Finelli, L.S.M. Miranda, R.O.M. a. de Souza, Chem. Commun. 51 (2015) 3708–3722.

40. I. Atodiresei, C. Vila, M. Rueping, ACS Catal. 5 (2015) 1972–1985.

41. R. Porta, M. Benaglia, A. Puglisi, Org. Process Res. Dev. 20 (2016) 2–25.

42. S. Shylesh, W.R. Thiel, ChemCatChem 3 (2011) 278–287.

43. A.A. Rownaghi, A. Kant, X. Li, H. Thakkar, A. Hajari, Y. He, P.J. Brennan, H. Hosseini, W.J. Koros, F. Rezaei, ChemSusChem 9 (2016) 1166–1177.

44. B.M. Choudary, M.L. Kantam, C. V Reddy, K.K. Rao, F. Figueras, Green Chem. 1 (1999) 187–189.

45. P. Borah, J. Mondal, Y. Zhao, J. Catal. 330 (2015) 129–134.

46. I. Union, O.F. Pure, A. Chemistry, Pure Appl.Chem. 57 (1985) 603–619.

47. E. Mäkilä, L.M. Bimbo, M. Kaasalainen, B. Herranz, A.J. Airaksinen, M. Heinonen, E. Kukk, J. Hirvonen, H. a. Santos, J. Salonen, Langmuir 28 (2012) 14045–14054.

48. C.J. Brinker, J. Non. Cryst. Solids 100 (1988) 31–50.

49. K.K. Sharma, A. V. Biradar, T. Asefa, ChemCatChem 2 (2010) 61–66.

50. C.C. Aquino, G. Richner, M. Chee Kimling, D. Chen, G. Puxty, P.H.M. Feron, R.A. Caruso, J. Phys. Chem. C 117 (2013) 9747–9757.

51. K.M. Parida, S. Mallick, P.C. Sahoo, S.K. Rana, Appl. Catal. A Gen. 381 (2010) 226–232.

52. W. Aperador, A. Delgado, M.D. Lagos, Int. J. Electrochem. Sci. 9 (2014) 4144–4157.

53. M.I. Zaki, M. a. Hasan, F. a. Al-Sagheer, L. Pasupulety, Colloids Surfaces A Physicochem. Eng. Asp. 190 (2001) 261–274.

54. M. Daturi, C. Binet, S. Bernal, J. a. Pe´rez Omil, J. Claude Lavalley, J. Chem. Soc. Faraday Trans. 94 (1998) 1143–1147.

55. G.J. a a Soler-illia, E.L. Crepaldi, M. Curie, P. Jussieu, P. Cedex, J. Mater. Chem. 14 (2004) 1879–1886.

56. V. a. Zeitler, C. a. Brown, a Brown, J. Phys. Chem. 61 (1957) 1174–1177.

57. M. Zhang, Y. Wu, X. Feng, X. He, L. Chen, Y. Zhang, J. Mater. Chem. 20 (2010) 5835–5842.

58. C. Xu, Z. Bacsik, N. Hedin, J. Mater. Chem. A 3 (2015) 16229–16234.

59. S. Mallick, S. Rana, K. Parida, Dalton Trans. 40 (2011) 9169–9175.

60. E. Parry, J. Catal. 2 (1963) 371–379.

61. R.K. Zeidan, S.J. Hwang, M.E. Davis, Angew. Chemie - Int. Ed. 45 (2006) 6332–6335.

62. R.K. Zeidan, M.E. Davis, J. Catal. 247 (2007) 379–382.

63. E.G. Moschetta, S. Negretti, K.M. Chepiga, N. a. Brunelli, Y. Labreche, Y. Feng, F. Rezaei, R.P. Lively, W.J. Koros, H.M.L. Davies, C.W. Jones, Angew. Chemie Int. Ed. 54 (2015) 6470–6474.

64. N. Kumagai, M. Shibasaki, Angew. Chemie - Int. Ed. 50 (2011) 4760–4772.

65. K.K. Sharma, T. Asefa, Angew. Chemie - Int. Ed. 46 (2007) 2879–2882.

66. A. Anan, K.K. Sharma, T. Asefa, J. Mol. Catal. A Chem. 288 (2008) 1–13.

67. M.R. Kosuri, W.J. Koros, J. Memb. Sci. 320 (2008) 65–72.

68. S. Luo, J. Falconer, Catal. Letters 57 (1999) 89–93.

69. Q. Wang, D.F. Shantz, J. Catal. 271 (2010) 170–177.

70. S. Rana, S. Mallick, K.M. Parida, Ind. Eng. Chem. Res. 50 (2011) 2055–2064.

SUPPORTING INFORMATION

Section S1:

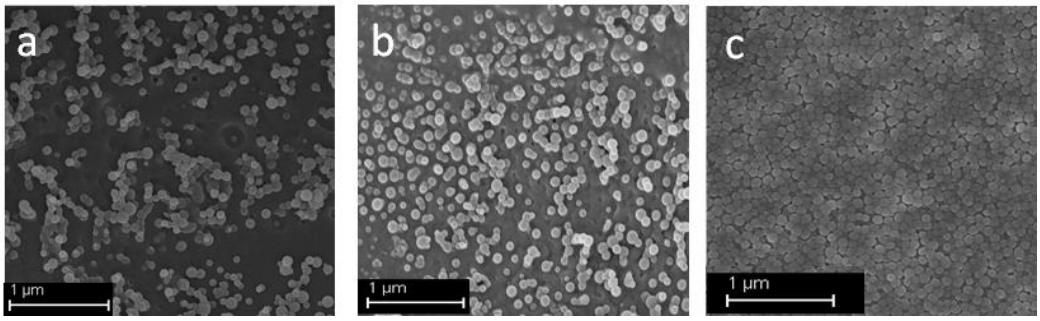

Figure S1: SEM image of bare zirconia (a) titinia (b) and silica (c).

Section S2:

This study focused on porous hollow fiber composites comprising catalyst nanoparticles (*i.e.*, zirconia, titania, and silica) embedded into a porous polymer matrix (*i.e.*, PAI). Creation of Zirconia, Titania and Silica Nanoparticle-Torlon Hollow Fibers. Commercial metal oxides including zirconia, titania, and silica (average particle size 100 nm, Sigma Aldrich) were used as the amine supports. The 3-Aminopropyltriethoxysilane (APS) (diaminosilane, Gelest, Inc.) was used as the grafting agents for functionalizing zirconia, titania, and silica-Torlon fiber sorbents. Torlon 4000T-HV, a commercially available polyamide-imide (PAI) (Solvay Advanced Polymers, Alpharetta, GA) and poly(vinylpyrrolidone) (PVP) (average Mw≈ 1300 K, Sigma Aldrich) were used for formation of the composite hollow fiber sorbents. Prior to use, PVP was dried at 80 °C for

24 h under vacuum to remove pre-sorbed water vapor, while Torlon was dried at 110 °C for 24 h. De-ionized (DI) water (18MU, Model: D4521, Barnstead International, Dubuque, IA) was added as a non-solvent into the fiber dope. N-Methyl-2-pyrrolidone (NMP) (Reagent Plus, 99%, Sigma-Aldrich, Milwaukee, WI) was used as the solvent to form the spinning dope due to its strong solvent power, low volatility, and good water miscibility. All solvents and nonsolvents were used as-received with no purification or modification. All liquid chemicals were reagent grade with 99% purity and purchased from Sigma Aldrich (Milwaukee, WI). Methanol (ACS grade, VWR) and hexane (ACS Reagent, >98.5%, VWR) was used for solvent exchange after fiber catalyst spinning. Moreover, methanol was used to remove excess water from the fibers.

A typical spinning dope to create a 20/80 (weight ratio) catalyst /Torlon sorbent contains the polymer PAI, sorbent particles, NMP (solvent), water (nonsolvent), and additives (PVP). The optimized polymer dope compositions and spinning conditions are presented in Table S1. The detail information of the hollow fiber sorbent formation setup along with the triple orifice spinneret and ternary phase diagram is discussed in detail in our previous work.[1] The water present in the fiber was then solvent exchanged with methanol (to remove excess water) followed by post-infusion functionalization by exposing fiber sorbents inappropriate aminosilane solutions (*i.e.,* APS,).

Figure S2 is a schematic representation of the hollow fiber creation process. A standard bore fluid used in this study comprise NMP and water with the weight ratio of 88:12. An appropriate Torlon core dope composition (determined by the cloud-point method and rheology measurements)] was fed to the middle spinneret compartment.

Table S1. Optimized spinning conditions for the formation of zirconia, titania and silica-PAI hollow fiber catalysts.

Dope composition (catalyst/PAI/PVP/NMP/H_2O) (wt %)	5/24/6/60.5/4.5
Dope flow rate	600 mL/hr
Bore fluid (NMP/H_2O)	88/12 wt %
Bore fluid flow rate	200 mL/hr
Sheath fluid (NMP/H_2O)	50/50 wt%
Sheath fluid flow rate	100 mL/hr
Sheath fluid (NMP/H_2O)	50/50 wt%
Sheath fluid flow rate	100 mL/hr
Air gap	0.15 m
Take up rate	8.5 m/min
Operating temperature	55 °C
Quench bath temperature	55 °C

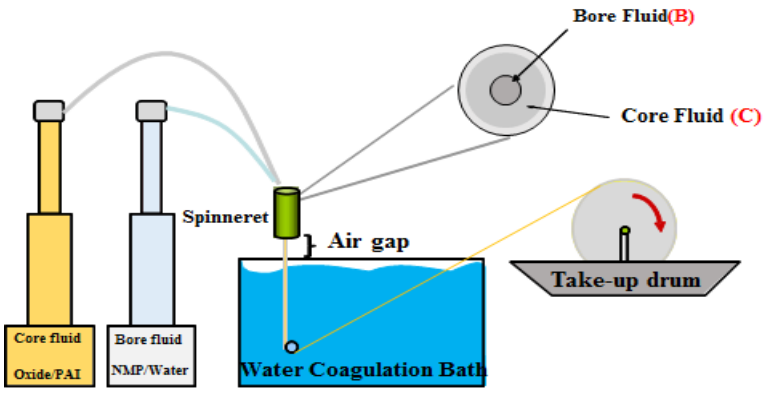

Figure 2S. Schematic diagram of fiber spinning apparatus

Section S3: Post spinning Infusion and Amine grafting of Zr/Ti/Si-Torlon Hollow Fiber Catalysts

The amine functionalization was performed in a mixture of a non-polar solvent (toluene) and a polar protic solvent (water). The water content of the mixture was kept within the range of 0.01- 2.00 wt%. Water is necessary for protonating APS and hydrolyzing

methoxy groups in dry liquid. As shown previously, exposure of APS to moisture disrupts strong hydrogen bonds and leads to the formation of polysiloxane.[1–3] It was found that a water content of 1.00 wt% gave rise to highest amine loading. As outlined above, after the Zr/Ti/Si-Torlon fiber composites were formed, they were subjected to a methanol solvent exchange process, followed by exposure to different APS/toluene/water (ratio 10:89:1 wt%) solution mixtures with varying immersion times, from 1 to 8 h. Subsequently, Zr/Ti/Si-Torlon fiber catalysts were removed from the amine solution, rinsed with hexane for 30 min at ambient temperature to wash away the ungrafted APS deposited on the fiber surface. Finally, APS/ Zr/Ti/Si-Torlon fiber catalysts were placed in a preheated vacuum oven and cured for 1 h at 60 °C. The APS aminosilane has the ability to form a durable bond with the zirconia, titania, and silica-Torlon hollow fibers in this post-spinning immersion step. The post-spinning infusion of aminosilane onto zirconia, titania, and silica nanoparticles-Torlon hollow fiber composites is schematically shown in Figure S3. The optimum infusion condition was determined by soaking 0.15 g of zirconia, titania, and silica -Torlon hollow fiber catalysts in a 100 g solution of different concentrations of APS in toluene/water mixture (*i.e.*, 5, 10, 15 and 20 wt.% APS) at room temperature for 1-8 h. APS concentration in toluene/water mixture was varied to determine the concentration that gives rise the highest equilibrium capacity. For 10 wt% APS/toluene/water solution and an infusion time of 2 h, the fibers exhibited an optimum amount of amine loading.

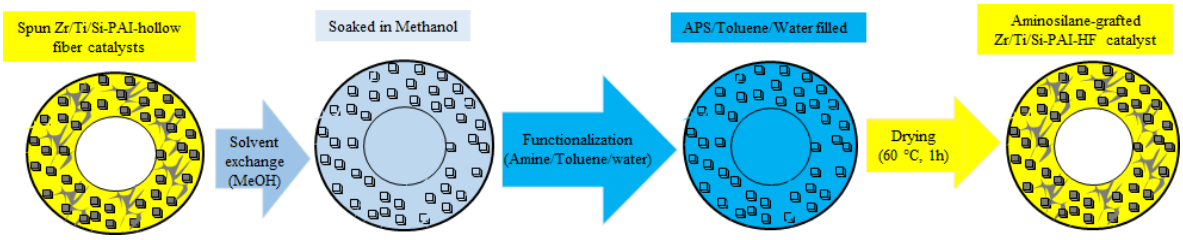

Figure S3. Amine grafting of Zr/Ti/Si-Torlon Hollow Fiber Catalysts Process.

REFERENCE

1. A. A. Rownaghi, F. Rezaei, Y. Labreche, P. J. Brennan, J. R. Johnson, S. Li, W. J. Koros, *ChemSusChem* **2015**, *8*, 3439–3450.

2. A. A. Rownaghi, A. Kant, X. Li, H. Thakkar, A. Hajari, Y. He, P. J. Brennan, H. Hosseini, W. J. Koros, F. Rezaei, *ChemSusChem* **2016**, 1–13.

3. F. S. Li, W. Qiu, R. P. Lively, J. S. Lee, A. A. Rownaghi, W. J. Koros, *ChemSusChem* **2013**, *6*, 1216–1223.

II. ENGINEERING POROUS POLYMER HOLLOW FIBER MICROFLUIDIC REACTORS FOR SUSTAINABLE C-H FUNCTIONALIZATION

Yingxin He,[‡] Fateme Rezaei,[‡] Shubhender Kapila,[†] Ali A. Rownaghi*[, ‡]

[‡] Department of Chemical & Biochemical Engineering, Missouri University of Science and Technology, 1101 N. State Street, Rolla, Missouri 65409, United States

[†]Department of Chemistry, Missouri University of Science and Technology, 400 W. 11th St., Rolla, MO, 65409, United States

* E-mail: rownaghia@mst.edu

ABSTRACT

The highly hydrophilic and solvent-stable porous polyamide-imide (PAI) hollow fibers were created by crosslinking of bare PAI hollow fibers with 3-aminopropyl trimethoxy silane (APS). The APS-grafted PAI hollow fibers were then functionalized with salicylic aldehyde for binding catalytically active Pd(II) ions through covalent post-modification method. The catalytic activity of the composite hollow fiber microfluidic reactors (Pd(II) immobilized APS-grafted PAI hollow fibers) was tested via heterogeneous Heck coupling reaction of aryl halides under both batch and continuous flow reaction in polar aprotic solvents at high temperature (120 °C) and low operating pressure. XPS and ICP analyses of the starting and recycled composite hollow fibers indicated that the fibers contain very similar loading of Pd(II), implying no degree of catalyst leaching from hollow fibers during the reaction. The composite hollow fiber microfluidic reactors showed long-term stability and strong control over the leaching of Pd species.

Keywords: polyamide-imide, immobilized Pd(II) ions, heterogeneous catalyst, hollow fiber microfluidic reactors, Heck coupling

1. INTRODUCTION

Over the past decade, laboratory-scale continuous-flow processes have witnessed explosive developments and have attracted a great deal of interest, in view of the significance of economic and environmentally-sustainable production of pharmaceuticals, fine chemicals, and agrochemicals, as well as upgrading of biomass feedstocks.[1–11] The immobilization of metal nanoparticles (MNPs) such as palladium, copper, ruthenium, and nickel on the surface of solid supports such as oxides and polymers offers a powerful catalytic system that exploits and enhances the advantages of both nanocatalysis and flow chemistry.[12–15]

In recent years, various approaches have been developed for stabilization and subsequent anchoring of the MNPs on solid surfaces and, in particular, within microstructured reactors.[5,6,16–19] Based on the methods used to incorporate and immobilize the MNPs in continuous-flow reactors, catalytic reactors may be divided into three main classes: (i) packed-bed; (ii) monolithic flow-through, and (iii) inner-wall catalysts embedded in nanotubes, nanowires, magnetic nanoparticles, and polymers.[8,9,20–24] In packed-bed reactors, the reaction mixture flows through the packed catalyst bed, leading to a very high ratio of the active catalyst and the substrates/reagents.[5,19] The high local concentration of the catalyst combined with an enhanced mass transfer in the reactor results in increased reaction rates and higher turnover numbers (TONs) as compared to a batch

reaction especially for the cases in which mass transfer is the limiting step.[6,18,21,25] However, packed-bed reactors typically result in uncontrolled fluid dynamics, hot-spot formation, broad residence time distribution, low selectivity, and overall low process efficiency.[6,18,25,26] Among possible alternatives, the use of macroporous monoliths comprised of polymer[5,19,27], silica[28], alumina[29], foam[30], and titania[31] in flow-through processes is a convenient approach to overcome the packed-bed drawbacks. The monoliths consist of well-defined hierarchical porous materials into which the MNPs can be supported. However, there are concerns associated with the use of monolithic reactors for chemical transformations including polymer swelling (in the case of organic monoliths) and clogging of inorganic monolith channels, mainly due to precipitation of solids or insoluble materials during the reaction.[5,19,27,32,33] In addition, inorganic monoliths are very expensive and fragile as a result of weak interactions between their aggregated colloidal particles.[28,29,31] Since all pharmaceuticals are currently produced through distinct batch processes, identification, screening, efficient preparation, and use of an alternative catalytic system would be a new powerful strategy for continuous manufacturing of various complex organic molecules, representing a paradigm shift for the pharmaceutical industry.

The major drawback of all the aforementioned continuous-flow reactors is leaching of the MNPs from the support and their subsequent transport to the product stream which will ultimately lead to significant catalyst loss and product contamination. Metal leaching can be critical, even in very small quantities in solution, which can further catalyze cross-coupling reactions with surprisingly high efficiency.[34–36] Therefore, a deep understanding of the fundamental interaction and permanent immobilization of the MNPs with the support is necessary in order to design an alternative catalytic system for cross-coupling reactions

under flow conditions. The immobilization of heterogeneous catalysts via covalent bonding could provide a general solution, preventing the leaching of catalytically-active centers out of the support. To date, a relatively simple and convenient method for permanent immobilization of various types of the MNPs within monolithic reactors that addresses stability, reactivity, and recyclability of the produced heterogeneous materials has not been established. In addition, most of the literature on monolithic flow reactors includes approaches that were inspired by earlier continuous packed-bed reactor literature and does not address issues of permanent immobilization of the MNPs into various monoliths.

Porous polymeric hollow fiber reactors are pseudo monolithic materials that have great potential to make the process more efficient and attractive by providing a high surface area to volume ratio, increase in flow pattern reliability for scale-up, and the ability to tune mass transfer resistances. Recently, we successfully demonstrated the concept of *in-situ* formation of organocatalysts hollow fiber continuous-flow reactors using a low-cost asymmetric hollow fiber polymer (AHFP) support and their utilization for aldol and nitroaldol condensation reactions.[37] This was achieved by precisely controlling the position, concentration, and temporal flow profiles of the porous hollow fiber formation and consequently aminosilane grafting of the outer shell side of the bare hollow fibers. A similar strategy will be attempted in this study to immobilize Pd(II) on hollow fibers that can be applied in the continuous-flow system at an elevated temperature.

In particular, this study aims at creating porous PAI hollow fibers crosslinked with 3-aminopropyl trimethoxy silane (APS) to make them solvent-resistant and suitable for application in microfluidic reactors with immobilized Pd(II) ions. We demonstrate that

Pd(II) ions can be immobilized permanently in microfluidic reactors by covalently bonding them to APS-grafted PAI hollow fiber surfaces. To the best of our knowledge, this is the first example of permanent immobilization of Pd(II) ions in a sealed microfluidic reactor. Although Pd(0) metallic nanoparticles have been successfully immobilized on various surfaces and investigated under continuous-flow conditions for Heck coupling reactions in the past,[8,38–40] their Pd(II)-catalyzed counterparts performance in continuous-flow reactor system still remains unexplored. This study tackles the challenge of catalyst leaching from the support under continuous-flow reaction that is suitable for continuous chemical transformations.

2. EXPERIMENTAL SECTION

2.1. CHEMICALS

4-vinylanisole (97%), styrene (99%), 2-bromoiodobenzene (99%), 2-iodotoluene (99%), 2-iodoanline (99%), 1-iodo-2-nitro-benzene (99 %), triethylamine (99%), tetra-n-butylammonium bromide [TBAB] (98%), dodecane (99%) and N,N-dimethylacetamide (DMA) (DMA, 99%), $PdCl_2(CH_3CN)_2$, and APS (95%) were purchased from Sigma-Aldrich (see Section S1, Supporting Information).

2.2. Pd(II) IMMOBILIZED APS-GRAFTED PAI HOLLOW FIBER FORMATIONS

The polymer dope composition, PAI hollow fiber formation, and aminosilane crosslinking approaches have been described in Supporting Information in detail (see Section S2, and Table S1, Supporting Information). The APS-grafted PAI-HFs were post-synthetically modified by reaction with salicylaldehyde in toluene to give the imine derivatives. Before metalation could be achieved, the imine-PAI-HFs were washed to

remove the excess salicylic acid. Then, solvent exchange with CH_2Cl_2 and $PdCl_2(CH_3CN)_2$ in CH_2Cl_2 was performed and allowed to stand at room temperature. After 48 h, the fibers were exchanged with CH_2Cl_2 to remove excess $PdCl_2(CH_3CN)_2$. Finally, the fibers were exposed to a vacuum (30 mTorr) at 85 °C to remove the residual solvent from the pores, yielding the Pd(II) immobilized APS-grafted PAI hollow fibers (Scheme 1).

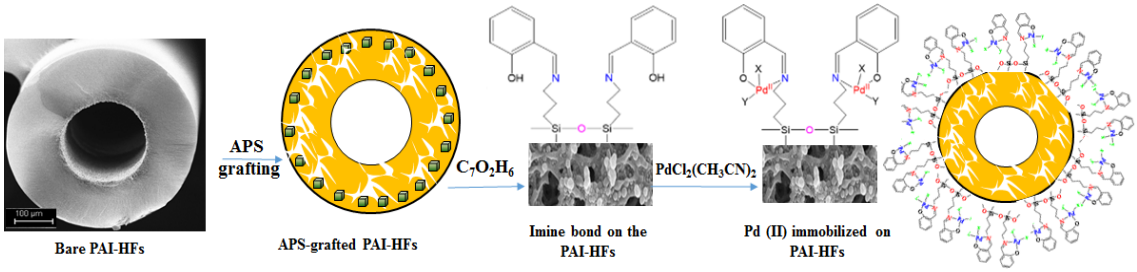

Scheme 1. Schematic representation of APS grafting and post-synthetic modification of APS-grafted PAI hollow fibers with salicylic aldehyde and Pd(II) ion immobilization, X and Y are Cl and CH_3CN, respectively.

2.3. Pd(II) IMMOBILIZED APS-GRAFTED PAI HOLLOW FIBER CATALYST AND REACTION PRODUCT CHARACTERIZATION

A high-resolution scanning electron microscope (Hitachi S-4700 FE-SEM) was used to assess the morphology of the hollow fibers before and after post-treatment. All bare and post-treated fibers were characterized by Fourier transform infrared spectroscopy (FTIR) at room temperature over a scanning range of 400-4000 cm^{-1} with a resolution of 4.0 cm^{-1}, using Bruker Tenser spectrophotometer. Bulk elemental analysis (ICP-MS) and XPS surface analysis (Kratos Axis 165 Photoelectron Spectroscopy System) were carried out to determine amine loading and Pd nanoparticles content of the hollow fibers. Nitrogen

physisorption isotherms were measured using a Micromeritics 3Flex surface characterization analyzer apparatus at 77 K. All hollow fibers were degassed at 110 °C under vacuum for 24 h prior to analysis. Surface area and pore volume were calculated from the isotherm data using the Brunauer-Emmett-Teller (BET) and Barrett-Joyner-Halenda (BJH) methods, respectively. The reaction products were analyzed by Gas Chromatography (GC) using a Varian 3800 equipped with a flame ionization detector (GC-FID) and a capillary column (DB-5) and mass spectrometry (GC-MS). In addition, ^{13}CNMR and ^{1}HNMR spectra were recorded at room temperature using a Bruker Avance III 400 WB and Bruker-DRX 500 MHz spectrometer, respectively.

2.4. BATCH CONDENSATION REACTIONS

About 5 mol% of Pd(II)/APS/PAI-HF catalyst (by Pd loading), 6 mL mixture containing 2 mmol iodobenzene para-substitutions and 3 mmol 4-vinylanisole or styrene as reactants, 3 mmol trimethylamine, 1 mmol tetra-n-butylammonium bromide [TBAB] and 1.0 mmol dodecane (internal standard) in N,N-dimethylacetamide (DMA) or methanol (as solvent) were added to a clean 25 mL one neck flask with magnetic stir bar. The reactions were run in an oil bath at 120 °C for 12 h. Reactant conversions for each Heck coupling reaction were monitored using the VARIAN gas chromatography CP-3800 equipped with a flame ionization detector (FID) and a DB-5 GC column (30 m, 0.25 mm inner diameter, 0.25 μm film thickness). For each reaction, dodecane was used as an internal standard to determine the reactant conversion.

2.5. CONTINUOUS FLOW CONDENSATION REACTIONS

To test the catalytic activity of Pd(II) ions immobilized on hollow fibers in microfluidic reactors, we carried out a proof-of-concept continuous-flow reaction study. The reaction was conducted in a stainless steel module containing five hollow fibers (fibers inner diameter 100 µm, length 15 cm, total volume 10 mL) at 120 °C. The microfluidic reactor was coiled in a heating jacket to adjust the temperature. The reactants were then continuously run through the hollow fiber reactor with 0.02 cm^3min^{-1} flow rate at 120 °C. A syringe pump equipped with two syringes was used to feed the microfluidic reactor with the reagents through a T-Junction. To start the reaction, in one syringe the reactant mixtures were introduced at one inlet (hollow fiber shell side) with the flow rate of 0.02 cm^3min^{-1}, while pure nitrogen was introduced from the other inlet (bore side) with 25 cm^3min^{-1} flow rate. Total outlet flow rate was 4.8-24 cm^3min^{-1} (various residence times). The schematic diagram of the system is illustrated in Scheme 2. The product was then cooled and collected from the boring side of the hollow fiber reactor. Pure nitrogen gas was passed through the hollow fibers bores to prevent pore blockage and also push the product out of the bore.

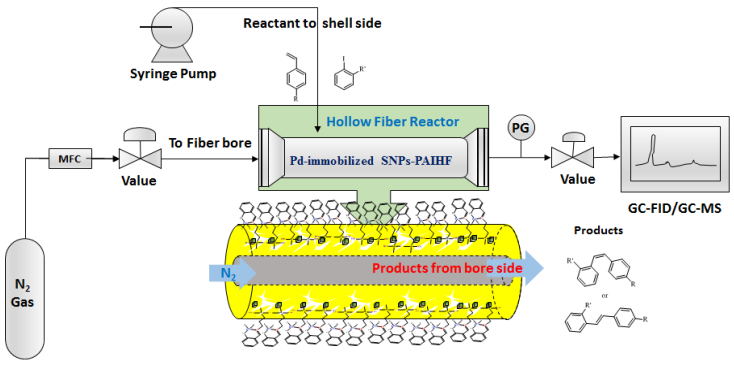

Scheme 2. Schematic diagram of microfluidic PAI hollow fiber reactors with immobilized Pd(II) for the continuous Heck coupling reactions.

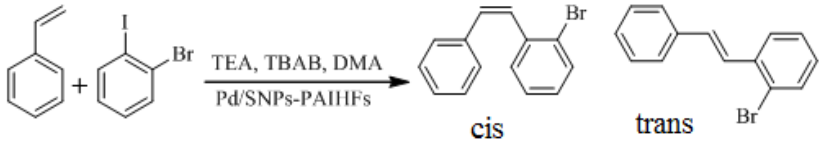

Scheme 2. Schematic diagram of microfluidic PAI hollow fiber reactors with immobilized Pd(II) for the continuous Heck coupling reactions.(cont.)

3. RESULTS AND DISCUSSION

3.1. Pd(II)/PAI HOLLOW FIBER CHARACTERIZATION

The textural properties and permeability of PAI hollow fibers before and after post-modification were characterized by N_2 physisorption and N_2 permeation, respectively and the corresponding results are shown in Table 1. Compared with bare PAI hollow fibers, BET surface area, pore volume, and N_2 flux of APS-grafted PAI hollow fibers (APS/PAI-HFs) decreased by approximately 50%. This effect is probably due to crosslinking of pore walls of PAI hollow fibers by APS through the ring-opening reaction. After anchoring Pd onto the APS-grafted PAI hollow fibers (Pd(II)/APS/PAI-HFs), the pore size and pore volume were slightly decreased in comparison to those of the APS-grafted fibers. This decrease in porosity is attributed to partially occupying the pores of hollow fibers with Pd(II) which further confirms the successful loading of Pd(II) into PAI hollow fibers. The textural properties Pd(II)/APS/PAI-HFs were found to be very similar before and after the continuous-flow reaction. Furthermore, N_2 physisorption profiles (Figure 1a) of all fibers were of type-IV isotherms, indicating a typical mesoporous structure, with H_1 type hysteresis according to IUPAC classification.[49] N_2 gas permeation measurements at 35 °C

and bore side pressure of 30 psig was carried out on PAI hollow fiber reactor before and after APS grafting and Pd(II) immobilization. It is apparent from the permeation data (Table 1) that the fiber reactor permeability was dramatically influenced upon functionalization. The nitrogen permeance decreased from 51,000 to 18,000 GPU after APS-grafting and 3,500 GPU after Pd(II) immobilization. The optimization of crosslinking conditions led to a good stability of the Pd(II)/APS/PAI-HFs in organic solvents and improved N_2 permeation. Moreover, the successful loading of Pd in the PAI hollow fibers was confirmed by the ICP and XPS analyses (Table 1).

Table 1: Textural properties, N_2 permeance, and palladium loading of the bare and postmodified PAI hollow fibers.

Materials	S_{BET}[a] m^2/g	V_{pore}[b] cm^3/g	N_2 Permeance[c] GPU	Pd loading (mmol)/g-fiber	
				ICP[d]	XPS[e]
Bare PAI-HF	40	0.14	51000	-	-
APS/PAI-HF	20	0.04	18000	-	-
Pd (II)/APS/PAI-HF (before reaction)	13	0.03	3500	0.40	0.40
Pd (II)/APS/PAI-HF (after reaction)	11	0.03	3000	0.39	0.38

[a]Determined by nitrogen physisorption experiments at 77 K.

[b]Determined by BJH method.

[c]GPU refers to $1x10^{-6}$ cc (STP)/(cm^2 s cmHg).

[d]Determined by ICP analysis.

[e]Determined by XPS analysis.

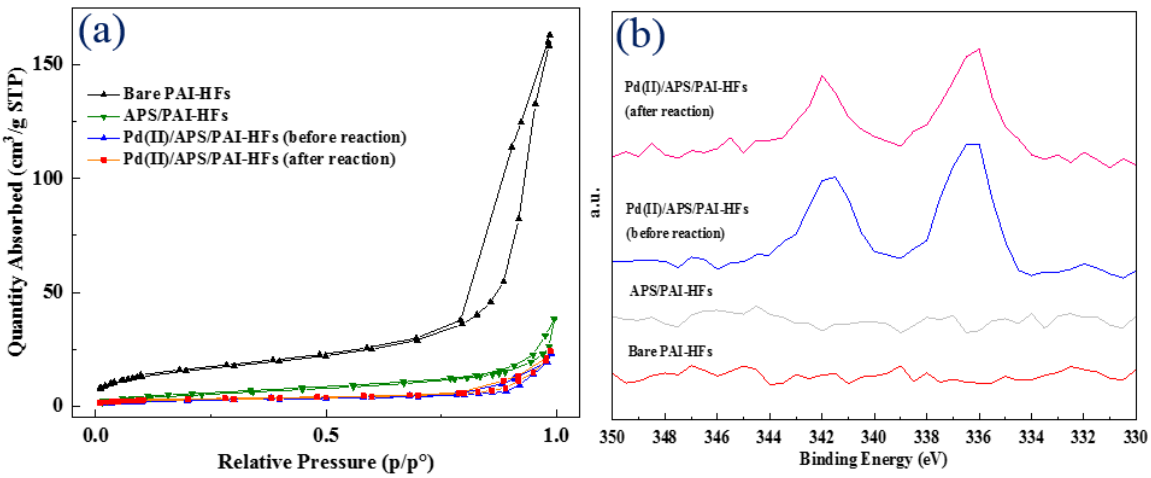

Figure 1: (a) Nitrogen adsorption/desorption isotherms at 77 K, and(b) X-ray photoelectron binding energy curves of bare and functionalized fibers before and after continuous-flow reaction for 2 h.

Furthermore, X-ray photoelectron spectroscopy (XPS) and inductively coupled plasma mass spectrometry (ICP-MS) analyses were used to obtain the concentrations of Pd(II) ions on fiber surfaces and bulk before and after modification and reaction. Figure 1(b) presents XPS spectra of Pd(II) 3d for all fibers. As this figure shows, the binding energies of Pd(II) $3d_{5/2}$ and $3d_{3/2}$ at 337 were found to be 342 eV respectively, which were very close to the typical values of Pd(II) species, confirming the presence of Pd(II) in APS/PAI-HFs.[50,51] As shown in Figure 1(b), no noticeable difference was observed in binding energy of the Pd(II)/APS/PAI-HFs before and after the reaction, implying that the chemical state of surface Pd species remained unchanged after the reaction. However, the amount of Pd on the fiber surface was found to decrease slightly (0.05%) after continuous-flow Heck reaction for 150 min (Table 1), in accordance with the results of ICP analysis (0.025%). These results clearly demonstrate that very small fraction of immobilized Pd(II) ions leached from the fibers to the product stream during the continuous-flow reaction.

However, we do not necessarily draw any conclusions by stating that Pd loading was different before and after reaction according to the respective Pd atomic concentrations obtained by XPS. The reason is that XPS results depend primarily on the area of the fiber selected for observation and the data obtained are representative of the surface only.

Although the hollow fiber module was heated at 120 °C and ran for 150 min, a negligible Pd leaching from the Pd(II)/APS/PAI-HFs bulk was observed after reaction by ICP-MS analysis. Furthermore, by operating under optimum conditions to achieve high conversion, minimal separation of unreacted products is required through this configuration and the hollow fiber catalysts can be easily regenerated and reused. These advantages render the microfluidic PAI hollow fiber reactor with immobilized Pd(II) as the most convenient configuration to perform a reaction under continuous-flow conditions. Figure 2 shows SEM images of bare PAI-HFs cross-section (2a) bare PAI-HFs surface (2b), APS/PAI-HFs (2c), and Pd(II)/APS/PAI-HFs before (2d) and after (2e) reaction. These micrographs qualitatively confirm that the fiber outer pore morphology collapsed during post-treatment processing and a highly porous state was not maintained after APS grafting and Pd(II) immobilization. Nevertheless, the Pd(II)/APS/PAI-HFs still retained a porous network, as can be inferred from Figure 2d and in agreement with the fibers textural properties, discussed earlier. In addition, as can be clearly seen from Figure 2e, the fiber surface layer displayed moderate porosity after continuous-flow reaction in DMA solvent, confirming a strong bonding between the immobilized Pd(II) ions and the polymer matrix as well as swelling resistance of APS-crosslinked PAI hollow fibers.

To further confirm the chemical bonding of Pd(II) ions with the amine functional groups on PAI hollow fibers surface, the Pd(II)/APS/PAI-HF was subjected to ^{13}CNMR

spectroscopy (Figure S2). The presence of the imine moiety was confirmed by a resonance at 119 ppm in the ^{13}CNMR spectrum. The X-ray diffraction pattern (XRD) spectra of bare and post-treated PAI hollow fibers are shown in Figure S3. The weak diffraction peaks of Pd(II) (JCPDS 05-0681) in the PAI hollow fibers catalyst appeared at 39.5° and 45.4° correspond to the (111) and (200) crystal facets of Pd, respectively, suggesting the high dispersion of Pd NPs in the PAI hollow fibers support and also interaction between APS and Pd(II) ions. FTIR spectra displayed distinct changes in the bare PAI hollow fiber chemical structure after APS grafting and Pd(II) immobilization treatments (Figure S4). These results indicate that the original imide rings in PAI-HFs were opened during APS functionalization reaction which was previously confirmed in our previous study.[41,43]

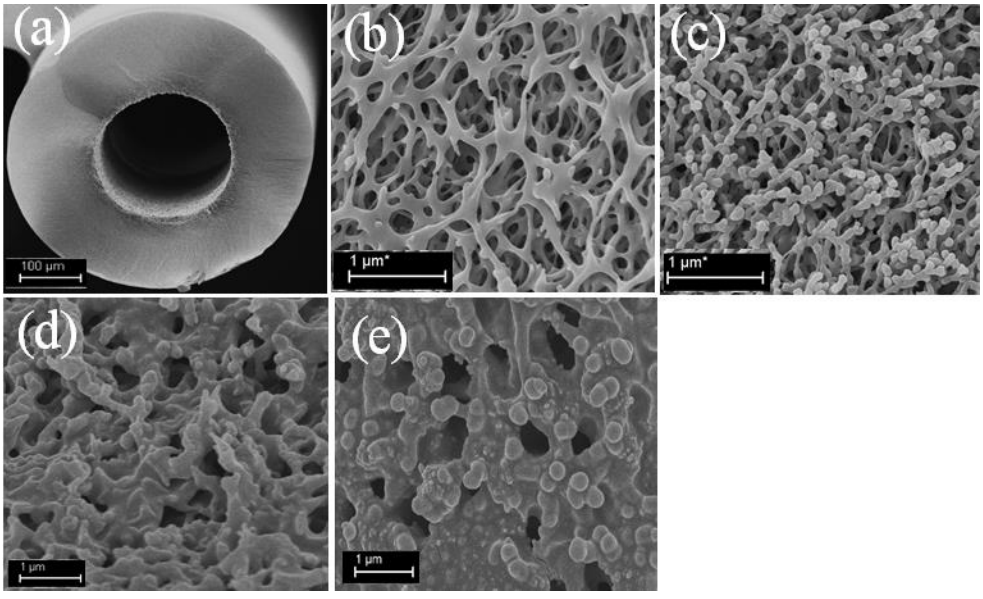

Figure 2. SEM images of (a) the cross-section of bare PAI-HF; (b) surface of bare PAI-HF; (c) surface of APS/ PAI-HF; (d) surface of Pd(II)/APS/PAI-HF (before reaction); (e) surface of Pd(II)/APS/PAI-HF (after reaction).

To evaluate the swelling properties of hollow fibers, the lengths of bare PAI-HFs, APS/PAI-HFs, and Pd(II)/APS/PAI-HFs were measured before and after immersion in DMA solvent. The bare PAI-HFs showed a 5% increase in length after immersion for 5 h and no noticeable change was observed after that. In contrast, the APS/PAI-HFs and Pd(II)/APS/PAI-HFs showed improved swelling resistance such that the length of fibers increased by only 2-3% and 1-2% after immersion, respectively. These results indicate that some swelling effects were still present in Pd(II)/APS/PAI-HFs although the degree of swelling was significantly reduced compared to the bare PAI-HFs. Crosslinking of PAI hollow fibers resulted in the formation of amine-tethered inorganic networks in the fiber structure, thus leading to improved stability and hydrophobicity of the fibers in aggressive solvents.

We used PAI polymer as Pd(II) support for microfluidic reactors due to its good chemical and thermal stability, excellent processability, and mechanical property.[41–43] The asymmetric polyamide-imide hollow fibers (PAI-HFs) were fabricated via a dry-jet/wet-quench spinning process,[41–43] as illustrated in Figure S1. During a spinning run, the dope (polymer solution) and bore fluid were coextruded from a spinneret into an air gap ("dry-jet") and then immersed into an aqueous quench bath ("wet-quench"). The optimized polymer dope compositions and spinning conditions are presented in Table S1. The water/N-methyl-2-pyrrolidone (NMP) solution mixture (50:50 wt%) was used in the outer orifice as alternate sheath side fluid to eliminate the fibers skin layer and facilitate *in-situ* formation of an extremely open surface on the outside of the fiber with a lacey structure, for subsequent surface modification (see Supporting Information for detailed synthetic procedure).

One of the key challenges faced in developing polymeric hollow fiber reactors for continuous-flow reactions lies in ensuring their excellent stability in organic solvents and achieving acceptable reactant diffusivity and target product formation and removing over long-term operation. To improve the PAI hollow fiber stability in aggressive solvents, the hollow fiber substrates were crosslinked with APS at 60 °C for 2 h that could form inorganic network structures inside of the substrates. To determine the optimal crosslinking temperature and time, PAI hollow fibers were treated with various amounts of APS in toluene solution at varying temperatures of 60-80 °C for 1-8 h (see Supporting Information for the detailed crosslinking procedure). The crosslinking of PAI hollow fibers with APS solution occurred through a ring-opening reaction between the amide groups of PAI polymer and amine groups of APS molecules.[41–43] Indeed, as shown in Scheme 1, the amine functional groups in APS-grafted molecules are also utilized for reaction with salicylaldehyde in toluene to give the imine derivatives for metalation with bis (acetonitrile) dichloro palladium(II) to immobilize Pd(II) ions in the APS/PAI-HFs through the formation of covalent amide bonds between activated imine and surface amino groups.

3.2. HECK REACTION IN MICROFLUIDIC Pd(II) IMMOBILIZED APS-GRAFTED PAI HOLLOW FIBER (Pd(II)/APS/PAI-HFs) MICROFLUIDIC REACTORS

The catalytic activity of Pd(II)/APS/PAI-HFs in heterogeneous Heck coupling reaction in batch and continuous-flow reactions were investigated. The reactants and reaction conditions were selected based on a previously published work involving homogenous and heterogeneous palladium catalysts.[44,45] The control reactions performed with the bare PAI-HFs (i.e., no amines grafted) and APS/PAI-HFs led to no observable C-C products. One interesting observation made from our control experiments was that the

aminosliane grafting of PAI hollow fibers was crucial for preventing fibers swelling since the bare PAI hollow fibers were dissolved in DMA solvent during the reaction. Initially, we performed the Heck cross-coupling reaction under batch conditions and the corresponding catalytic performance of Pd(II)/APS/PAI-HFs estimated from the GC-FID analysis is reported in Table 2. The apparent initial turnover frequency (TOF) was estimated to be 50 h^{-1} which were slightly lower compared with Pd(0) nanoparticles studied previously.[8,40] These data may appear to suggest that the immobilized Pd(II) ions attached to the polymer backbone were inherently less active than those associated with the Pd(0) in homogeneous catalysts. As shown in Table 2, the reaction gave a product mixture with the 1:4 ratio of cis to trans, except for entries that used 1-iodo-2-nitro-benzene. Almost 100% selectivity toward trans product was obtained by using 1-iodo-2-nitro-benzene which could be correlated with the strong electron-withdraw ability of the nitro functional group. This observation is consistent with published reports using heterogeneous Pd (II) ions.[45,46] The GC-MS were utilized to identify the ratio of isomers and the corresponding results are provided in supporting information (see Section S4).

After demonstrating the efficiency of Pd(II)/APS/PAI-HFs in Heck coupling reaction in the batch reactor, the hollow fiber module was formed using five fibers (with a total volume of 10 mL) and evaluated under the same conditions as for the batch reactor to demonstrate the compatibility and stability of the catalytically active Pd(II) ions in a continuous-flow system. In particular, the catalytic activities of microfluidic PAI-HF reactors with immobilized Pd(II) for the continuous-flow Heck coupling reaction between styrene and 2-bromoiodobenzene in DMA solvent were evaluated. As shown in Scheme 2, the catalytically active Pd(II) ions were immobilized and resided within the porous wall

while the reagents were passed through the fiber shell and products were collected from the bore side, thus in principle, no separation of the products from the catalyst is required using this novel microfluidic hollow fiber reactor. The experiments were carried out by feeding the reactants into the reactor for 150 min and then analyzing the products every 20 min. A syringe pump was used to introduce reactants (styrene and 2-bromoiodobenzene) continuously onto the shell side of the hollow fiber reactor at 120 °C.

Table 2. Heck cross-coupling reaction over Pd(II)/APS/PAI-HFs under batch conditions.

Entry	Reactant 1	Reactant 2	-R	TOF (h^{-1})	Con. (%)	Sel. (%) (trans/cis)
1	4-Vinylanisole	2-bromoiodobenzene	-Br	61	100	80/20
2		2-iodotoluene	$-CH_3$	56	100	71/29
3		1-iodo-2-nitro-benzene	$-NO_2$	49	100	71/29
5	Styrene	2-bromoiodobenzene	-Br	55	100	100
6		2-iodotoluene	$-CH_3$	47	100	67/33
7		1-iodo-2-nitro-benzene	$-NO_2$	48	100	100

Reaction condition: 120 °C for 12 h, 6 mL DMA (solvent), TEA 1mmol, TBAB 1 mmol, catalysts 100 mg, 3 mmol reactant 1 and 2 mmol reactant 2. The conversion and selectivity data were obtained by GC-FID. Initial turnover frequencies (TOFs) are measured in the first 30 min.

Figure 3 shows the relationship between catalyst performance (product selectivity and conversion of 2-bromoiodobenzene) and reaction time in a continuous hollow fiber module for the Heck reaction. A mixture of trans and cis product isomers with different ratios was obtained upon 50 % conversion of 2-bromoiodobenzene in the continuous-flow

system. After the catalytic reaction reached a steady state, the amount of products increased linearly with reactant solution permeation. The ratio of isomers slightly changed over time while the catalyst was found to be very stable (i.e., constant conversion). In this continuous-flow reactor, a different ratio of trans and cis products isomers was obtained than in the batch reactor under the same reaction conditions. This difference could be attributed to the shorter contact time for Heck coupling reaction under the continuous-flow condition since trans isomers are much more stable than cis isomers, therefore, increasing the contact time could lead to the more stable product (i.e., trans isomer), as was the case in the batch reaction. The higher ratio of cis isomer in the first 80 min continuous-flow reaction further proved this hypothesis. Therefore, with increasing the reaction time, the amount of trans isomer increased substantially. As shown in Figure 3, about 45% reactants conversion was obtained with 41 and 59% selectivity toward cis and trans products, respectively at 120 °C and ambient pressure. These values are slightly lower than those obtained in the batch system which can be attributed to different residence times. Both ^{1}H NMR and GC-MS were utilized to identify the ratio of isomers and the corresponding results are provided in Supporting Information (see Section S4). Basically, in this continuous-flow system, the product mixture is obtained in three steps: (1) mass transfer of 2-bromoiodobenzene and styrene to the Pd(II) ions immobilized in the PAI hollow fiber pores; (2) catalytic conversion of reactants into the products by Heck coupling reaction; and (3) products diffusion through the fiber matrix and collection from the fiber bore. According to Seto et. al, the rate-determining step in the continuous-flow coupling reaction is typically the first step (i.e., reactants diffusion).[47]

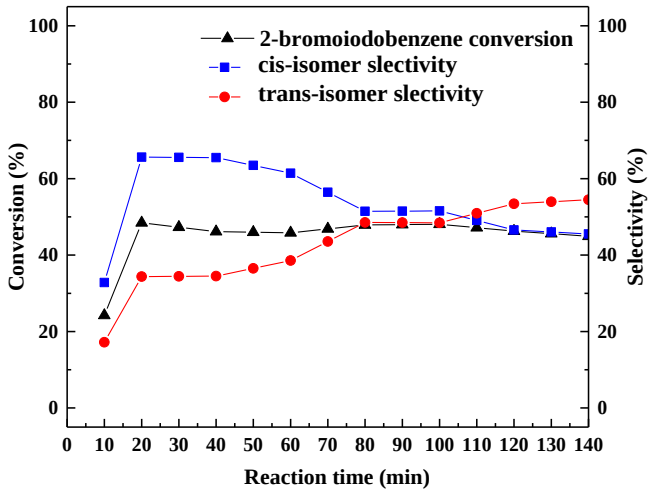

Figure 3. Conversion of 2-bromoiodobenzene in microfluidic hollow fiber reactor with immobilized Pd(II) under continuous flow reaction.

In order to assess the leaching of Pd species from the microfluidic reactor, all product samples were analyzed with ICP-MS. It is noteworthy that the amount of Pd maybe below the ICP-MS detection limit (i.e., <1 ppm) in all cases. Furthermore, all samples used for real-time analysis with GC-FID were sealed and remeasured after storing for 1 month at room temperature. While no increase in the conversion was detected in the case of a batch reaction, a negligible product formation (approximately 0.05%) was detected outside the reactor at room temperature for the samples from the continuous-flow reaction. Furthermore, the hollow fiber module was unpacked and the used Pd(II)/APS/PAI-HFs were characterized and compared with the fresh fibers. Although continuous-flow processing by using a homogeneous and heterogeneous Pd catalysts for Heck coupling reaction has been extensively studied before,[8,38,39,48] such investigations in the context of microfluidic reactor with immobilized Pd(II) ions, as both a highly selective heterogeneous catalyst toward C-C bond formation and a microfluidic reactor, are reported herein for the

first time. Compared to existing homogeneous and heterogeneous Pd catalysts for continuous-flow reaction,[8,38,39] the catalytically active Pd(II) ions are immobilized on the highly porous surface, thus allowing for strong interactions between the catalyst MNPs and the substrate.

4. CONCLUSION

This work is a proof-of-concept study that demonstrates Pd(II) can be immobilized permanently into microstructured hollow fibers for utilization in microfluidic reactors. The anchoring of catalytically active Pd(II) ions within porous PAI-HFs offered a powerful catalytic system that demonstrated the advantages of nanocatalysts in the continuous-flow reaction without significant Pd nanoparticles leaching. Although the conversion and selectivity achieved so far in a continuous-flow mode are close to those obtained in a batch mode, the concept reported herein can facilitate the ultimate scale-up of continuous Heck coupling reaction. Successful fabrication of the PAI hollow fiber support was accomplished with a range of microstructural properties, composed of a large number of interconnected cells or channels and high surface/volume ratios, which provide excellent mass transfer properties and low resistance to flow during the continuous-flow reaction.

ACKNOWLEDGMENTS

The authors would like to thank the University of Missouri Research Board (UMRB) for supporting this work. The authors acknowledge Professor William J. Koros from the School of Chemical and Biomolecular Engineering at the Georgia Institute of Technology for giving access to his fiber spinning facilities.

REFERENCES

1. Hartman, R. L.; Naber, J. R.; Buchwald, S. L.; Jensen, K. F. Multistep Microchemical Synthesis Enabled by Microfluidic Distillation. *Angew. Chemie - Int. Ed.* **2010**, *49* (5), 899–903.

2. McMullen, J. P.; Stone, M. T.; Buchwald, S. L.; Jensen, K. F. An Integrated Microreactor System for Self-Optimization of a Heck Reaction: From Micro- to Mesoscale Flow Systems. *Angew. Chemie - Int. Ed.* **2010**, *49* (39), 7076–7080.

3. Molnár, Á. Efficient, Selective, and Recyclable Palladium Catalysts in Carbon-Carbon Coupling Reactions. *Chem. Rev.* **2011**, *111* (3), 2251–2320.

4. Johansson Seechurn, C. C. C.; Kitching, M. O.; Colacot, T. J.; Snieckus, V. Palladium-Catalyzed Cross-Coupling: A Historical Contextual Perspective to the 2010 Nobel Prize. *Angew. Chemie - Int. Ed.* **2012**, *51* (21), 5062–5085.

5. Irfan, M.; Glasnov, T. N.; Kappe, C. O. Heterogeneous Catalytic Hydrogenation Reactions in Continuous-Flow Reactors. *ChemSusChem* **2011**, *4* (3), 300–316.

6. Porta, R.; Benaglia, M.; Puglisi, A. Flow Chemistry: Recent Developments in the Synthesis of Pharmaceutical Products. *Org. Process Res. Dev.* **2016**, *20*, 2–25.

7. Noël, T.; Buchwald, S. L. Cross-Coupling in Flow. *Chem. Soc. Rev.* **2011**, *40* (10), 5010.

8. Ricciardi, R.; Huskens, J.; Verboom, W. Nanocatalysis in Flow. *ChemSusChem* **2015**, *8* (16), 2586–2605.

9. Battilocchio, C.; Hawkins, J. M.; Ley, S. V. Mild and Selective Heterogeneous Catalytic Hydration of Nitriles to Amides by Flowing through Manganese Dioxide. *Org. Lett.* **2014**, *16* (4), 1060–1063.

10. Kant, A.; He, Y.; Jawad, A.; Li, X.; Rezaei, F.; Smith, J. D.; Rownaghi, A. A. Hydrogenolysis of Glycerol over Ni, Cu, Zn, and Zr Supported on H-Beta. *Chem. Eng. J.* **2017**, *317*, 1–8.

11. Brennführer, A.; Neumann, H.; Beller, M. Palladium-Catalyzed Carbonylation Reactions of Aryl Halides and Related Compounds. *Angew. Chemie - Int. Ed.* **2009**, *48* (23), 4114–4133.

12. Odedra, A.; Seeberger, P. H. 5-(Pyrrolidin-2-Yl)tetrazole-Catalyzed Aldol and Mannich Reactions: Acceleration and Lower Catalyst Loading in a Continuous-Flow Reactor. *Angew. Chemie - Int. Ed.* **2009**, *48* (15), 2699–2702.

13. Porta, R.; Benaglia, M.; Coccia, F.; Rossi, S.; Puglisi, A. Enantioselective Organocatalysis in Microreactors: Continuous Flow Synthesis of a (S)-Pregabalin Precursor and (S)-Warfarin. *Symmetry (Basel).* **2015**, *7* (3), 1395–1409.

14. Koreniuk, A.; Maresz, K.; Odrozek, K.; Jarzebski, A. B.; Mrowiec-Biaton, J. Highly Effective Continuous-Flow Monolithic Silica Microreactors for Acid Catalyzed Processes. *Appl. Catal. A Gen.* **2015**, *489*, 203–208.

15. Wu, X. F.; Anbarasan, P.; Neumann, H.; Beller, M. From Noble Metal to Nobel Prize: Palladium-Catalyzed Coupling Reactions as Key Methods in Organic Synthesis. *Angew. Chemie - Int. Ed.* **2010**, *49* (48), 9047–9050.

16. Jumde, R. P.; Marelli, M.; Scotti, N.; Mandoli, A.; Psaro, R.; Evangelisti, C. Ultrafine Palladium Nanoparticles Immobilized into poly(4-Vinylpyridine)-Based Porous Monolith for Continuous-Flow Mizoroki–Heck Reaction. *J. Mol. Catal. A Chem.* **2016**, *414*, 55–61.

17. Wiles, C.; Watts, P. Continuous Flow Reactors: A Perspective. *Green Chem.* **2012**, *14* (1), 38–54.

18. Wegner, J.; Ceylan, S.; Kirschning, A. Flow Chemistry - A Key Enabling Technology for (Multistep) Organic Synthesis. *Adv. Synth. Catal.* **2012**, *354* (1), 17–57.

19. Frost, C. G.; Mutton, L. Heterogeneous Catalytic Synthesis Using Microreactor Technology. *Green Chem.* **2010**, *12*, 1687–1703.

20. Nikbin, N.; Ladlow, M.; Ley, S. V. Continuous Glow Ligand-Free Heck Reactions Using Monolithic Pd(0) Nanoparticles. *Org. Proc. Res. Dev.* **2007**, *11* (5), 458–462.

21. Munirathinam, R.; Huskens, J.; Verboom, W. Supported Catalysis in Continuous-Flow Microreactors. *Adv. Synth. Catal.* **2015**, *357* (6), 1093–1123.

22. Wang, G.; Yuan, C.; Fu, B.; He, L.; Reichmanis, E.; Wang, H.; Zhang, Q.; Li, Y. Flow Effects on the Controlled Growth of Nanostructured Networks at Microcapillary Walls for Applications in Continuous Flow Reactions. *ACS Appl. Mater. Interfaces* **2015**, *7* (38), 21580–21588.

23. Buchmeiser, M. R.; Lubbad, S.; Mayr, M.; Wurst, K. Access to Silica- and Monolithic Polymer Supported C-C-Coupling Catalysts via ROMP: Applications in High-Throughput Screening, Reactor Technology and Biphasic Catalysis. *Inorganica Chim. Acta* **2003**, *345*, 145–153.

24. Barlow, K. J.; Bernabeu, V.; Hao, X.; Hughes, T. C.; Hutt, O. E.; Polyzos, A.; Turner, K. A.; Moad, G. Triphenylphosphine-Grafted, RAFT-Synthesised, Porous Monoliths as Catalysts for Michael Addition in Flow Synthesis. *React. Funct. Polym.* **2015**, *96*, 89–96.

25. Gutmann, B.; Cantillo, D.; Kappe, C. O. Continuous-Flow Technology - A Tool for the Safe Manufacturing of Active Pharmaceutical Ingredients. *Angew. Chemie - Int. Ed.* **2015**, *54* (23), 6688–6728.

26. Kirschning, A.; Solodenko, W.; Mennecke, K. Combining Enabling Techniques in Organic Synthesis: Continuous Flow Processes with Heterogenized Catalysts. *Chem. - A Eur. J.* **2006**, *12* (23), 5972–5990.

27. Kirschning, A.; Altwicker, C.; Dräger, G.; Harders, J.; Hoffmann, N.; Hoffmann, U.; Schönfeld, H.; Solodenko, W.; Kunz, U. PASS Flow Syntheses Using Functionalized Monolithic Polymer/Glass Composites in Flow-Through Microreactors. *Angew. Chem. Int. Ed.* **2001**, *40* (21), 3995–3998.

28. El Kadib, A.; Chimenton, R.; Sachse, A.; Fajula, F.; Galarneau, A.; Coq, B. Functionalized Inorganic Monolithic Microreactors for High Productivity in Fine Chemicals Catalytic Synthesis. *Angew. Chemie - Int. Ed.* **2009**, *48* (27), 4969–4972.

29. Łojewska, J.; Kołodziej, A.; Żak, J.; Stoch, J. Pd/Pt Promoted Co3O4 Catalysts for VOCs Combustion. *Catal. Today* **2005**, *105* (3–4), 655–661.

30. Wickenheisser, M.; Paul, T.; Janiak, C. Prospects of Monolithic MIL-MOF@poly(NIPAM)HIPE Composites as Water Sorption Materials. *Microporous Mesoporous Mater.* **2016**, *220*, 258–269.

31. Linares, N.; Hartmann, S.; Galarneau, A.; Barbaro, P.; Organo, C.; Nazionale, C.; Fiorentino, S. Continuous Partial Hydrogenation Reactions by Pd@unconventional Bimodal Porous Titania Monolith Catalysts. *ACS Catal.* **2012**, *2*, 2194−2198.

32. Anderson, E. B.; Buchmeiser, M. R. Catalysts Immobilized on Organic Polymeric Monolithic Supports: From Molecular Heterogeneous Catalysis to Biocatalysis. *ChemCatChem* **2012**, *4* (1), 30–44.

33. He, P.; Haswell, S. J.; Fletcher, P. D. I.; Kelly, S. M.; Mansfield, A. Scaling up of Continuous-Flow, Microwave-Assisted, Organic Reactions by Varying the Size of Pd-Functionalized Catalytic Monoliths. *Beilstein J. Org. Chem.* **2011**, *7*, 1150–1157.

34. Arvela, R. K.; Leadbeater, N. E.; Sangi, M. S.; Williams, V. A.; Granados, P.; Singer, R. D. A Reassessment of the Transition-Metal Free Suzuki-Type Coupling Methodology. *J. Org. Chem.* **2005**, *70* (1), 161–168.

35. Thomé, I.; Nijs, A.; Bolm, C. Trace Metal Impurities in Catalysis. *Chem. Soc. Rev.* **2012**, *41* (3), 979.

36. Thathagar, M. B.; Ten Elshof, J. E.; Rothenberg, G. Pd Nanoclusters in C-C Coupling Reactions: Proof of Leaching. *Angew. Chemie - Int. Ed.* **2006**, *45* (18), 2886–2890.

37. He, Y.; Jawad, A.; Li, X.; Atanga, M.; Rezaei, F.; Rownaghi, A. A. Direct Aldol and Nitroaldol Condensation in an Aminosilane-Grafted Si/Zr/Ti Composite Hollow Fiber as a Heterogeneous Catalyst and Continuous-Flow Reactor. *J. Catal.* **2016**, *341*, 149–159.

38. Oger, N.; Le Grognec, E.; Felpin, F. X. Continuous-Flow Heck - Matsuda Reaction: Homogeneous versus Heterogeneous Palladium Catalysts. *J. Org. Chem.* **2014**, *79* (17), 8255–8262.

39. Solodenko, W.; Wen, H.; Leue, S.; Stuhlmann, F.; Sourkouni-Argirusi, G.; Jas, G.; Sch??nfeld, H.; Kunz, U.; Kirschning, A. Development of a Continuous-Flow System for Catalysis with palladium(0) Particles. *European J. Org. Chem.* **2004**, No. 17, 3601–3610.

40. Ricciardi, R.; Huskens, J.; Verboom, W. Dendrimer-Encapsulated Pd Nanoparticles as Catalysts for C-C Cross-Couplings in Flow Microreactors. *Org. Biomol. Chem.* **2015**, *13* (17), 4953–4959.

41. Rownaghi, A. A.; Kant, A.; Li, X.; Thakkar, H.; Hajari, A.; He, Y.; Brennan, P. J.; Hosseini, H.; Koros, W. J.; Rezaei, F. Aminosilane-Grafted Zirconia-Titiania-Silica Nanoparticles/Torlon Hollow Fiber Composites for CO2 Capture. *ChemSusChem* **2016**, *9*, 1166–1177.

42. Brennan, P. J.; Thakkar, H.; Li, X.; Rownaghi, A. A.; Koros, W. J.; Rezaei, F. Effect of Post-Functionalization Conditions on the Carbon Dioxide Adsorption Properties of Aminosilane-Grafted Zirconia/Titania/Silica-Poly (Amide-Imide) Composite Hollow Fiber Sorbents. *Energy Technol.* **2017**, *5*, 327–337.

43. Rownaghi, A. A.; Rezaei, F.; Labreche, Y.; Brennan, P. J.; Johnson, J. R.; Li, S.; Koros, W. J. In Situ Formation of a Monodispersed Spherical Mesoporous Nanosilica – Torlon Hollow-Fiber Composite for Carbon Dioxide Capture. *ChemSusChem* **2015**, *8*, 3439–3450.

44. Botella, L.; Nájera, C. Synthesis of Methylated Resveratrol and Analogues by Heck Reactions in Organic and Aqueous Solvents. *Tetrahedron* **2004**, *60* (26), 5563–5570.

45. Brown, J. W.; Jarenwattananon, N. N.; Otto, T.; Wang, J. L.; Glöggler, S.; Bouchard, L.-S. Heterogeneous Heck Coupling in Multivariate Metal–organic Frameworks for Enhanced Selectivity. *Catal. Commun.* **2015**, *65*, 105–107.

46. Gaikwad, A. V.; Holuigue, A.; Thathagar, M. B.; Ten Elshof, J. E.; Rothenberg, G. Ion- and Atom-Leaching Mechanisms from Palladium Nanoparticles in Cross-Coupling Reactions. *Chem. - A Eur. J.* **2007**, *13* (24), 6908–6913.

47. Ferreira, L. S.; Trierweiler, J. O. Membrane Reactor Immobilized with Palladium-Loaded Polymer Nanogel for Continuous-Flow Suzuki Coupling Reaction. *AIChE J.* **2014**, *61* (PART 1), 582–589.

48. Viviano, M.; Glasnov, T. N.; Reichart, B.; Tekautz, G.; Kappe, C. O. A Scalable Two-Step Continuous Flow Synthesis of Nabumetone and Related 4-Aryl-2-Butanones. *Org. Process Res. Dev.* **2011**, *15* (4), 858–870.

49. Sing, K. S. W.; Everett, D. H.; Haul, R. A. W.; Moscou, L.; Pierotti, R. A.; Rouquero, J.; Siemieniewska, T. Reporting Physisorption Data for Gas/solid Systems with Special Reference to the Determination of Surface Area and Porosity. *Pure Appl.Chem.* **1985**, *57* (4), 603–619.

50. Chavan, S. P.; Varadwaj, G. B. B.; Parida, K.; Bhanage, B. M. Palladium Anchored on Amine-Functionalized K10 as an Efficient, Heterogeneous and Reusable Catalyst for Carbonylative Sonogashira Reaction. *Appl. Catal. A Gen.* **2015**, *506*, 237–245.

51. Tan, L.; Dong, H.; Liu, X.; He, J.; Xu, H.; Xie, J. Mechanism of Palladium(II) Biosorption by Providencia Vermicola. *RSC Adv.* **2017**, *7* (12), 7060–7072.

SUPPORTING INFORMATION

Section S1: Materials

A commercially available polyamide-imide (PAI) (Torlon® 4000T-HV, Solvay Advanced Polymers, Alpharetta, GA) and poly(vinylpyrrolidone) (PVP) (average Mw≈ 1300 K, Sigma Aldrich) was used for formation of the composite hollow fibers. Prior to use, PVP was dried at 80 °C for 24 h under vacuum to remove pre-sorbed water vapor, while Torlon was dried at 110 °C for 24 h. De-ionized (DI) water (18MU, Model: D4521, Barnstead International, Dubuque, IA) was added as a non-solvent into the fiber dope. N-Methyl-2-pyrrolidone (NMP) (Reagent Plus, 99%, Sigma-Aldrich, Milwaukee, WI) was used as the solvent to form the spinning dope due to its strong solvent power, low volatility, and good water miscibility. All solvents and nonsolvents were used as-received with no purification or modification. All liquid chemicals were reagent grade with 99% purity and purchased from Sigma Aldrich (Milwaukee, WI). Methanol (ACS grade, VWR) and

hexane (ACS Reagent, >98.5%, VWR) was used for solvent exchange after fiber sorbent spinning. Moreover, methanol was used to remove excess water from the fibers. Inert UHP nitrogen gas was also purchased from Airgas.

Section S2: Formation of PAI Hollow Fibers

The optimized polymer dope compositions and spinning conditions are presented in Table S1. The detail information of the hollow fiber sorbent formation setup along with the triple orifice spinneret and ternary phase diagram is discussed in detail in our previous work.[1] The water present in the fiber was then solvent exchanged with methanol (to remove excess water) followed by post-infusion functionalization by exposing fiber sorbents inappropriate 3-Aminopropyltriethoxysilane (APS) solutions.

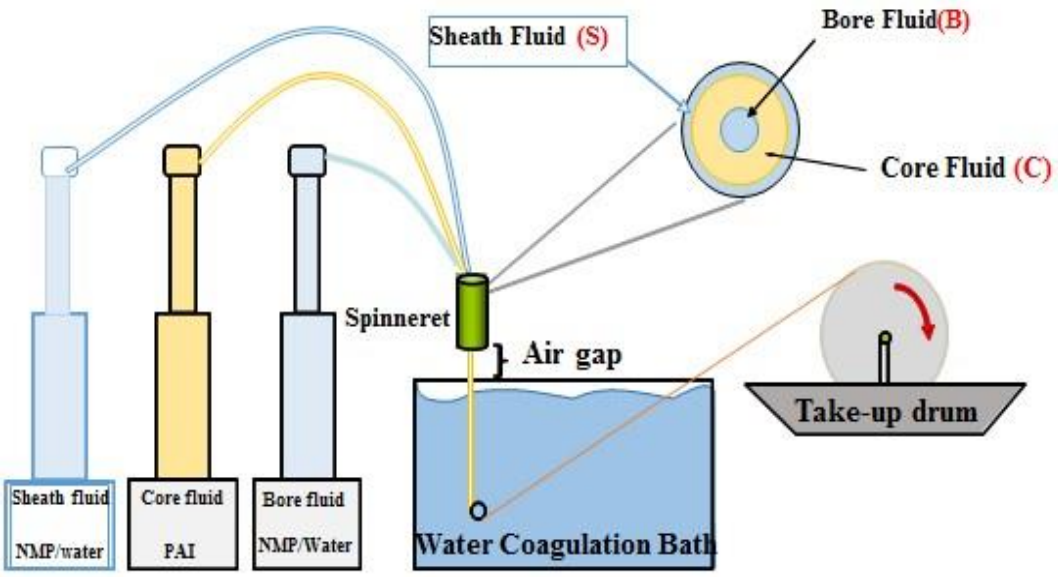

Figure S1. Schematic diagram of fiber spinning apparatus; cross-section view of triple orifice spinneret (S: Sheath channel, C: Core channel, B: Bore channel).

Table S1. Optimized spinning conditions for PAI hollow fiber formation

Dope composition (PAI/PVP/NMP/H_2O) (wt %)	5/25/7/63/5
Dope flow rate	600 mL/hr
Bore fluid (NMP/H_2O)	88/12 wt %
Bore fluid flow rate	200 mL/hr
Sheath fluid (NMP/H_2O)	50/50 wt%
Sheath fluid flow rate	100 mL/hr
Air gap	0.15 m
Take up rate	8.5 m/min
Operating temperature	55 °C
Quench bath temperature	55 °C

The aminosilane crosslinking was performed in a mixture of a non-polar solvent (toluene) and a polar protic solvent (water). The water content of the mixture was kept within the range of 0.01- 2.00 wt%. Water is necessary for protonating APS and hydrolyzing methoxy groups in dry liquid. As shown previously, exposure of APS to moisture disrupts strong hydrogen bonds and leads to the formation of polysiloxane.[1–4]It was found that a water content of 1.00 wt% gave rise to highest amine loading. As outlined above, after the PAI hollow fibers were formed, they were subjected to a methanol solvent exchange process, followed by exposure to different APS/toluene/water (ratio 10:89:1 wt%) solution mixtures with varying immersion times, from 1 to 8 h. Subsequently, crosslinked PAI hollow fibers were removed from the amine solution, rinsed with hexane for 30 min at ambient temperature to wash away the ungrafted APS deposited on the fiber surface. Finally, APS-grafted PAI hollow fibers (APS/PAI-HFs)were placed in a preheated vacuum oven and cured for 1 h at 60 °C. The APS aminosilane has the ability to form a durable bond with the PAI polymer in this post-spinning immersion step.

Section S3: Bare PAI-HFs, APS/PAI-HF, Pd(II)/APS/PAI-HF characterization

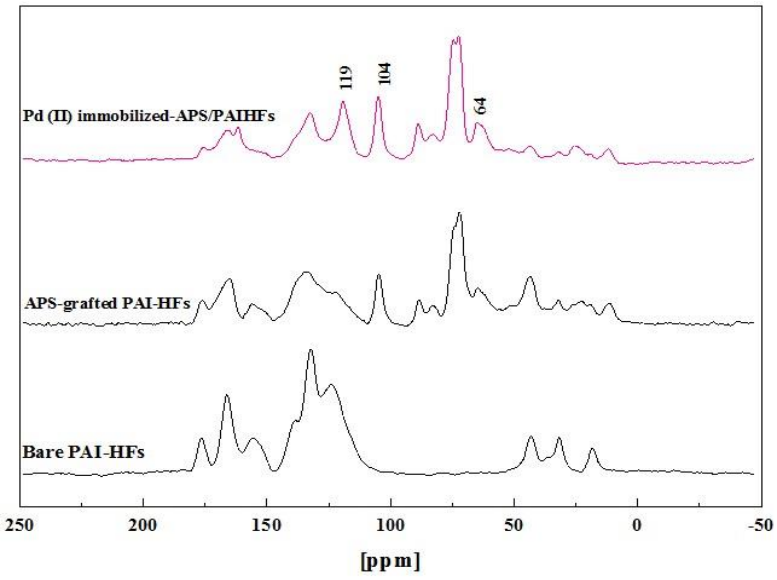

Figure S2. Solid state ^{13}C NMR data of bare PAI-HF, APS/PAI-HF, Pd(II)/APS/PAI-HF before and after the reaction.

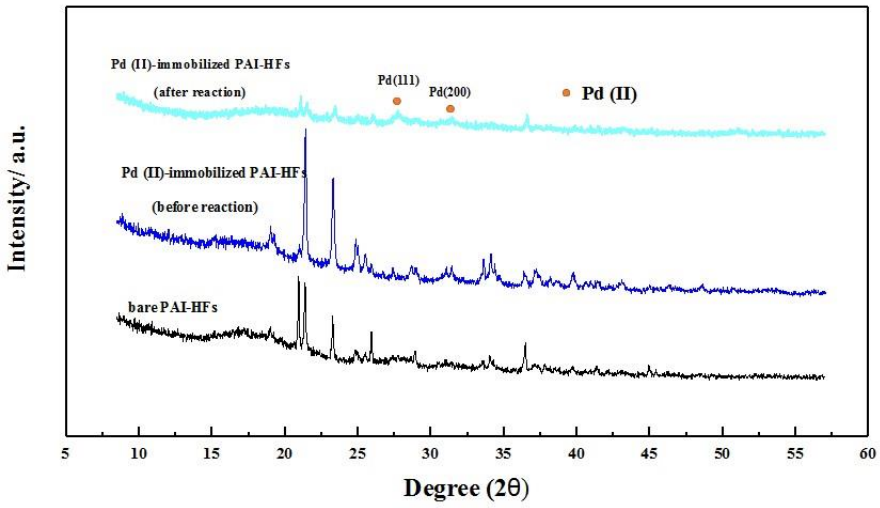

Figure S3. XRD diffraction of bare PAI-HF, APS/PAI-HF, Pd(II)/APS/PAI-HF before and after the reaction.

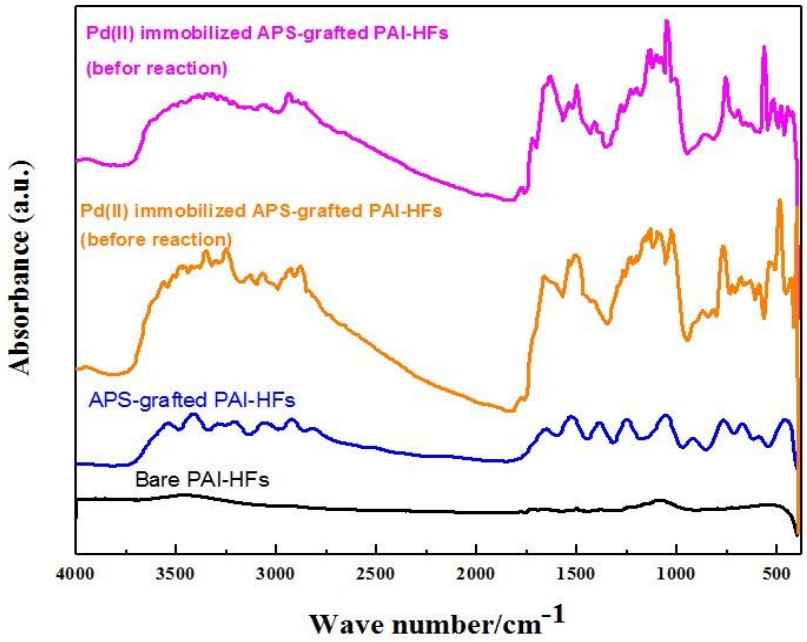

Figure S4. FT-IR spectra of bare PAI-HF, APS/PAI-HF, Pd(II)/APS/PAI-HF before and after the reaction.

Section S4: Product characterization

4-vinylanisole and 2-bromoiodobenezene

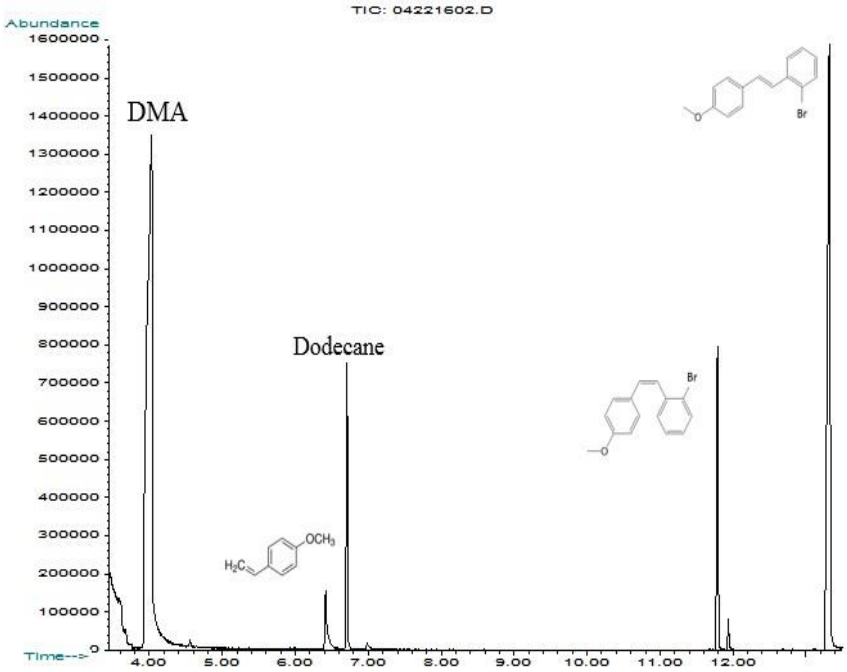

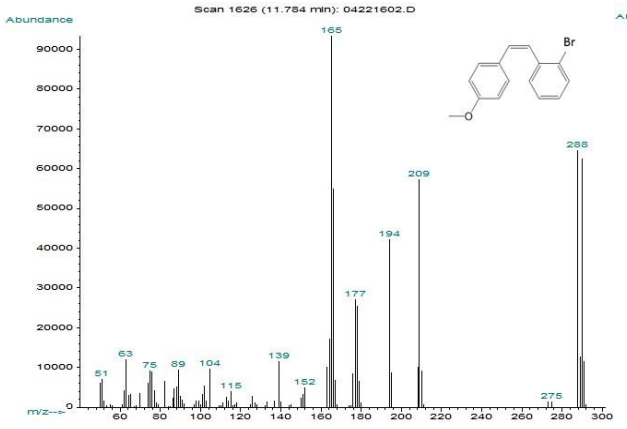

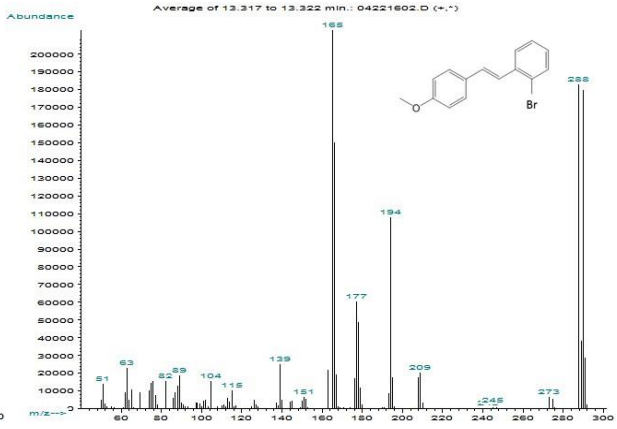

4-vinylanisole and 2-iodotoluene

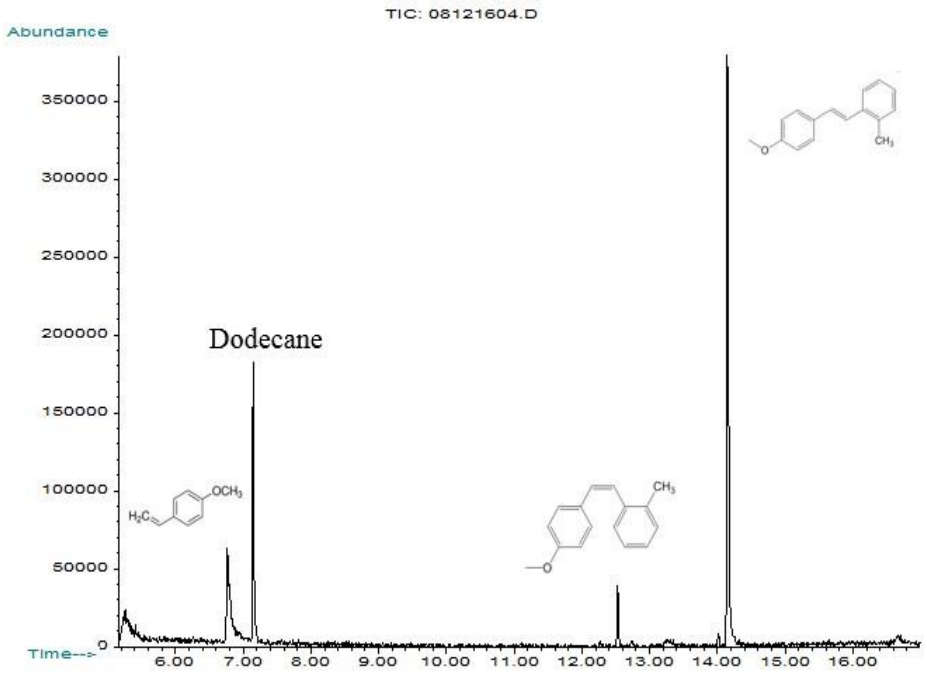

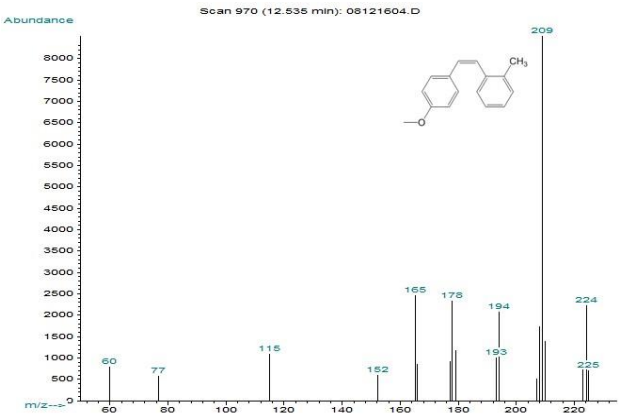

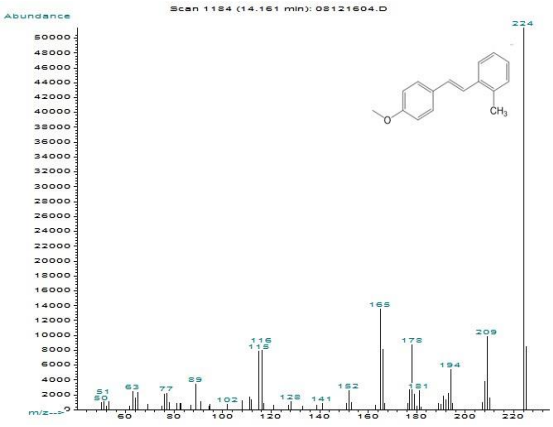

4-vinylanisole and 1-iodo-2-nitro-benzene

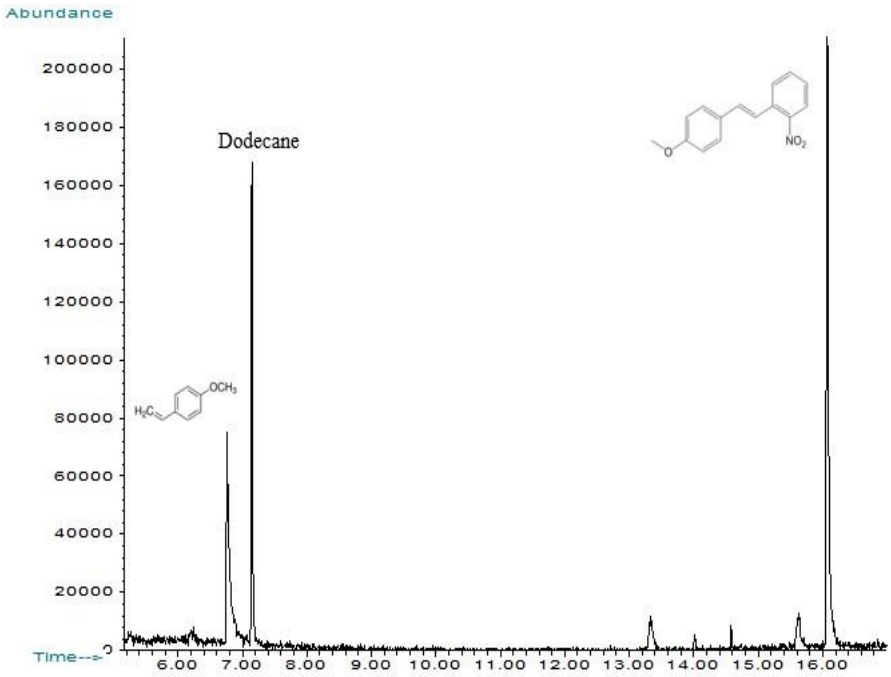

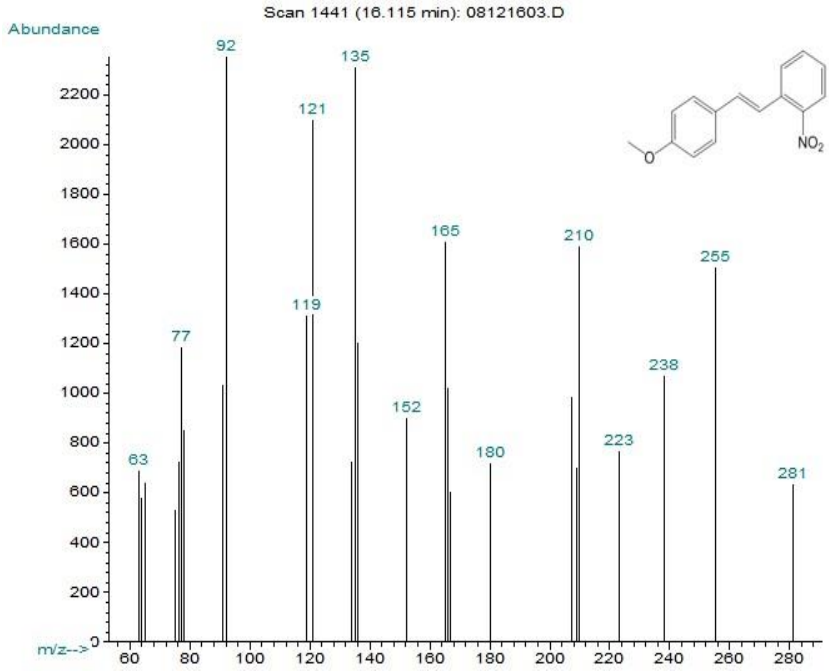

Styrene and 2-bromoiodobenezene

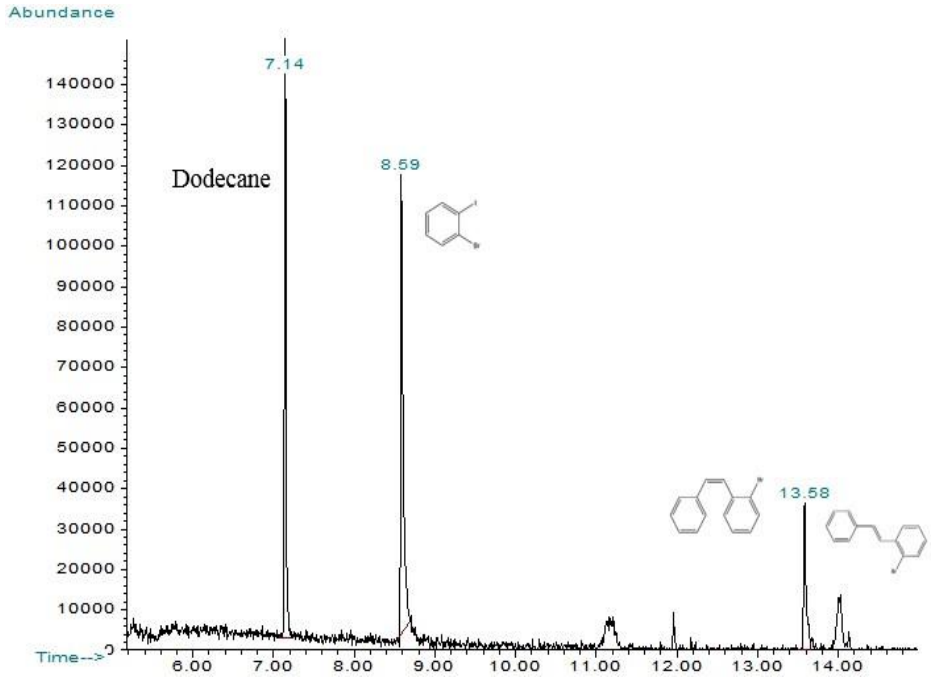

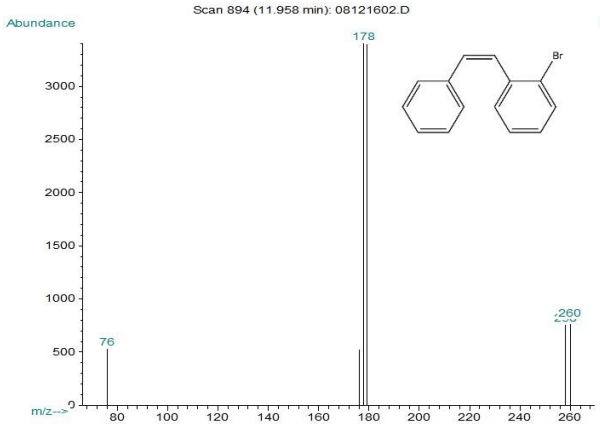

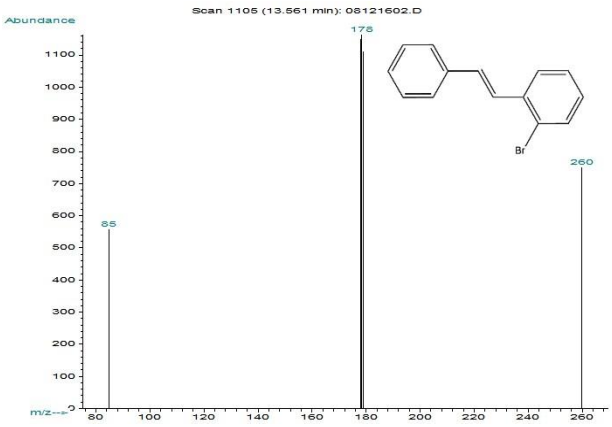

Styrene and 2-iodotoluene

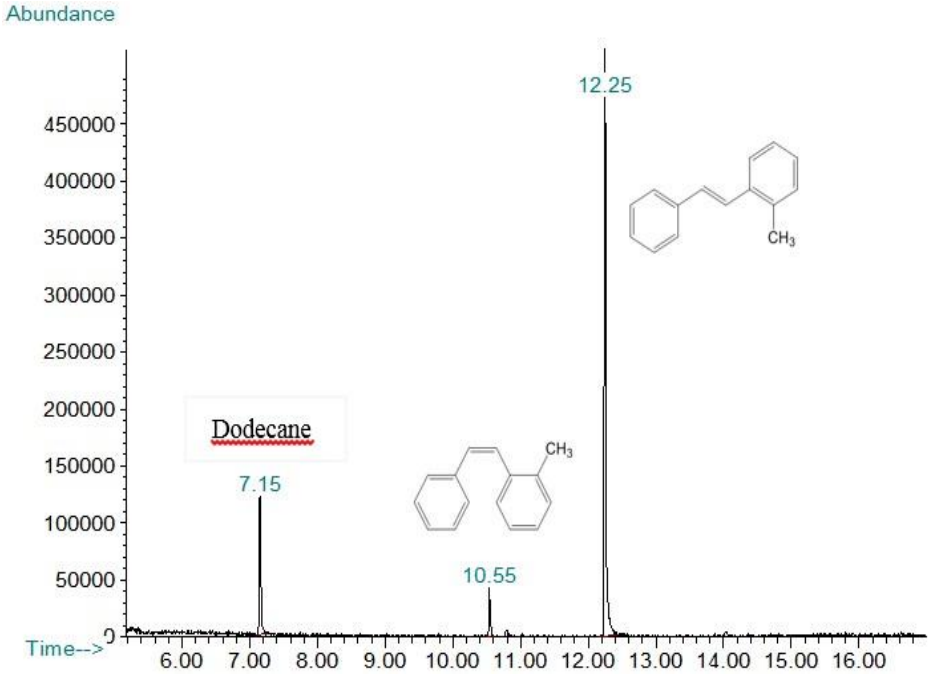

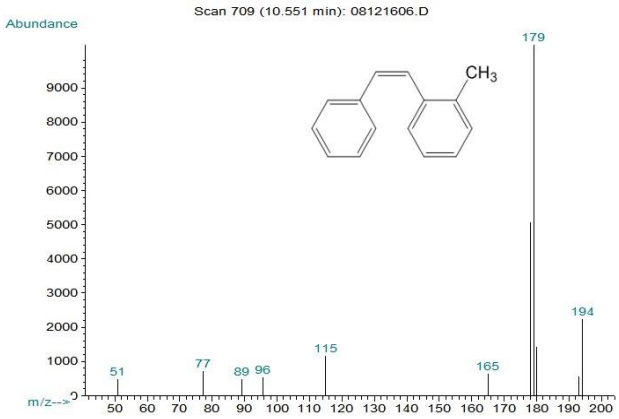

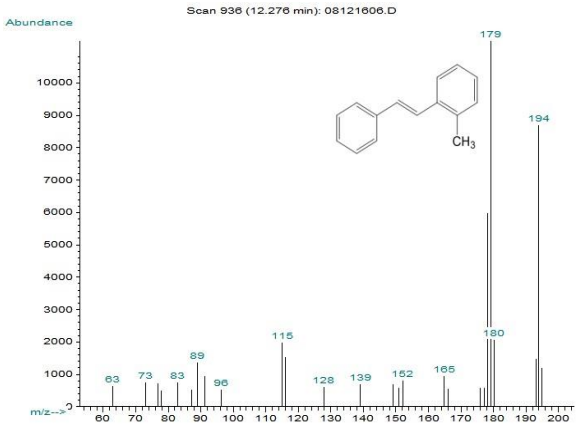

Styrene and 1-iodo-2-nitro-benzene

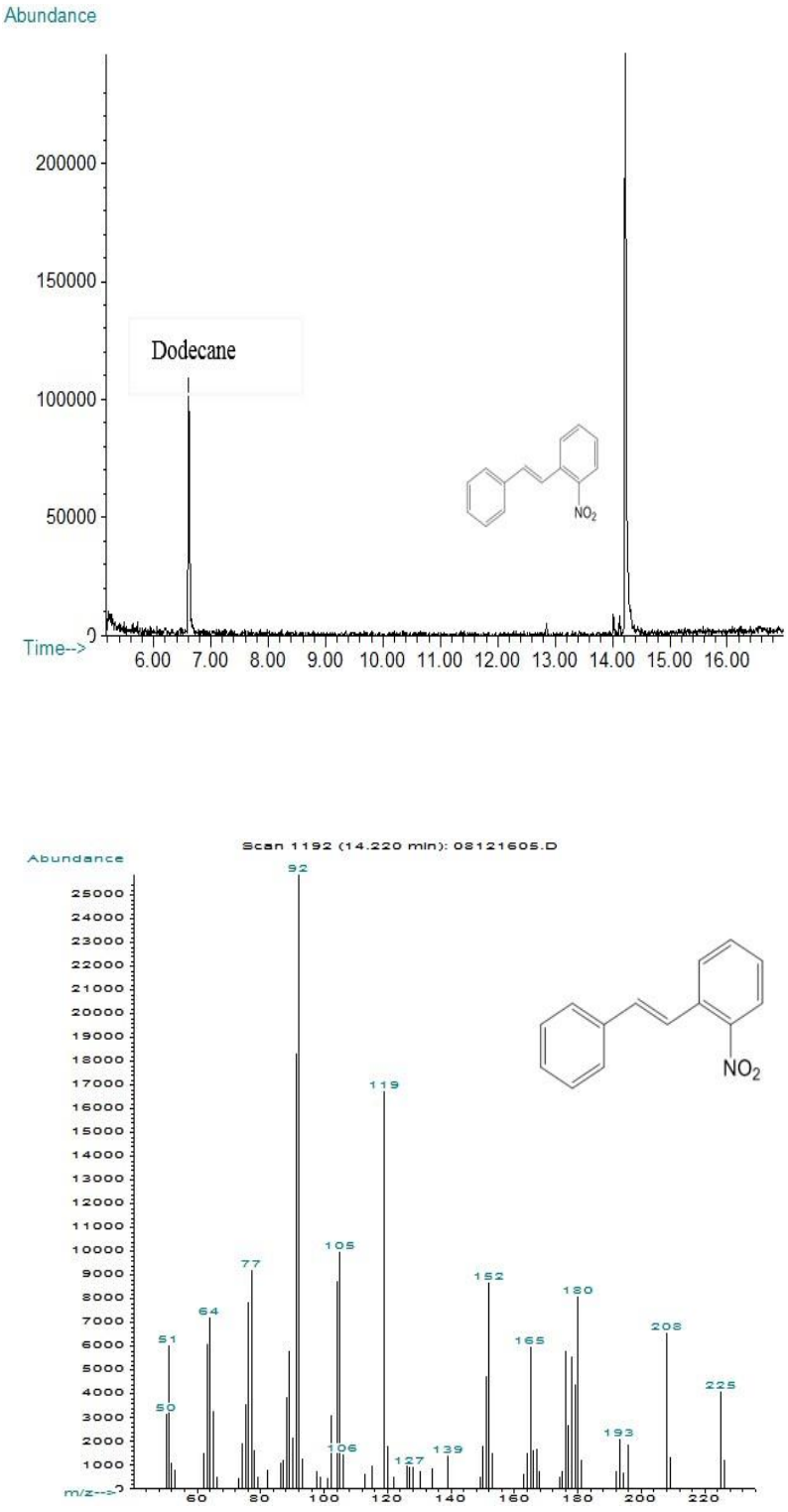

Figure S5. GC-MS spectra for the reaction product of batch Heck coupling reactions over Pd(II)/APS/PAI-HF catalysts.

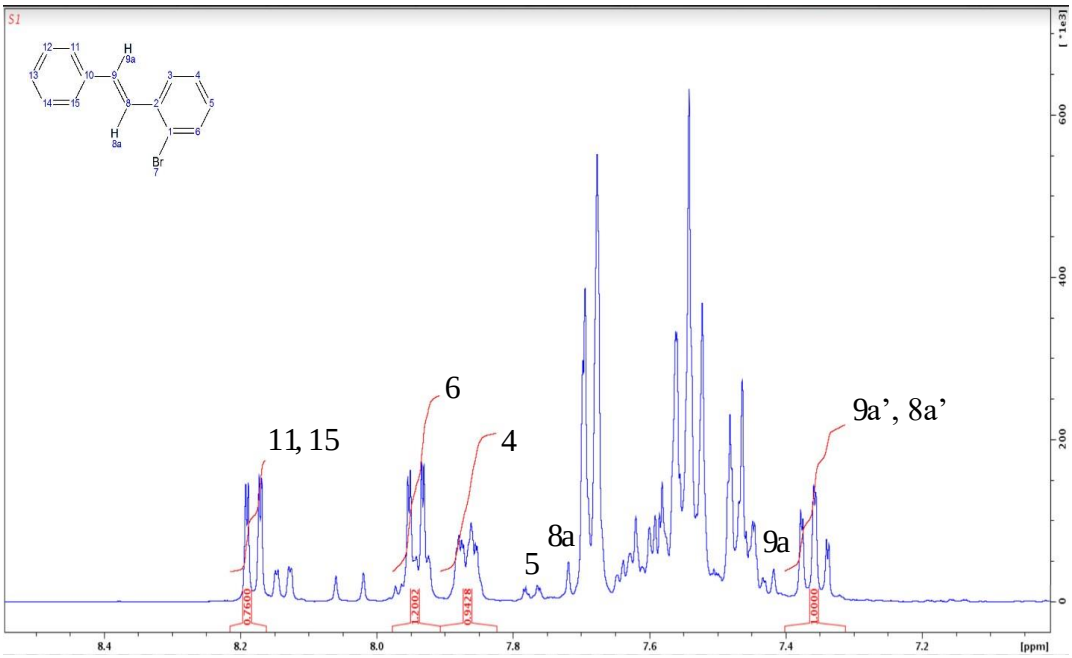

Figure S6. ^{1}H NMR spectra for the reaction product of continuous Heck coupling reactions (styrene and 2-bromoiodobenzene) over Pd(II)/APS/PAI-HF.

REFERENCES

1. Rownaghi, A. A.; Rezaei, F.; Labreche, Y.; Brennan, P. J.; Johnson, J. R.; Li, S.; Koros, W. J. In Situ Formation of a Monodispersed Spherical Mesoporous Nanosilica – Torlon Hollow-Fiber Composite for Carbon Dioxide Capture. *ChemSusChem* **2015**, *8*, 3439–3450.

2. Vandenberg, E. T.; Bertilsson, L.; Liedberg, B.; Uvdal, K.; Erlandsson, R.; Elwing, H.; Lundström, I. Structure of 3-Aminopropyl Triethoxy Silane on Silicon Oxide. *J. Colloid Interface Sci.* **1991**, *147* (1), 103–118.

3. Brennan, P. J.; Thakkar, H.; Li, X.; Rownaghi, A. A.; Koros, W. J.; Rezaei, F. Effect of Post-Functionalization Conditions on the Carbon Dioxide Adsorption Properties of Aminosilane-Grafted Zirconia/Titania/Silica-Poly (Amide-Imide) Composite Hollow Fiber Sorbents. *Energy Technol.* **2017**, *5*, 327–337.

4. Rownaghi, A. A.; Kant, A.; Li, X.; Thakkar, H.; Hajari, A.; He, Y.; Brennan, P. J.; Hosseini, H.; Koros, W. J.; Rezaei, F. Aminosilane-Grafted Zirconia-Titania-Silica Nanoparticles/Torlon Hollow Fiber Composites for CO2 Capture. *ChemSusChem* **2016**, *9*, 1166–1177.

III. AMINOSILANE-GRAFTED SiO_2-ZrO_2 POLYMER HOLLOWFIBERS AS BIFUNCTIONAL MICROFLUIDIC REACTOR FOR TANDEM REACTION OF GLUCOSE AND FRUCTOSE TO 5-HYDROXYMETHYFURFURAL

Yingxin He[a], Arun K. Itta[b], Abdo-alslam Alwakwak[a], Ming Huang[c], Fateme Rezaei[a], Ali A. Rownaghi[a*]

[a]Department of Chemical and Biochemical Engineering, Missouri University of Science and Technology, 1101 N State St., Rolla, MO 65409, United States

[b]School of Chemical & Biomolecular Engineering Georgia Institute of Technology 311 Ferst Dr. NW, Atlanta, GA 30332, United States

[c]Department of Chemistry, Missouri University of Science and Technology, 400 West 11th Street, Rolla, Missouri 65409, United States

ABSTRACT

In this study, we demonstrate the concept of tandem reaction for glucose and fructose to 5-hydroxymethylfurfural (HMF) in an aminosilane-grafted SiO_2-ZrO_2 polyamide-imide hollow fiber that acts as a bifunctional heterogeneous catalyst and microfluidic reactor. The bifunctional catalysts were formed by embedding SiO_2 and ZrO_2 nanoparticles into polyamide-imide polymer dope that underwent subsequent phase inversion through "dry-jet, wet-quench spinning" process to form hollow fibers, followed by post-grafting with aminosilane to incorporate amine moieties into the hollow fibers. The tandem strategy integrated the first step of glucose isomerization with the subsequent step of dehydration of fructose to HMF over bifunctional Lewis and

Brønsted acid sites of hollow fiber microfluidic reactor at different temperatures (100-150 °C) and reaction times (1- 8 h). Our results indicated through optimizing the Lewis to Brønsted sites acid ratio in hollow fiber catalysts, the HMF selectivity enhances from 21 to 82% and 21 to 34% by using fructose and glucose as feedstock's, respectively. The effect of water on glucose isomerization and fructose dehydration to HMF was also studied. Investigation of the stability and efficiency of bifunctional catalysts through recycling experiments revealed that this tandem microfluidic system enables precise control of the reaction flow rate, temperature, and time while eliminates the need for additional catalyst separation step and opens up new opportunities for the conversion of sugar molecules in a continuous-flow system.

Keywords: Fructose; 5-hydroxymethylfurfural; Tandem reactions; Bifunctional Lewis and Brønsted catalysts; Continuous-flow reactor.

1. INTRODUCTION

5-hydroxymethylfurfural (HMF) is an important bio-based precursor molecule for various building blocks such as liquid biofuels, polymers, and intermedia organic compounds that can be converted into a wide variety of valuable chemicals.[1–5] U.S. Department of energy has listed this chemical as one of the top value-added biochemicals due to its versatility and multifunctionality. Nevertheless, HMF is yet to be produced at an industrial scale. Therefore, it is highly desirable to develop efficient processed for the production of HMF from sugar molecules such as glucose and fructose. It has been

demonstrated that catalytic materials are critical for enhancing isomerization of glucose to fructose, which is an equilibrium-limited reaction, and fructose dehydration to HMF.[6] In this regard, transformation of glucose and fructose to HMF has been studied over both homogeneous catalysts such as $CrCl_3$, $SnCl_4$, $AlCl_3$, and liquid acids, and heterogeneous catalysts such as $H_3PW_{12}O_{40}$ salts, hydrotalcites, hybrid organic-inorganic anatase (such as hybrid-TiO_2), cationized zeolites, organic bases, anionized resins, porous coordination polymers, and phosphoric-acid-treated metal oxides.[3,6–18] Compared with homogeneous analogues, heterogeneous catalysts have attracted increasing attention owing to their facile recovery and adjustable acidity as well as a wide range of operation conditions.[1,19]

Interest in fructose and glucose to HMF reaction has been greatly expanded with the discovery of bifunctional catalysts that contain two distinct catalytic sites that can act as cooperative catalysts for achieving a higher reaction rate than that achieved by using either of the catalytic species independently or their homogeneous analogs.[16,19–22]

The tandem reaction of glucose to HMF over bifunctional Lewis and Brønsted acid sites has been studied since this approach enhances the glucose isomerization reaction equilibrium and does not require separation of intermediates.[18,19,23–26] It has been well-documented in the literature that the Brønsted-Lewis bifunctional sites are necessary for the one-pot conversion of glucose to HMF. [2,7,16,19,27] Previous studies reported that Lewis-acidic TiO_2 and ZrO_2 particles can improve HMF yield from glucose and demonstrated that more effective organocatalysts-stabilizing sites can be created upon incorporation of zirconia-titania-silica particles.[9,18,19,28–32] However, it has been reported that the reaction rates are limited by surface reaction and mass transfer during the tandem reactions of glucose isomerization and fructose dehydration over bifunctional catalysts.[33] Among

various heterogeneous catalysts investigated to date, catalyst embedded in porous polymers have been shown to exhibit high catalytic activity towards HMF owing to their large surface area, tunable pore size, and versatile architecture.[2,6,8,34,35] However, catalyst deactivation presumably through leaching of catalytically active species in polar reaction media from the porous polymer as well as their unknown reaction mechanism limit their widespread use in such processes. Compared to solid catalysts, immobilized Lewis acid/Brønsted acid on porous polymers have significant processing advantages including improved thermal management, mixing control and the application of extreme reaction conditions that can enhance the catalytic activity.

Furthermore, in recent years, various approaches have been developed for immobilization and subsequent anchoring of the homogeneous catalysts on solid surfaces and, in particular, within microstructured reactors.[36–41]

However, many applications of microfluidic reactor-supported catalysts are still hampered by linkers/catalysts decomposition and their subsequent leaching from the microfluidic reactor to the product stream.[42,43] In addition, most of the literature on flow reactors have taken approaches inspired by earlier continuous packed-bed microreactor studies and do not address issues of permanent immobilization of catalyst species, economic feasibility, and scalability.

Incorporating bifunctional catalysts into the walls of the porous polymer presents an alternative to traditional monoliths.[44–46] The porous polymer networks consist of hierarchical pore structure which could be used to support catalyst active species. The porous polymer formation allows a variety of Lewis acid/Brønsted acid catalysts to be immobilized upon the surface, thus leading to catalysis of numerous reaction steps in a

continuous-flow platform. With the aim of demonstrating the concept of hollow fiber microreactor for chemical transformations, we previously immobilized organocatalysts and Pd nanoparticles on the surface of polyamide−imide (PAI) hollow fibers.[44,45] This novel hollow fiber microreactor was used as heterogeneous bifunctional catalysts and continuous-flow reactor for Heck coupling,[45] CO_2 cycloaddition,[46] and aldol and nitroaldol condensation[44] reactions. The results revealed a high conversion and modular selectivity toward different products with very short reaction times (1−5 min) at 50−150 °C and ambient pressure. Our findings also revealed that the turnover frequency (TOF) and selectivity can be tuned and controlled by adjusting the chemistry and cooperative interaction of bifunctional catalysts, reaction solvents, reactants, and flow rates. Furthermore, porous hollow fiber polymer with tunable bifunctional catalysts can meet or exceed those achievable by other heterogeneous catalysts reported previously.[1,7,16,25] The active sites are immobilized in the microchannels of the composite catalyst permanently without the loss of stability, which eliminates the necessity for further catalyst separation from the product.

In this investigation, we describe an integrated microfluidic transformation platform for efficient and direct conversion of fructose and glucose to HMF without the need for separation of intermediates and catalysts, in continuous-flow fashion. As shown in Scheme 1, this tandem strategy integrates the first step of glucose isomerization with the subsequent step of dehydration of fructose to HMF over bifunctional Lewis and Brønsted acid sites in the single hollow fiber microfluid reactor at different temperatures and reaction times. A series of Lewis acid/Brønsted acid catalysts were immobilized on the surface of silica−zirconia-incorporated polymeric hollow fibers by surface grafting and investigated

in glucose/fructose conversion to HMF. To the best of our knowledge, this is the first microfluidic hollow fiber reactor system for HMF formation. The amine functional groups in APS-grafted hollow fibers can also be utilized as bifunctional catalysts for cooperative interactions in tandem reactions (i.e., acid−base catalysis).[21,44,46]

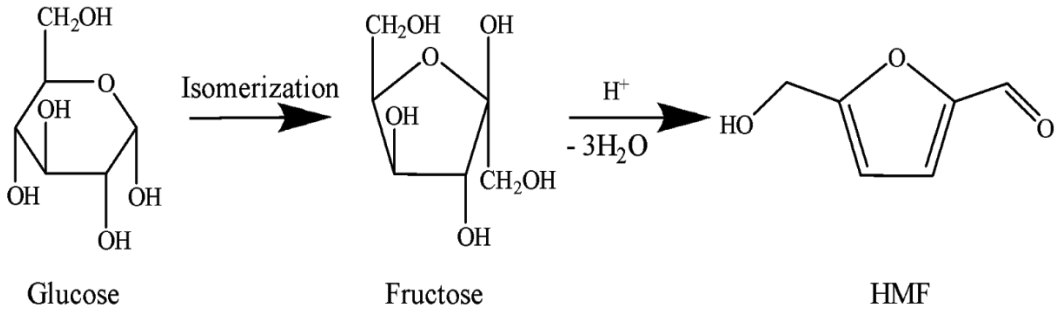

Scheme 1. Reaction scheme of direct glucose conversion to HMF.

2. EXPERIMENTAL SECTION

2.1. MATERIALS

Composite hollow fiber catalysts were spun by using polyamide−imide (PAI) was supplied from Solvay Advanced Polymers (Alpharetta, GA), pore former polyvinylpyrrolidone (average MW ≈ 1 300 000) and N-methyl-2-pyrrolidone (anhydrous NMP, ACS reagent, >98.5%, 99.5%), zirconia (average particle size 100 nm, surface area of 600 m^2/g, and pore size of 5 nm) and silica (average particle size 100 nm, surface area of 300 m^2/g, and pore size of 4 nm) were purchased from Sigma-Aldrich used for polymer dope preparation. The heterogeneous organocatalysts were prepared using a primary

aminosilane (3-aminopropyltrimethoxysilane, APS 95% from Sigma-Aldrich) that was grafted to zirconia−silica/PAI hollow fibers. Glucose (99%), D-(−)-fructose (99%), lauric acid (99%), 5-hydroxymethylfurfural (HMF), dimethyl sulfoxide (99.5%, DMSO), dimethylformamide (DMF), acetonitrile, and methanol were also purchased from Sigma-Aldrich and used without further treatment for the catalytic test. Nitrogen was purchased from Airgas and used to purge the sample in a continuous-flow system.

2.2. FORMATION OF BIFUNCTIONAL SiO_2-ZrO_2 HOLLOW FIBER CATALYSTS

The "dry-jet, wet-quench spinning" method was used for formation of SiO_2−ZrO_2 poly(amide-imide) hollow fibers (PAI-HFs) in this work has been described in detail in previous works.[44−48] PAI hollow fibers readily dissolve in polar aprotic solvents, and thus, they should be post treated prior to utilization as heterogeneous catalysts and as a flow reactor. To improve the hollow fiber stability and compatibility in polar aprotic solvents (e.g., DMSO, NMP, and DMF) that are commonly used in chemical transformation reactions in flow, the porous PAI hollow fibers were grafted with aminosilane inorganic network structures by further condensation of APS at 80 °C for 2 h in a mixture of toluene and water. Finally, the APS-exposed SiO_2-ZrO_2 PAI hollow fibers were washed with ethanol and dried under vacuum at 80 °C for 2 h. Three sets of hollow fiber reactors were developed for conversion of glucose to fructose and fructose dehydration to HMF, namely, aminebased catalyst (APS/PAI-HF) and bifunctional catalysts (APS/SiO_2/PAI-HF and APS/SiO_2-ZrO_2/PAI-HF). As a control material, bare SiO_2-ZrO_2/PAI-HF that contained weakly acidic silanol groups and Lewis acid sites was also developed and evaluated.

2.3. CHARACTERIZATION OF HOLLOW FIBER CATALYSTS AND REACTION PRODUCTS

Aminosilane grafting onto SiO_2-ZrO_2/PAI hollow fibers were confirmed by Fourier transform infrared spectroscopy (FTIR) in the range of 400−4000 cm^{-1} by a Bruker Tenser instrument. The spectra were acquired at a 4 cm^{-1} resolution. Amine loading and SiO_2/ZrO_2 content were determined by inductively coupled plasma optical emission spectroscopy (ICP-MS). The corresponding results are given in Table 1. The BET surface area, BJH pore volume, and average pore size of hollow fiber catalysts were determined using nitrogen isotherms (−196 °C) in a Micromeritics 3Flex. Prior to analysis, the PAI hollow fiber catalysts were degassed at 110 °C under vacuum for 12 h to remove any preadsorbed species from the pores of the materials. The high-resolution scanning electron microscope (Hitachi S-4700 FESEM) was used to assess the morphology of the bare and grafted hollow fibers. The total amount of Brønsted acid sites and Lewis acid sites were determined on a Bruker Tensor 27 FTIR spectrometer.

To analyze the reaction products, the samples were quenched by submergence in a water bath followed by separation and filtration of liquid phases. The characterization was carried out by ^{1}H NMR spectra at room temperature using a Bruker-DRX 400 MHz spectrometer ^{1}H liquid-state NMR CPMAS TOSS (^{1}H NMR). In addition, the analysis of products was performed by using high-performance liquid chromatography (HPLC) system. The Agilent HPLC equipped with ultraviolet (UV) and refractive index (RI) detectors, C18 reversed phase column (100 mm × 4.6 mm, 4 μm), and Aminex HPX-87H (300 mm × 7.8 mm, 5 μm) columns. UV and RI detectors were used for measuring HMF and sugar molecules, respectively. Both glucose and fructose were monitored using an RI detector for aqueous phase, while HMF production was monitored using a UV detector.

The mobile phases used for these analyses consisted of acetonitrile/water = 80:20 (V/V) (with the flow rate of 0.6 mL/min) for Luna C18, and 0.01 mol/ L H_2SO_4 (with the flow rate of 0.6 mL/min) for Aminex HPX-87H, being the columns at room temperature and 60 °C, respectively.

2.4. ISOMERIZATION OF GLUCOSE TO FRUCTOSE AND FRUCTOSE DEHYDRATION TO HMF REACTIONS

2.4.1. Batch Dehydration Reaction of Fructose to HMF. All fructose dehydration batch reactions were performed in the presence of three different catalysts (e.g., APS/PAI-HF, APS/SiO_2/PAI-HF, and APS/SiO_2-ZrO_2/PAI-HF) catalysts in a 25 mL one-neck flask reactor equipped with a reflux glass condenser. In a typical procedure, 10 mL mixture of 0.5 g D-(−)-Fructose was dissolved in 10 mL DMSO. After that, about 20 mol% of hollow fiber catalysts (by amine loading, about 50 mg) was added to a clean 25 mL one-neck flask with the fructose DMSO solution. The system was then heated under a thermostatically and timer-controlled oil bath with a magnetic stir bar. The experiments over various hollow fiber catalysts were conducted under different reaction temperature (100, 125, and 150 °C) and reaction time (1, 2, 4, and 6 h) to identify the best reaction conditions that yield the best reaction performance. Reactants conversion for fructose dehydration were determined using HPLC equipped with UV detector (at about 284 nm), and ^{1}H NMR.

2.4.2. Batch Isomerization/Dehydration Reactions of Glucose to HMF. Two sets of glucose dehydration reaction in a batch system were conducted over various hollow fiber catalysts in a 25 mL of one-neck flask reactor equipped with a reflux glass condenser under 150 °C with different reaction times. For the first set, 10 mL mixture of 0.5 g glucose was first dissolved in 10 mL DMSO followed by the addition of about 20 mol% of hollow

fiber catalysts into the solution. The other set of the reaction was conducted under similar conditions except for the use of a different solvent (20% H_2O in 80% DMSO) to study the effect of the existence of H_2O on the glucose dehydration reaction.

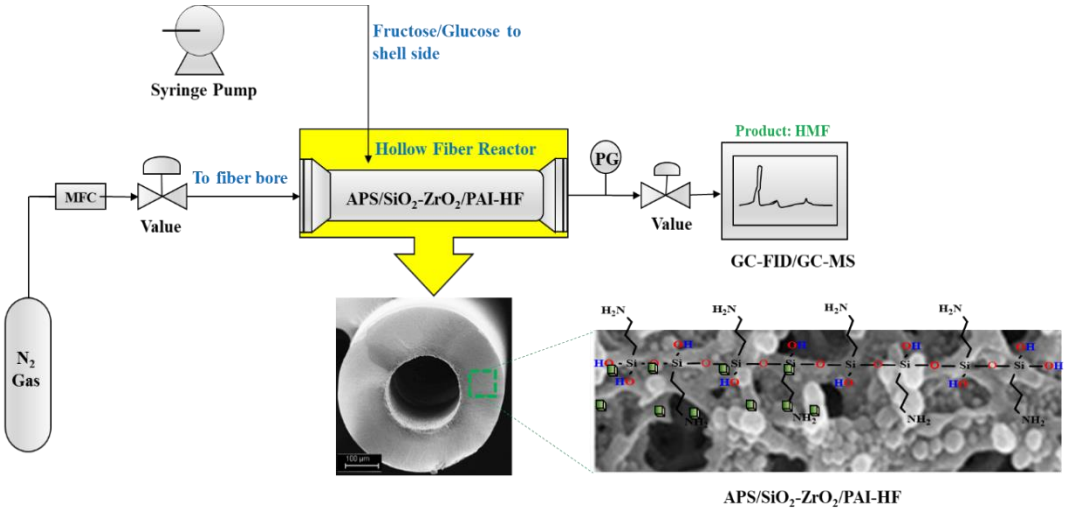

Figure 1. Schematic diagram of a hollow fiber microfluidic reactor for fructose dehydration reaction.

2.4.3. Continuous Flow Dehydration Reaction of Fructose to HMF. To test the cooperative Lewis acid/Brønsted acid-catalyzed conversion of fructose to HMF over SiO_2-ZrO_2/PAI-HFs in continuous-flow platform, a hollow fiber module with inner diameter of 0.1 μm, length of 15 cm, total volume of 10 mL, and five fibers was constructed and exposed to reaction mixture at flow rate of 0.02 mL/min and different reaction temperatures (100 and 125 °C). The schematic diagram of the experimental setup is shown in Figure 1. To start the fructose dehydration reaction, the mixture solution was introduced from hollow fiber shell side at a flow rate of 0.02 mL/min, while nitrogen was introduced from hollow

fiber bore side at 25 mL/min flow rate to prevent pore blockage and also push the product out of the bore. The schematic diagram of the system is depicted in Figure 1.

2.4.4. Catalyst Recycling. Recycling experiments with all hollow fiber catalysts were also undertaken to determine the degree of reusability and extent of oxides leaching from the fibers. After each reaction cycle, the used hollow fiber catalysts were dried in vacuum oven at 80 °C for 3 h to completely remove all the reactants and products molecules adsorbed in/on the pores prior to the next cycle. The textural properties and catalyst activity of the catalysts were investigated after three cycles and compared with those of fresh materials.

3. RESULTS AND DISCUSSION

3.1 CHARACTERIZATION OF HOLLOW FIBER CATALYSTS

Successful aminosilane grafting was confirmed by comparing the FTIR spectra of hollow fiber catalysts before and after APS exposure (Figure S1, Supporting Information). The characteristic imide peaks such as C=O absorbance at 1778 and 1719 cm^{-1}, and C-N stretching vibration at 1360 cm^{-1} disappeared in the spectra of bare aminosilane-grafted fiber catalysts. On the other hand, several new absorption bands appeared at 3367-3371 cm^{-1} and 3301-3308 cm^{-1} which were correlated to asymmetric and symmetric NH_2 stretching vibrations, respectively. Moreover, another clear peak at 1515-1570 cm^{-1}, related to NH_2 deformation, was observed after amine incorporation. For APS/SiO_2-ZrO_2/PAI-HF, there was a slight shift towards lower wavenumbers in the position of the NH_2 symmetric vibration which may be due to the bonding of zirconia, titania, and silica nanoparticles with the amine groups, in agreement with the literature.[48,50,51]

The amine loading and metal oxide content of the hollow fiber catalysts were determined by elemental analysis and the results are presented in Table 1. The total amount of amine loading and SiO_2, the ZrO_2 content of hollow fiber catalysts were found to be approximately 20 wt.% of fiber weight (~7 wt.% each oxide). Moreover, the APS/SiO_2-ZrO_2/PAI-HF with 20 wt.% metal loading was demonstrated to have a nitrogen loading of 6.2 mmol N/g. The scanning electron microscopy (SEM) images of the hollow fiber catalysts (shown in Figure S2, Supporting Information) demonstrated that the fiber catalysts retained sufficient porosity after aminosilane grafting for effective catalytic performance.

The N_2 physisorption isotherms for bare, APS-grafted and used SiO_2-ZrO_2/PAI-HF are shown in Figure 2. As evident from this figure, all hollow fiber catalysts exhibited type IV isotherm with H_2-type hysteresis between adsorption and desorption branches according to the IUPAC classification. Nitrogen uptake dropped after incorporation of metal oxides and aminosilane grafting, suggesting that the pore structure of hollow fiber catalysts partially collapsed after aminosilane grafting as a result of successful incorporation of APS moieties into the hollow fibers and partial filling of the smaller pores of the corrugated fiber substructure. The reaction of aminosilane molecules with the imide groups of PAI polymer occurred through ring-opening of phthalimide matrix, as demonstrated before.[48,50,51]

The surface area and pore volume (at P/P_0 = 0.99) of fibers estimated from physisorption data are summarized in Table 1. The SiO_2-ZrO_2/PAI-HF showed higher surface area and porosity before and after reaction than the SiO_2/PAI-HF and pure PAI-HF. Furthermore, compared with bare hollow fibers, the BET surface area, pore volume,

and N_2 flux (determined from permeance experiments) of used hollow fibers decreased by approximately 50% after reaction at 150 °C and run for 6 h. In addition, the metal loading data indicated negligible SiO_2 and ZrO_2 leaching from the hollow fibers after fructose dehydration reaction.

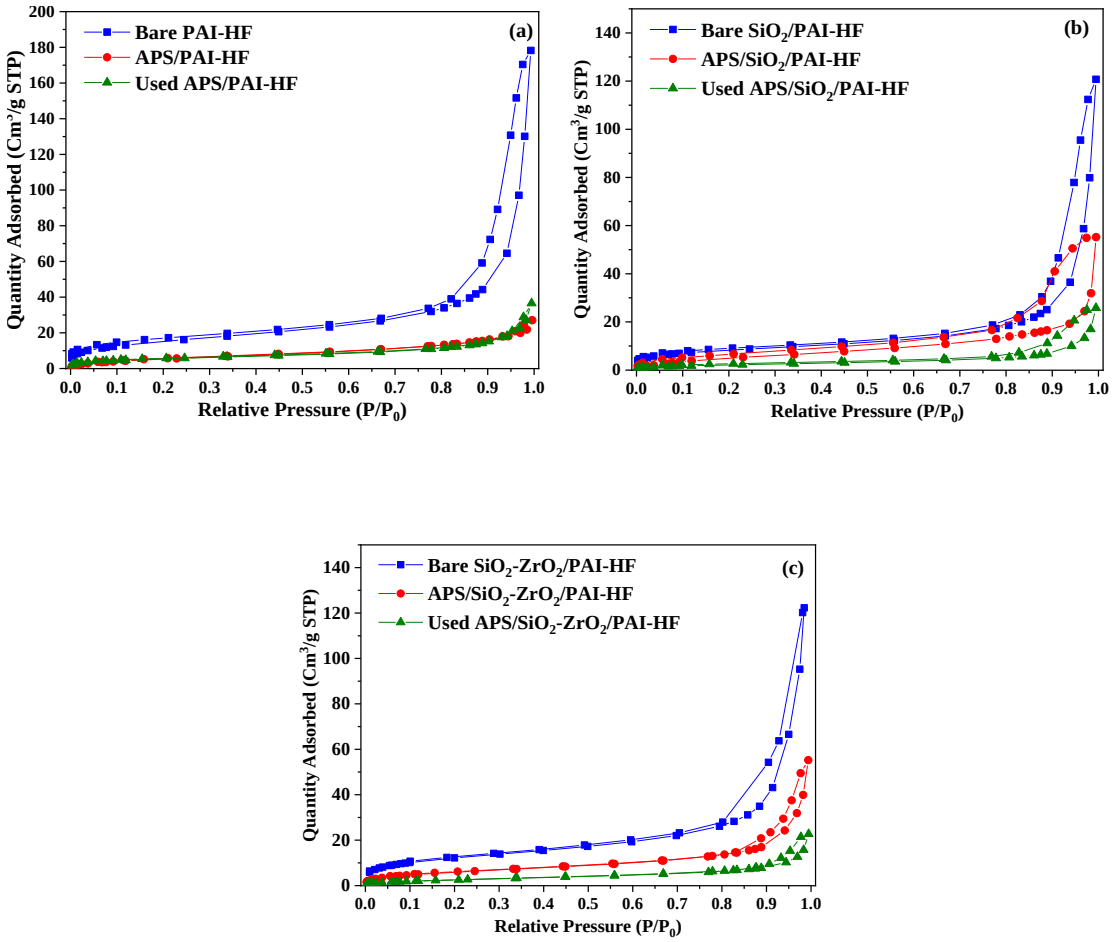

Figure 2. Nitrogen adsorption/desorption isotherms for bare, APS-grafted, and used (a) PAI-HF, (b) SiO_2/PAI-HF, and (c) SiO_2-ZrO_2/PAI-HF.

Table 1. Textural properties N_2 permeance and amine and metal oxide loading of the resulting aminosilica bifunctional hollow fiber catalysts.

Catalyst	S_{BET} (m^2/g)[a]	V_{pore} (cm^3/g)[a]	Permeance (GPU)[b]	Amine loading (mmol N/g)[c]	Metal oxide loading (wt.%)[b]	
					SiO_2	ZrO_2
PAI-HF	56	0.27	88,000	0.00	-	-
APS/PAI-HF	21	0.14	35,000	-	0.1	-
Used APS/PAI-HF	8	0.04	6,000	-	0.1	-
SiO_2/PAI-HF	40	0.14	100,000	0.00	19.5	-
APS/SiO_2/PAI-HF	20	0.08	35,000	5.82	20.5	-
Used APS/ SiO_2/PAI-HF	15	0.07	9,000	-	18.0	-
SiO_2-ZrO_2/PAI-HF	45	0.19	112,000	0.00	11.0	8.5
APS/SiO_2-ZrO_2/PAI-HF	27	0.12	40,000	5.73	12.0	8.5
Used APS/SiO_2-ZrO_2/PAI-HF	10	0.06	8,000	-	10.5	8.0

[a] Determined by nitrogen physisorption experiments at 77 K.

[b] GPU refers to 1×10^6 cc (STP)/(cm^2 s cmHg).

[C] Amine and metal oxide loadings determined by elemental analysis.

Previous studies have pointed out that maximum activity in glucose dehydration reactions could be achieved when surface acid sites such as Brønsted and Lewis acid sites with amines provide cooperative catalysis character.[1,8,18,19] The number of Brønsted and Lewis acid sites on each of the hollow fiber catalysts was determined by pyridine IR spectroscopy measurements and the corresponding spectra are presented in Figure 3. High-intense characteristic peaks of Brønsted acid sites[49] at 1675, 1620, and 1500 cm^{-1} and Lewis acid sites[49] at 1443, 1550, and 1625 cm^{-1} were observed on the APS/SiO_2-ZrO_2/PAI-

HF; the intensity of these peaks was found to be much smaller for APS/PAI-HF and SiO_2/PAI-HF, indicating a much less amount of Brønsted acid sites in these fibers. Notably, the observed peak at 1600 cm^{-1} in the spectra of APS/PAI-HF and SiO_2-ZrO_2/PAI-HF was attributed to weakly physisorbed (hydrogen-bonded) pyridine.[21,49] In addition, Figure 3 shows that the Brønsted and Lewis acids sites on APS/SiO_2-ZrO_2/PAI-HF were better balanced than those on APS/SiO_2/PAI-HF. These results demonstrate that the APS/SiO_2-ZrO_2/PAI-HF catalyst possessed a sufficient number of Brønsted and Lewis acid sites for synergistic cooperation with APS moieties, thereby imparting cooperative catalysis character to the catalyst.

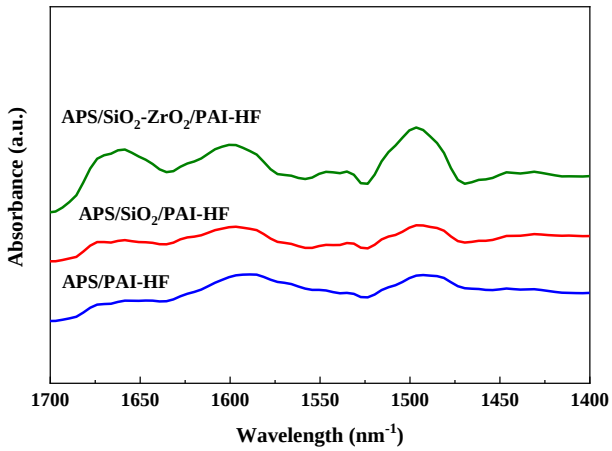

Figure 3. Pyridine IR spectra of hollow fiber catalysts obtained at 50 °C.

The amount of both acid sites for different hollow fiber catalysts are listed in Table 2. Whereas negligible acid site density was estimated for APS/PAI-HFs and APS/SiO_2/PAI-HFs, the APS/SiO_2-ZrO_2/PAI-HFs exhibited 7 and 13 μmol/g Brønsted

acid and Lewis acid sites, respectively. The significant discrepancy in the acidity of the hollow fiber catalysts stems from the presence of Zr^{IV} in APS/SiO_2-ZrO_2/PAI-HF. It has been shown that the Lewis acid sites are mainly ascribed to the Zr^{IV}. These FTIR results are consistent with the ICP-MS elemental analysis, by which the amount of Zr^{IV} in SiO_2-ZrO_2/PAI-HF was determined to be 8.5 wt %. It has been shown that Brønsted acidic sites can enhance the dehydration of fructose into HMF, whereas the Lewis acidic sites play an important role in the glucose isomerization[16]. Therefore, the ratio of Brønsted/Lewis acids is another important metric impacting the yield of HMF.

Table 2. Total amounts of Brønsted and Lewis acid sites for the aminosilica bifunctional hollow fiber catalysts, determined by pyridine IR experiments at 50 °C.

Materials	**Brønsted acid sites** (μmol/g-fiber)	**Lewis acid sites** (μmol/g-fiber)
APS/PAI-HF	2	0
APS/SiO_2/PAI-HF	4	0
APS/SiO_2-ZrO_2/PAI-HF	7	13

3.2 DEHYDRATION REACTION OF FRUCTOSE TO HMF-BATCH EXPERIMENTS

Before catalytic conversion of glucose into HMF, the catalytic activity of bare and APS grafted-hollow fiber catalysts was assessed in the heterogeneous dehydration of fructose to HMF as represented in Scheme 1 in both batch and continuous-flow reactions. The corresponding fructose conversion and HMF selectivity results obtained by HPLC and NMR are shown in Table 3 and Figure S4 (Supporting Information), respectively. The

control reactions performed with PAI-HF, SiO_2/PAI-HF, and SiO_2-ZrO_2/PAI-HF (no aminosilane grafted) led to no observable HMF products.

Control experiments showed that bare hollow fiber catalysts were swelled and dissolved in DMSO solvent. Therefore, aminosilane grafting of fibers for formation of amine-tethered inorganic networks in the fiber structure is necessary to prevent fibers swelling and improve their chemical stability and hydrophobicity in aggressive solvents. In these reactions, the activity of APS/PAI-HF and APS/SiO_2/PAI-HF was also evaluated. These hollow fiber catalysts that contain only weakly acidic silanol groups on the silica surface, and weakly basic functional groups (i.e., -NH_2), serve as control materials to exemplify the improvement in catalyst activity from immobilizing aminosilanes that have the ability to behave in a cooperative manner. For APS/PAI-HF, the initial fructose conversion at 100 °C was only 25%, however, it was dramatically increased to 99% by raising the temperature to 150 °C and also increasing the reaction time to 6 h. APS/SiO_2/PAI-HF exhibited improved conversion relative to APS/PAI-HF under the same condition. Interestingly, with the loading of zirconia into SiO_2/PAI-HFs and APS grafting, both Brønsted and Lewis acid sites further increased, as noted before, resulting in much better fructose conversion and HMF selectivity over APS/SiO_2-ZrO_2/PAI-HF catalyst. At 100 °C and after 6 h reaction period, fructose conversion and HMF selectivity over this catalyst reached 100 and 24%, respectively. The combination of weakly Bronsted acidic (silanol groups), Lewis acidic (Zr^{IV}) and basic groups (amines) in APS/SiO_2-ZrO_2/PAI-HF make them bifunctional catalysts for cooperative interactions (i.e., acid-base catalysis). Overall, the results indicate that the ZrO_2 embedded into the polymer hollow fiber matrix is effective for dehydration of fructose to HMF.

The data in Table 3 also demonstrate the effects of reaction time and temperature on fructose conversion and HMF selectivity over three types of catalysts. As can be observed, both parameters had a favorable influence on HMF yield and fructose conversion. The maximum HMF selectivity was obtained after 4 h time on stream, while it slightly dropped at longer reaction time due to the hydrolyzation of HMF and production of side products.[16] Fructose conversion was about 100% over APS/SiO_2-ZrO_2/PAI-HF at 125 and 150 °C. Notably, the conversion of fructose reached 100% over APS/SiO_2-ZrO_2/PAI-HF at a lower reaction temperature of 100 °C. These results further confirm that bifunctional groups can act together to undergo cooperative catalysis, which is not possible with only one monofunctional catalyst.

Table 3. Comparison of the performance of different hollow fiber catalysts in fructose conversion to HMF.

Reaction Temperature (°C)	Reaction time (h)	APS/PAI-HF		APS/SiO_2/PAI-HF		APS/SiO_2-ZrO_2/PAI-HF	
		Fructose Con. (%)	HMF Sel. (%)	Fructose Con. (%)	HMF Sel. (%)	Fructose Con. (%)	HMF Sel. (%)
100	2	25	10.5	60	25	65	22
	4	55	15	93	26	100	30
	6	87	13	96	18	100	24
125	2	69	15	95	18	86	32
	4	97	16	99	14	100	64
	6	97	17	100	17	100	80
150	2	98	21	98	24	98	62
	4	99	23	99	25	100	82
	6	99	23	99	23	100	44

It should be pointed out here that whereas the control materials (bare PAI-HFs, SiO_2/PAI-HFs, and SiO_2-ZrO_2/PAI-HFs) exhibited no activity and resulted in no observable HMF product, the APS/PAI-HF achieved a fructose conversion of 25% with an HMF selectivity of 10.5% after 2 h reaction. These findings highlight the synergistic effect of Brønsted and Lewis acid sites on dehydration of fructose to HMF and the dependency of the of HMF yield on the cooperative interactions of acid-base pairs. The turnover frequencies (TOFs) of APS/SiO_2-ZrO_2/PAI-HF, APS/SiO_2/PAI-HF, and APS/PAI-HF were estimated to be 2.11, 1.05 and 0.60 h^{-1} after the first hour of reaction, respectively, indicating the advantage of embedding zirconia into the composite hollow fiber.

3.3 REUSE OF HOLLOW FIBER CATALYSTS

To evaluate the stability of the bifunctional hollow fiber catalysts, recycling experiments were carried out in which the used hollow fiber catalysts were first recovered from the solvent mixtures, dried under vacuum to sufficiently remove water and other solvents, and then reused in fructose dehydration reaction in fresh reaction mixture under the same reaction conditions as fresh catalysts. The corresponding catalytic results are reported in Table 4 and Figure S3, Supporting Information. It is apparent from these results that both fructose conversion and HMF selectivity were comparable to those obtained with fresh hollow fiber catalysts. The slight activity decrease was possibly due to the loss of accessibility to some of the active sites on porous hollow fiber catalysts and catalyst leaching due to fiber swelling.

Among all hollow fiber catalysts, the recycled APS/SiO_2-ZrO_2/PAI-HF maintained its activity and gave rise to 99% fructose conversion and ~50% HMF yield, respectively implying that they can be reused without significant loss of catalyst active sites. The

recycling experiment demonstrated that the hollow fiber catalyst can be utilized as a heterogeneous catalyst and microfluidic reactor for fructose dehydration.

Table 4. Reuse of different hollow fiber catalysts for fructose dehydration reaction.

Reaction cycle	Reaction time (h)	APS/PAI-HF		APS/SiO_2/PAI-HF		APS/SiO_2-ZrO_2/PAI-HF	
		Fructose Con. (%)	HMF Sel. (%)	Fructose Con. (%)	HMF Sel. (%)	Fructose Con. (%)	HMF Sel. (%)
1st	1	94	22	93	23	98	53
	2	98	22	98	24	98	62
	4	99	23	99	26	100	82
	6	99	23	99	23	100	44
2nd	1	92	21	93	23	98	52
	2	94	24	98	25	99	61
	4	97	26	99	25	97	80
	6	98	20	99	22	99	44
3rd	1	92	22	98	23	99	52
	2	92	22	99	25	99	62
	4	95	24	99	24	99	78
	6	96	23	99	22	99	43

3.4. DEHYDRATION REACTION OF FRUCTOSE TO HMF-CONTINUOUS FLOW EXPERIMENTS

After demonstrating the efficiency, stability, and reusability of APS/SiO_2-ZrO_2/PAI-HF in fructose dehydration reaction in the batch reactor, the performance of this bifunctional catalyst was further evaluated on a continuous-flow platform. Immobilization of bifunctional acid-base character and zirconium nanoparticles within porous polymeric hollow fiber reactor system offer an alternative flow-based synthesis platform for chemical transformation. We carried out a set of proof-of-concept tests to assess the cooperative

catalytic activity of immobilized bifunctional catalysts upon hollow fibers in a continuous-flow system in a stainless-steel module containing five hollow fibers at 150 °C.

As shown in Figure 1, diluted fructose continuously flow through the shell side of the microfluidic reactor containing APS/SiO_2-ZrO_2/PAI-HF with precise control of flow rate (0.02 cm^3 /min), temperature (150 °C), and pressure (1 bar).The HPLC data in Figure 4 show that, after 5 min of reaction, the conversion of fructose and selectivity toward HMF reached 25% and 30%, respectively. These results indicated that the conversion of fructose was lower than that under batch reaction which could be associated with the shorter contact time. Both fructose conversion and HMF selectivity can be optimized by controlling the reactant flow rate. Moreover, as evident from this figure, the catalyst retained its activity for HMF formation within 120 min time on stream at 125 °C. To assess the leaching of silica and zirconia species from the microfluidic reactor, the product samples were analyzed with ICP-MS. Considering the ICP-MS detection limit of <1 ppm, there was no leaching of SiO_2 and ZrO_2. It should be noted that the bifunctional heterogeneous catalysts developed here achieve the same conversion and selectivity compared to recent studies reported by Li et al.[16] on the use of tin porous coordination polymer (SnPCP), and Jeong et al.[25] on the use of sulfonic acid functionalized silica capillary for the same reaction, while being resistant to deactivation and active sites leaching. Another advantage of such systems for tandem reactions of fructose to HMF is the facile control of contact time by varying the flow rate which may prevent over-reactions and production of side products. The hollow fiber could be utilized in microfluidic synthesized functional materials in chemical transformation and separation by simply assembling different catalysts immobilized within

porous hollow fibers for tandem conversion of fructose to HMF into furfuryl alcohol (FFA), 2,5-diformylfuran (2,5-DFF), and 2,5-dimethylfuran (2,5-DMF).

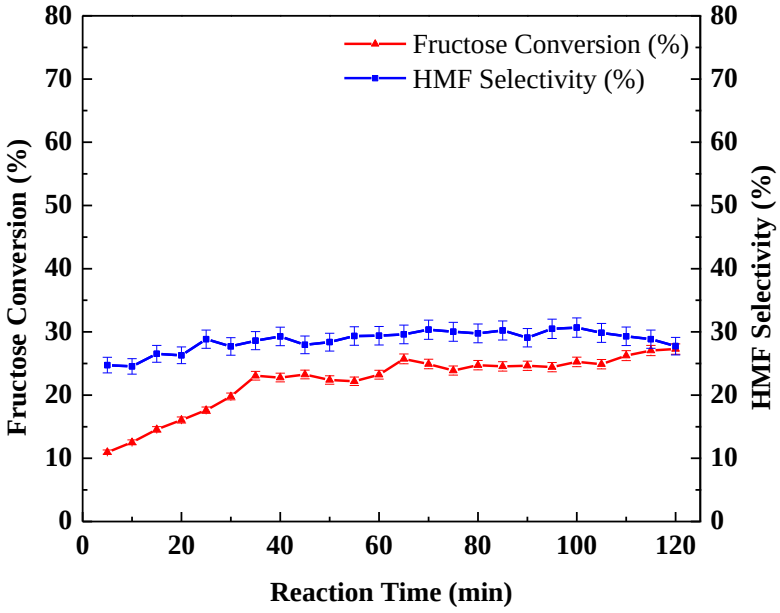

Figure 4. Fructose conversion and HMF selectivity as a function of reaction time over APS/SiO_2-ZrO_2/PAI-HF in DMSO 150 °C.

3.5. TANDEM REACTION OF GLUCOSE TO HMF USING HOLLOW FIBER CATALYSTS

The catalytic conversion of glucose to HMF in the presence of bifunctional Lewis and Brønsted acid sites of hollow fiber catalysts proceeds through a tandem pathway involving isomerization of glucose to fructose, followed by dehydration of fructose to HMF that requires a balance between different catalyst active species to optimize HMF yield. The obtained HPLC and NMR results are summarized in Table 5 and Figure S4, respectively. All three bifunctional hollow fiber catalysts effectively catalyzed the glucose

conversion into HMF at 150 °C from 1-8 h reaction time. In general, the conversion of glucose was enhanced with the longer reaction time overall catalysts. In DMSO solution, the best performing material, APS/SiO_2-ZrO_2/PAI-HF, exhibited a glucose conversion of 100% and an HMF selectivity of 34% after 8 h time-on-stream. Moreover, we explored the effect of Lewis to Brønsted acid (L/B) ratio on the tandem reaction and the behavior of hollow fiber bifunctional catalysts by changing L/B ratio for the first time. We found that APS/SiO_2-ZrO_2/PAI-HF with L/B ratio of ~2 exhibits good catalytic activity in terms of glucose conversion and HMF selectivity.

Zhou et al. [17] reported that the water molecule can facilitate the proton transfer process and enhance the rate of glucose isomerization reaction. To assess this effect on the performance of our composite catalysts, in addition to DMSO being used as a reaction solvent, the mixture of DMSO/distilled water (80:20 wt. %) was also investigated as a solvent indirect conversion of glucose to HMF. As the data in Table 5 suggest, the involvement of water did not promote the glucose conversion and the maximum glucose conversion reached after 8 h reaction time was around 18-40%, which was about three times lower compared to the pure DMSO reaction system. As the glucose dehydration reaction involves losing water from the glucose, thus the presence of higher levels of H_2O in the reaction solvent is generally harmful to the dehydration reaction and slows down the glucose dehydration reaction.

Table 5. Glucose conversion and HMF selectivity in DMSO and DMSO/water solvents.

Reaction cycle	Reaction time (h)	APS/PAI-HF		APS/SiO_2/PAI-HF		APS/SiO_2-ZrO_2/PAI-HF	
		Glucose Con. (%)	HMF Sel. (%)	Glucose Con. (%)	HMF Sel. (%)	Glucose Con. (%)	HMF Sel. (%)
DMSO	1	40	3	53	4	53	6
	2	73	7	71	11	79	20
	4	89	18	95	25	96	27
	8	95	21	97	31	100	34
20% H_2O + 80% DMSO	1	2	-	10	-	4	-
	2	23	-	10	-	10	5
	4	18	4	16	2	38	6
	8	16	5	28	6	40	10

Reaction condition: Reaction temp. 150 °C; 0.5 g glucose; 50 mg Catalysts; DMSO=10 mL.

4. CONCLUSION

In summary, the development of aminosilane-grafted SiO_2-ZrO_2/PAI-HF as a bifunctional heterogeneous catalyst (cooperative acid-base catalyst) and a continuous-flow reactor for the conversion of fructose and glucose to HMF using tandem reactions was investigated. Our results indicated that both aminosilane grafting and cooperation of Lewis acid/Brønsted acid are key factors for catalytic activity. The good catalytic efficiency and excellent stability at different reaction temperatures make the APS/SiO_2-ZrO_2/PAI-HF a promising microfluidic system for tandem Lewis acid/Brønsted acid-catalyzed conversion of carbohydrates by simply controlling contact time and reaction temperature. Hollow fiber catalysts were recycled three times with more than 50% HMF yield. The composite APS/SiO_2-ZrO_2/PAI-HF possesses a bifunctional catalysis ability, catalyzing the tandem reactions of glucose isomerization to fructose and fructose dehydration to HMF with

conversions of 100% and HMF selectivity of 34%. This work demonstrates the utility of an integrated continuous-flow microfluidic system for efficient conversion of fructose into HMF.

Supporting Information

The supporting Information covers SEM image and FTIR results of bare and aminosilane-grafted SiO_2-ZrO_2 polyamide-imide hollow fibers, ^1H NMR spectrum of fructose and glucose conversion to HMF over various hollow fiber catalysts.

Author Information

Corresponding Author

*Email: rownaghia@mst.edu

ORCID

Ali Rownaghi: 0000-0001-5228-5624

Notes

The authors declare no competing financial interest.

ACKNOWLEDGMENT

We thank the University of Missouri Research Board (UMRB) for supporting this work. We acknowledge Professor William J. Koros from the School of Chemical and Biomolecular Engineering at Georgia Institute of Technology for giving us access to his fiber-spinning facilities.

REFERENCES

1. Hou, Q.; Zhen, M.; Liu, L.; Chen, Y.; Huang, F.; Zhang, S.; Li, W.; Ju, M. Tin Phosphate as a Heterogeneous Catalyst for Efficient Dehydration of Glucose into 5-Hydroxymethylfurfural in Ionic Liquid. *Appl. Catal. B Environ.* **2018**, *224* (September 2017), 183–193.

2. Zhao, P.; Zhang, Y.; Wang, Y.; Cui, H.; Song, F.; Sun, X.; Zhang, L. Conversion of Glucose into 5-Hydroxymethylfurfural Catalyzed by Acid–base Bifunctional Heteropolyacid-Based Ionic Hybrids. *Green Chem.* **2018**, *20* (7), 1551–1559.

3. Rathod, P. V.; Nale, S. D.; Jadhav, V. H. Metal Free Acid Base Catalyst in the Selective Synthesis of 2,5-Diformylfuran from Hydroxymethylfurfural, Fructose, and Glucose. *ACS Sustain. Chem. Eng.* **2017**, *5* (1), 701–707.

4. Graça, I.; Iruretagoyena, D.; Chadwick, D. Glucose Isomerisation into Fructose over Magnesium-Impregnated NaY Zeolite Catalysts. *Appl. Catal. B Environ.* **2017**, *206*, 434–443.

5. Wang, T.; Gallo, J. M. R.; Shanks, B. H.; Dumesic, J. A. Production of 5-Hydroxymethylfurfural from Glucose Using a Combination of Lewis and Brønsted Acid Catalysts in Water in a Biphasic Reactor with an Alkylphenol Solvent. *ACS Catal.* **2012**, *2*, 930–934.

6. Deshpande, N.; Pattanaik, L.; Whitaker, M. R.; Yang, C. T.; Lin, L. C.; Brunelli, N. A. Selectively Converting Glucose to Fructose Using Immobilized Tertiary Amines. *J. Catal.* **2017**, *353*, 205–210.

7. Wang, X.; Zhang, H.; Ma, J.; Ma, Z.-H. Bifunctional Brønsted–Lewis Solid Acid as a Recyclable Catalyst for Conversion of Glucose to 5-Hydroxymethylfurfural and Its Hydrophobicity Effect. *RSC Adv.* **2016**, *6* (49), 43152–43158.

8. Chen, D.; Liang, F.; Feng, D.; Xian, M.; Zhang, H.; Liu, H.; Du, F. An Efficient Route from Reproducible Glucose to 5-Hydroxymethylfurfural Catalyzed by Porous Coordination Polymer Heterogeneous Catalysts. *Chem. Eng. J.* **2016**, *300*, 177–184.

9. Lanziano, C. A. S.; Moya, S. F.; Barrett, D. H.; Teixeira-Neto, E.; Guirardello, R.; de Souto da Silva, F.; Rinaldi, R.; Rodella, C. B. Hybrid Organic–Inorganic Anatase as a Bifunctional Catalyst for Enhanced Production of 5-Hydroxymethylfurfural from Glucose in Water. *ChemSusChem* **2018**, *11* (5), 872–880.

10. Osatiashtiani, A.; Lee, A. F.; Wilson, K. Hydrothermally Stable , Conformal Sulfated Zirconia Monolayer Catalysts for Sustainable Chemical Processes. *ACS Catal.* **2015**, *5* (7), 4345–4352.

11. Saravanamurugan, S.; Paniagua, M.; Melero, J. A.; Riisager, A. Efficient Isomerization of Glucose to Fructose over Zeolites in Consecutive Reactions in Alcohol and Aqueous Media. *J. Am. Chem. Soc.* **2013**, *135* (14), 5246–5249.

12. Liu, C.; Carraher, J. M.; Swedberg, J. L.; Herndon, C. R.; Fleitman, C. N.; Tessonnier, J. P. Selective Base-Catalyzed Isomerization of Glucose to Fructose. *ACS Catal.* **2014**, *4* (12), 4295–4298.

13. Delidovich, I.; Palkovits, R. Structure-Performance Correlations of Mg-Al Hydrotalcite Catalysts for the Isomerization of Glucose into Fructose. *J. Catal.* **2015**, *327*, 1–9.

14. Rajabbeigi, N.; Torres, A. I.; Lew, C. M.; Elyassi, B.; Ren, L.; Wang, Z.; Je Cho, H.; Fan, W.; Daoutidis, P.; Tsapatsis, M. On the Kinetics of the Isomerization of Glucose to Fructose Using Sn-Beta. *Chem. Eng. Sci.* **2014**, *116*, 235–242.

15. Yue, C.; Magusin, P. C. M. M.; Mezari, B.; Rigutto, M.; Hensen, E. J. M. Hydrothermal Synthesis and Characterization of a Layered Zirconium Silicate. *Microporous Mesoporous Mater.* **2013**, *180*, 48–55.

16. Li, K.; Du, M.; Ji, P. Multifunctional Tin-Based Heterogeneous Catalyst for Catalytic Conversion of Glucose to 5-Hydroxymethylfurfural. *ACS Sustain. Chem. Eng.* **2018**, acssuschemeng.8b00745.

17. Zhou, F.; Sun, X.; Wu, D.; Zhang, Y.; Su, H. Role of Water in Catalyzing Proton Transfer in Glucose Dehydration to 5-Hydroxymethylfurfural. *ChemCatChem* **2017**, *9* (14), 2784–2789.

18. Osatiashtiani, A.; Lee, A. F.; Granollers, M.; Brown, D. R.; Olivi, L.; Morales, G.; Melero, J. A.; Wilson, K. Hydrothermally Stable, Conformal, Sulfated Zirconia Monolayer Catalysts for Glucose Conversion to 5-HMF. *ACS Catal.* **2015**, *5* (7), 4345–4352.

19. Swift, T. D.; Nguyen, H.; Erdman, Z.; Kruger, J. S.; Nikolakis, V.; Vlachos, D. G. Tandem Lewis Acid/Brønsted Acid-Catalyzed Conversion of Carbohydrates to 5-Hydroxymethylfurfural Using Zeolite Beta. *J. Catal.* **2016**, *333*, 149–161.

20. Margelefsky, E. L.; Zeidan, R. K.; Davis, M. E. Cooperative Catalysis by Silica-Supported Organic Functional Groups. *Chem. Soc. Rev.* **2008**, *37* (6), 1118.

21. Moschetta, E. G.; Brunelli, N. a.; Jones, C. W. Reaction-Dependent Heteroatom Modification of Acid–base Catalytic Cooperativity in Aminosilica Materials. *Appl. Catal. A Gen.* **2015**, *504*, 429–439.

22. Marcoux, L.; Florek, J.; Kleitz, F. Critical Assessment of the Base Catalysis Properties of Amino-Functionalized Mesoporous Polymer-SBA-15 Nanocomposites. *Appl. Catal. A Gen.* **2015**, *504*, 493–503.

23. Jing Luo, Lisandra Arroyo-Ram ırez, Raymond J. Gorte, D. T. and D. G. V. Hydrodeoxygenation of HMF Over Pt/C in a Continuous Flow Reactor. *AIChE J.* **2015**, *61* (2), 590–597.

24. Luo, J.; Arroyo-Ramírez, L.; Wei, J.; Yun, H.; Murray, C. B.; Gorte, R. J. Comparison of HMF Hydrodeoxygenation over Different Metal Catalysts in a Continuous Flow Reactor. *Appl. Catal. A Gen.* **2015**, *508*, 86–93.

25. Jeong, G. Y.; Singh, A. K.; Sharma, S.; Gyak, K. W.; Maurya, R. A.; Kim, D. P. One-Flow Syntheses of Diverse Heterocyclic Furan Chemicals Directly from Fructose via Tandem Transformation Platform. *NPG Asia Mater.* **2015**, *7* (4), e173-8.

26. Adamo, A.; Beingessner, R. L.; Behnam, M.; Chen, J.; Jamison, T. F.; Jensen, K. F.; Monbaliu, J. C. M.; Myerson, A. S.; Revalor, E. M.; Snead, D. R.; Stelzer, T.; Weeranoppanant, N.; Wong, S. Y.; Zhang, P. On-Demand Continuous-Flow Production of Pharmaceuticals in a Compact, Reconfigurable System. *Science (80-.).* **2016**, *352* (6281), 61–67.

27. Yang, L.; Tsilomelekis, G.; Caratzoulas, S.; Vlachos, D. G. Mechanism of Brønsted Acid-Catalyzed Glucose Dehydration. *ChemSusChem* **2015**, *8* (8), 1334–1341.

28. Wang, Q.; Shantz, D. F. Nitroaldol Reactions Catalyzed by Amine-MCM-41 Hybrids. *J. Catal.* **2010**, *271* (2), 170–177.

29. Biradar, A. V.; Sharma, K. K.; Asefa, T. Continuous Henry Reaction to a Specific Product over Nanoporous Silica-Supported Amine Catalysts on Fixed Bed Reactor. *Appl. Catal. A Gen.* **2010**, *389* (1–2), 19–26.

30. Rana, S.; Mallick, S.; Parida, K. M. Facile Method for Synthesis of Polyamine-Functionalized Mesoporous Zirconia and Its Catalytic Evaluation toward Henry Reaction. *Ind. Eng. Chem. Res.* **2011**, *50* (4), 2055–2064.

31. Luo, S.; Falconer, J. Aldol Condensation of Acetaldehyde to Form High Molecular Weight Compounds on TiO2. *Catal. Letters* **1999**, *57*, 89–93.

32. Mazzotta, M. G.; Gupta, D.; Saha, B.; Patra, A. K.; Bhaumik, A.; Abu-Omar, M. M. Efficient Solid Acid Catalyst Containing Lewis and Brønsted Acid Sites for the Production of Furfurals. *ChemSusChem* **2014**, *7* (8), 2342–2350.

33. Guo, F.; Fang, Z.; Zhou, T. J. Conversion of Fructose and Glucose into 5-Hydroxymethylfurfural with Lignin-Derived Carbonaceous Catalyst under Microwave Irradiation in Dimethyl Sulfoxide-Ionic Liquid Mixtures. *Bioresour. Technol.* **2012**, *112*, 313–318.

34. Woodward, R. T.; Kessler, M.; Lima, S.; Rinaldi, R. Hypercrosslinked Microporous Polymer Sorbents for the Efficient Recycling of a Soluble Acid Catalyst in Cellulose Hydrolysis. *Green Chem.* **2018**, *20*, 2374–2381.

35. Detoni, C.; Gierlich, C. H.; Rose, M.; Palkovits, R. Selective Liquid Phase Adsorption of 5-Hydroxymethylfurfural on Nanoporous Hyper-Cross-Linked Polymers. *ACS Sustain. Chem. Eng.* **2014**, *2* (10), 2407–2415.

36. Jumde, R. P.; Marelli, M.; Scotti, N.; Mandoli, A.; Psaro, R.; Evangelisti, C. Ultrafine Palladium Nanoparticles Immobilized into Poly(4-Vinylpyridine)-Based Porous Monolith for Continuous-Flow Mizoroki–Heck Reaction. *J. Mol. Catal. A Chem.* **2016**, *414*, 55–61.

37. Porta, R.; Benaglia, M.; Puglisi, A. Flow Chemistry: Recent Developments in the Synthesis of Pharmaceutical Products. *Org. Process Res. Dev.* **2016**, *20*, 2–25.

38. Wiles, C.; Watts, P. Continuous Flow Reactors: A Perspective. *Green Chem.* **2012**, *14* (1), 38–54.

39. Wegner, J.; Ceylan, S.; Kirschning, A. Flow Chemistry - A Key Enabling Technology for (Multistep) Organic Synthesis. *Adv. Synth. Catal.* **2012**, *354* (1), 17–57.

40. Irfan, M.; Glasnov, T. N.; Kappe, C. O. Heterogeneous Catalytic Hydrogenation Reactions in Continuous-Flow Reactors. *ChemSusChem* **2011**, *4* (3), 300–316.

41. Frost, C. G.; Mutton, L. Heterogeneous Catalytic Synthesis Using Microreactor Technology. *Green Chem.* **2010**, *12*, 1687–1703.

42. Arvela, R. K.; Leadbeater, N. E.; Sangi, M. S.; Williams, V. A.; Granados, P.; Singer, R. D. A Reassessment of the Transition-Metal Free Suzuki-Type Coupling Methodology. J. Org. Chem. 2005, 70 (1), 161−168.

43. Thome, I.; Nijs, A.; Bolm, C. Trace Metal Impurities in Catalysis.́Chem. Soc. Rev. 2012, 41 (3), 979.

44. He, Y.; Jawad, A.; Li, X.; Atanga, M.; Rezaei, F.; Rownaghi, A. A. Direct Aldol and Nitroaldol Condensation in an Aminosilane-Grafted Si/Zr/Ti Composite Hollow Fiber as a Heterogeneous Catalyst and Continuous-Flow Reactor. J. Catal. 2016, 341, 149−159.

45. He, Y.; Rezaei, F.; Kapila, S.; Rownaghi, A. A. Engineering Porous Polymer Hollow Fiber Micro Fluidic Reactors for Sustainable C-H Functionalization. ACS Appl. Mater. Interfaces 2017, 9, 16288−16295.

46. Jawad, A.; Rezaei, F.; Rownaghi, A. A. Porous Polymeric Hollow Fibers as Bifunctional Catalysts for CO2 Conversion to Cyclic Carbonates. J. CO2 Util. 2017, 21, 589−596.

47. Rownaghi, A. A.; Bhandari, D.; Burgess, S. K.; Mikkilineni, D. S. Effects of Coating Solvent and Thermal Treatment on Transport and Morphological Characteristics of PDMS/Torlon® Composite Hollow Fiber Membrane. J. Appl. Polym. Sci. 2017, 134 (42), 45418.

48. Rownaghi, A. A.; Rezaei, F.; Labreche, Y.; Brennan, P. J.; Johnson, J. R.; Li, S.; Koros, W. J. In Situ Formation of a Monodispersed Spherical Mesoporous Nanosilica − Torlon Hollow-Fiber Composite for Carbon Dioxide Capture. ChemSusChem 2015, 8, 3439−3450.

49. Parry, E. P. An Infrared Study of Pyridine Adsorbed on Acidic Solids. Characterization of Surface Acidity. J. Catal. 1963, 2 (5), 371− 379.

50. Rownaghi, A. A.; Kant, A.; Li, X.; Thakkar, H.; Hajari, A.; He, Y.; Brennan, P. J.; Hosseini, H.; Koros, W. J.; Rezaei, F. AminosilaneGrafted Zirconia-Titiania-Silica Nanoparticles/Torlon Hollow Fiber Composites for CO2 Capture. ChemSusChem 2016, 9 (10), 1166− 1177.

51. Brennan, P. J.; Thakkar, H.; Li, X.; Rownaghi, A. A.; Koros, W. J.; Rezaei, F. Effect of Post-Functionalization Conditions on the Carbon Dioxide Adsorption Properties of Aminosilane-Grafted Zirconia/ Titania/Silica-Poly(Amide-Imide) Composite Hollow Fiber Sorbents. Energy Technol. 2017, 5 (2), 327−337.

SUPPORTING INFORMATION

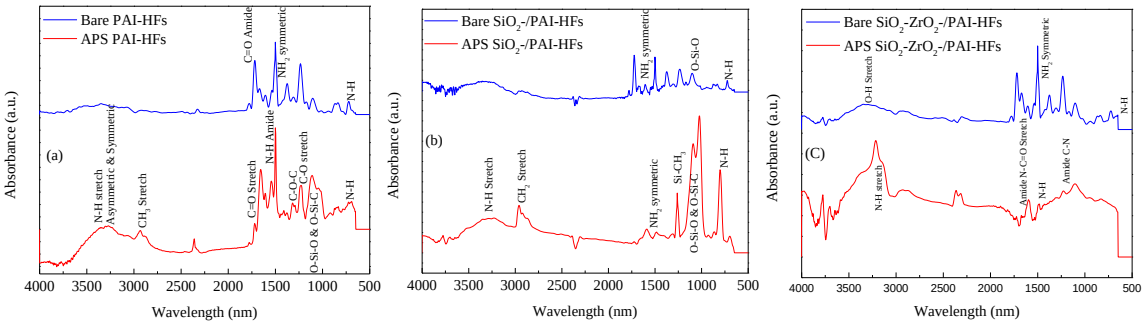

Figure S1: FTIR spectroscopy of hollow fiber catalysts before and after APS exposure

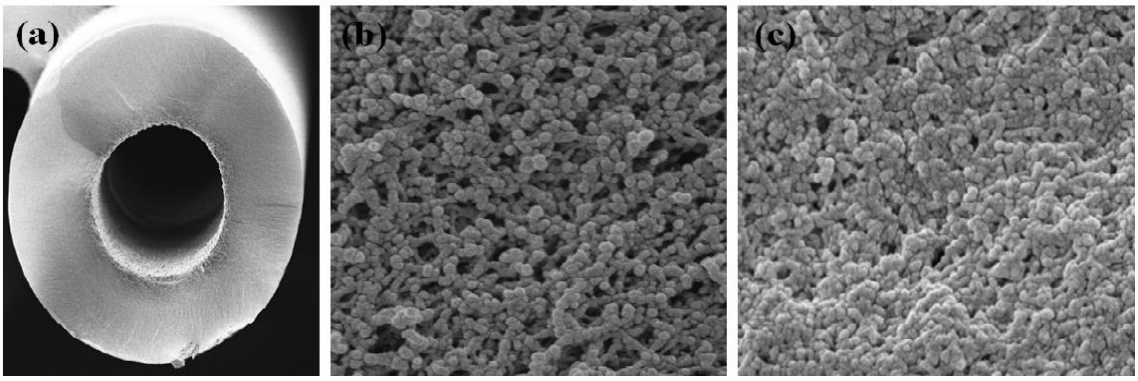

Figure S2: SEM images of a) the cross-section of APS-grafted SiO_2-ZrO_2/PAI-HF; b) the outer surface of bare SiO_2-ZrO_2/PAI-HF; and c) the outer surface of APS-grafted SiO_2-ZrO_2/PAI-HF.

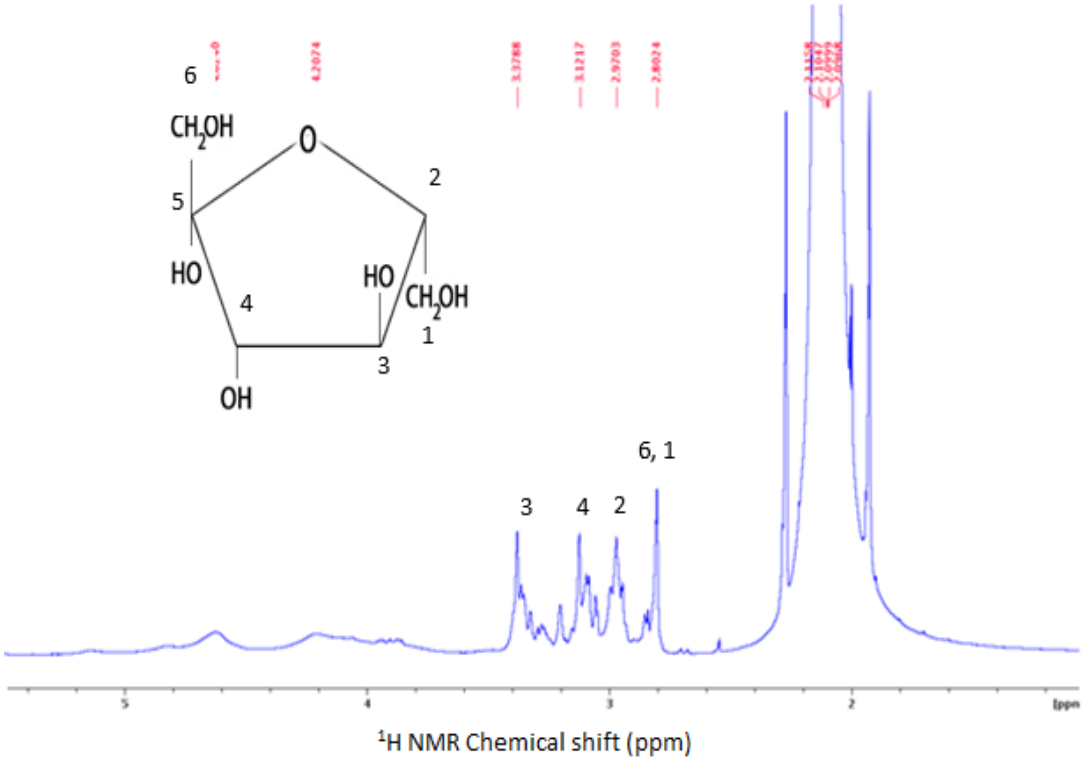

Figure S3-1: 400-MHz ^{1}H NMR spectrum of fructose (0.5 g) dissolved in DMSO (10 mL). Because no deuterated solvent, and thus no field-frequency lock was used, the singlet signal of the DMSO CH_3 group was used as chemical-shift reference and set to 2.09 ppm (m, 6 H). The fructose NMR signals (1, 2, 3, 4, and 6 in the spectrum) correlate with protons in the 1, 2, 3, 4, and 6 position of the fructose structures. While the chemical shift of the protons 1 and 6 are identical (2.80-2.89 ppm), protons 2, 3, and 4 are assigned to the signals at 2.97 - 3.01 ppm, 3.35 - 3.38 ppm, and 3.02 - 3.12 ppm, respectively. Some unidentified minor impurities are observed in the range of 3.9 - 5.1 ppm.

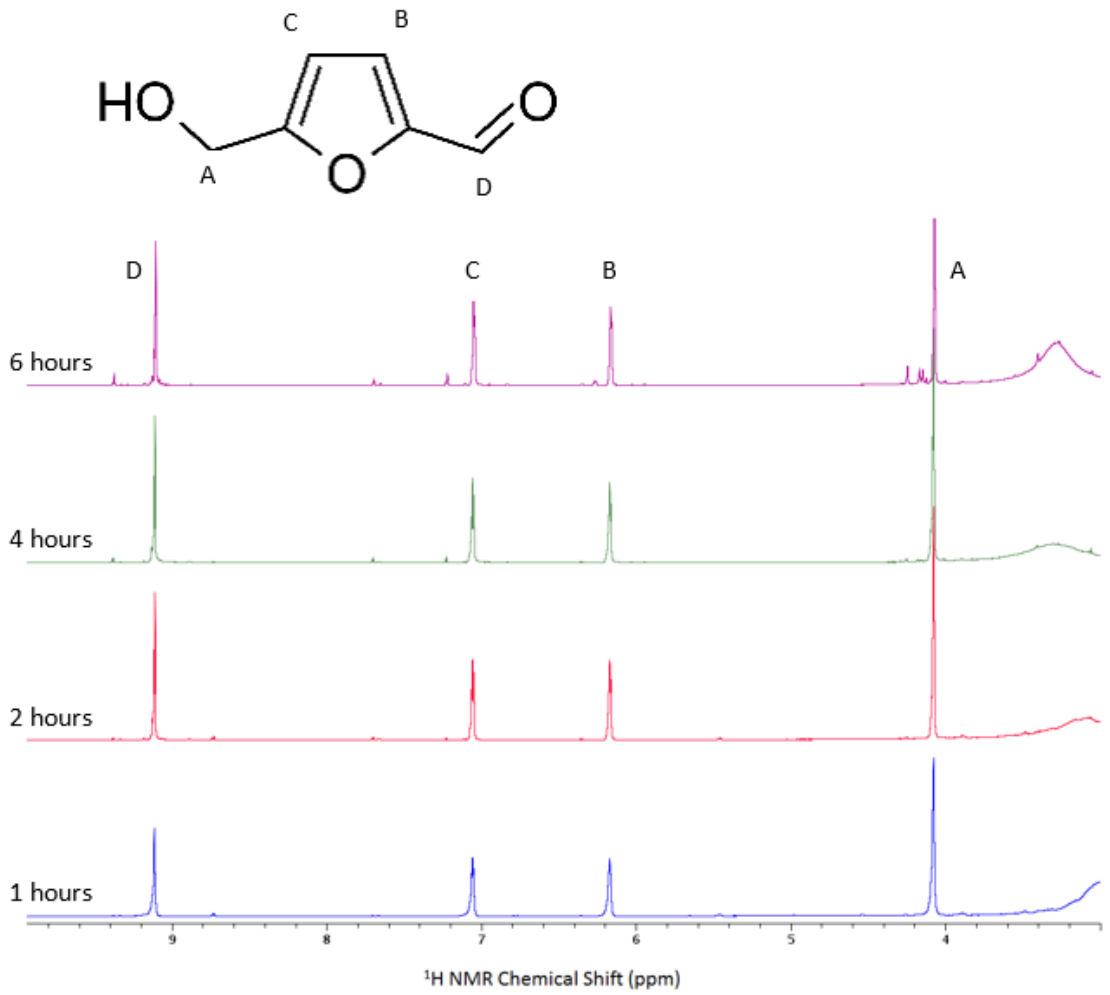

Figure S3-2: 400 MHz NMR spectra of samples drawn after different reaction times (1, 2, 4, and 6 hours) of fructose in DMSO at 150 °C using APS-grafted PAI-HFs as the catalyst. The DMSO signal at 2.50 ppm was used as chemical-shift reference. The NMR signals are assigned to the reaction product HMF) as indicated in the chemical structure above (A: 4.15 ppm, B: 6.21 ppm, C: 7.15 ppm, D: 9.20 ppm). The majority of the reaction occurs within the first two hours, while undesirable side products are visible at longer reaction times.

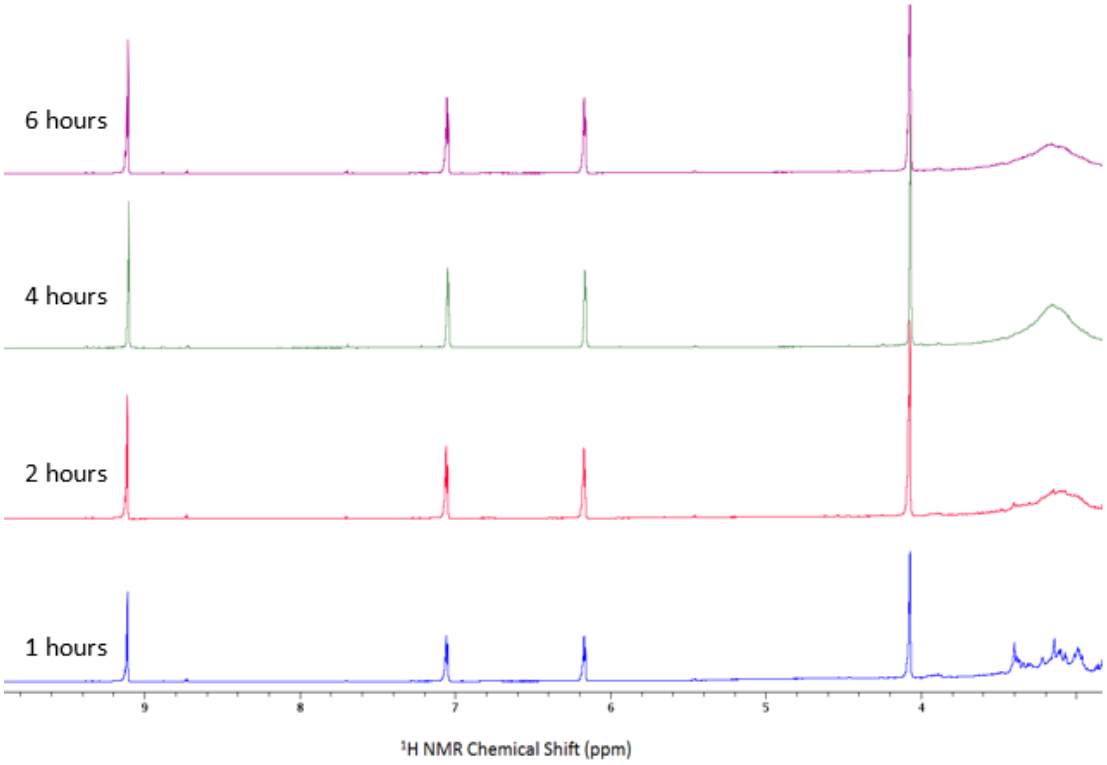

Figure S3-3: 400 MHz NMR spectra of samples drawn after different reaction times (1, 2, 4, and 6 hours) of fructose in DMSO at 150 ^{o}C using APS-grafted SiO_2/PAI-HFs as the catalyst. The DMSO signal at 2.50 ppm was used as a chemical-shift reference. The NMR signals at 4.15 ppm, 6.21 ppm, 7.15 ppm, 9.20 ppm are assigned to the reaction product HMF as shown in Figure 2.

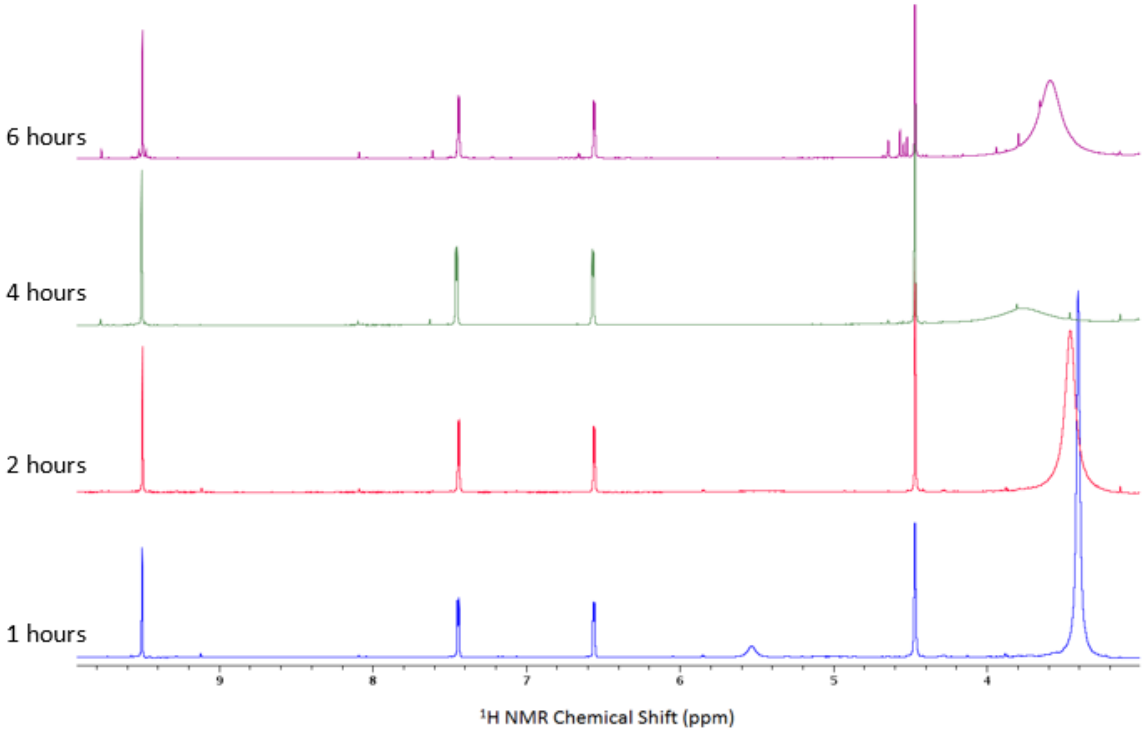

Figure S3-4: 400 MHz NMR spectra of samples drawn after different reaction times (1, 2, 4, and 6 hours) of fructose in DMSO at 150 ^{o}C using APS-grafted SiO_2-ZrO_2/PAI-HFs as the catalyst. The DMSO signal at 2.09 ppm was used as a chemical-shift reference. The NMR signals at 4.42 ppm, 6.59 ppm, 7.42 ppm, 9.50 ppm are assigned to the reaction product HMF as shown in Figure 2.

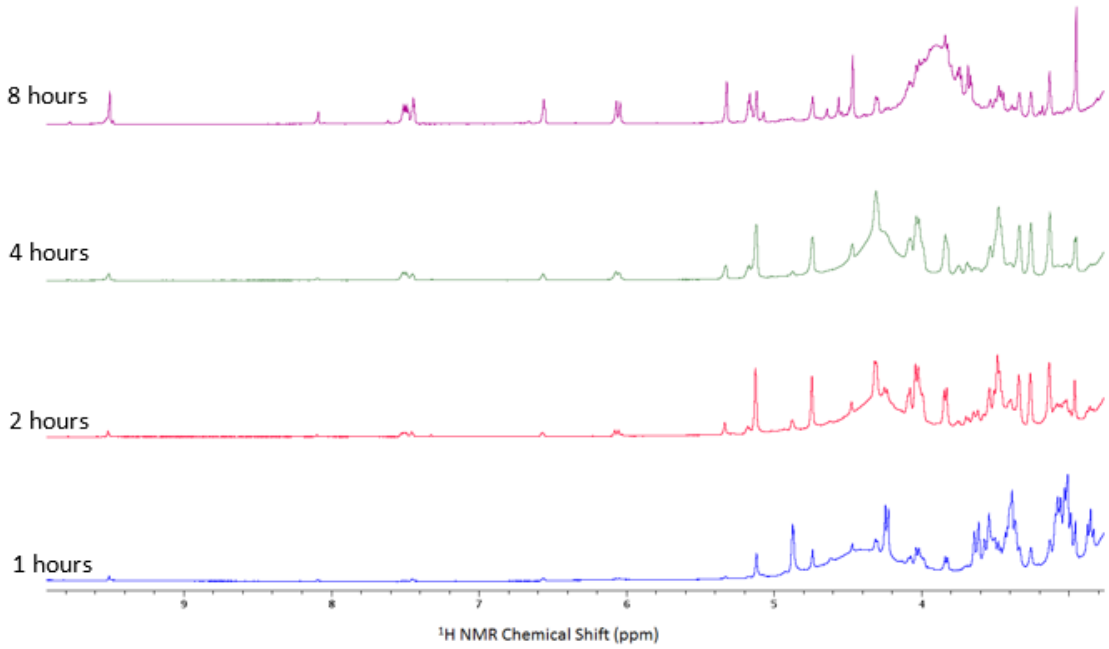

Figure S4-1: 400 MHz NMR spectra of samples drawn after different reaction times (1, 2, 4, and 8 hours) of glucose in DMSO at 150 ºC using APS-grafted PAI-HFs as the catalyst. The DMSO signal at 2.50 ppm was used as a chemical-shift reference. The NMR signals at (4.15 ppm, 6.21 ppm, and 7.15 ppm, 9.20 ppm are assigned to the reaction product HMF as shown in Figure 2. There are a lot of side product and also some unidentified impurities product observed in the sample NMR spectrum. Compare to the fructose reaction, the glucose converted to HMF is more impurity signals at 9.3, 7.0-7.2, 5.60-5.70, and so on.

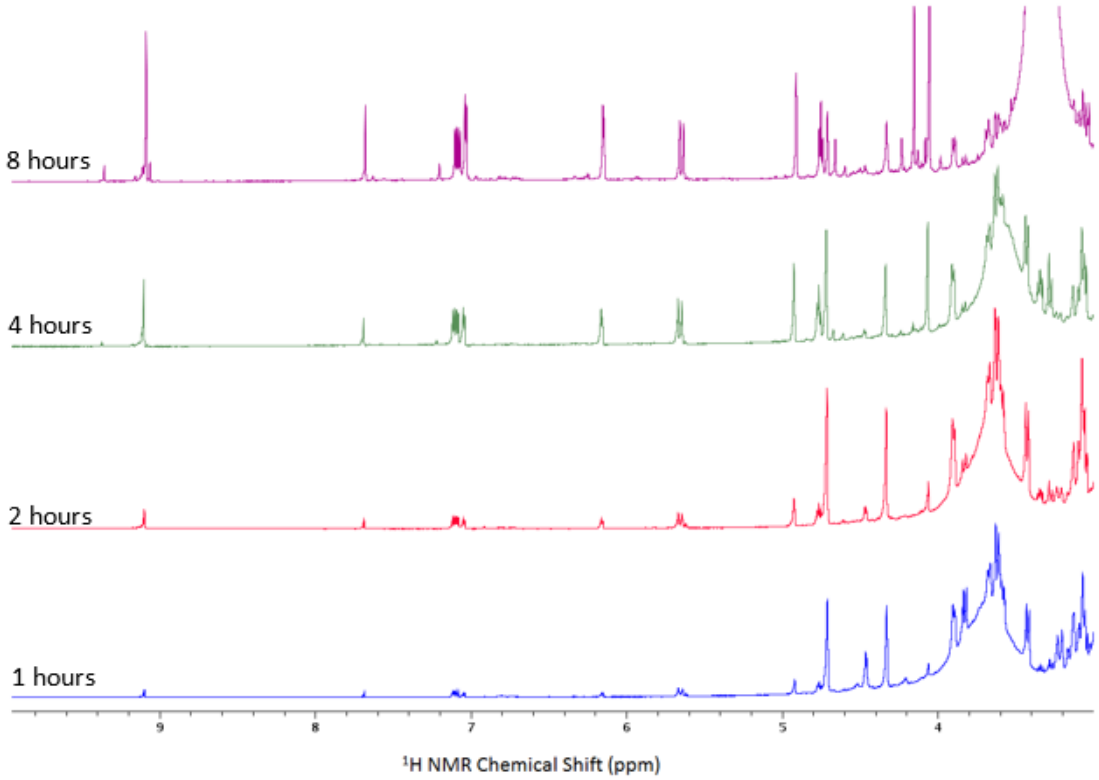

Figure S4-2: 400 MHz NMR spectra of samples drawn after different reaction times (1, 2, 4, and 8 hours) of glucose in DMSO at 150 ^{o}C using APS-grafted SiO_2/PAI-HFs as the catalyst. The DMSO signal at 2.50 ppm was used as a chemical-shift reference. The NMR signals at (4.15 ppm, 6.21 ppm, and 7.15 ppm, 9.20 ppm are assigned to the reaction product HMF as shown in Figure 2. There are a lot of side product and also some unidentified impurities product observed in the sample NMR spectrum. Compare to the fructose reaction, the glucose converted to HMF is more impurity signals at 9.3, 7.0-7.2, 5.60-5.70, and so on.

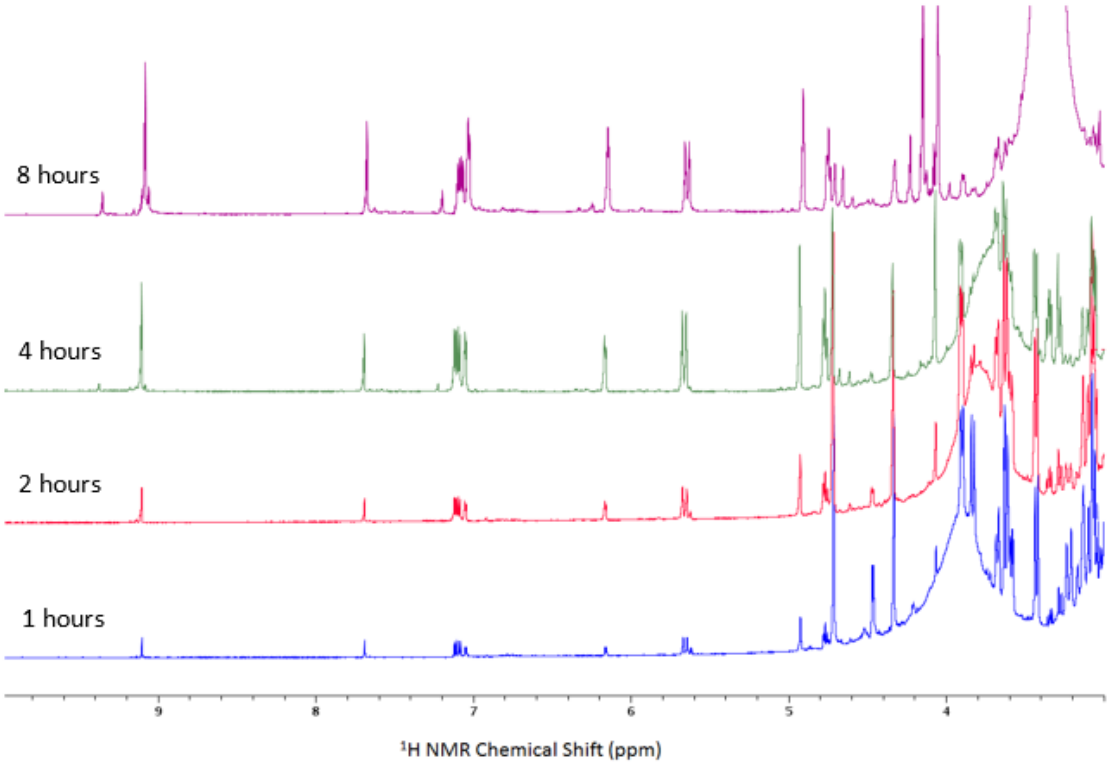

Figure S4-3: 400 MHz NMR spectra of samples drawn after different reaction times (1, 2, 4, and 8 hours) of glucose in DMSO at 150 ^{o}C using APS-grafted SiO_2-ZrO_2/PAI-HFs as the catalyst. The DMSO signal at 2.50 ppm was used as a chemical-shift reference. The NMR signals at (4.15 ppm, 6.21 ppm, and 7.15 ppm, 9.20 ppm are assigned to the reaction product HMF as shown in Figure 2. There are a lot of side product and also some unidentified impurities product observed in the sample NMR spectrum. Compare to the fructose reaction, the glucose converted to HMF has more impurity signals at 9.3, 7.0-7.2, 5.60-5.70, and so on.

IV. A Pd-IMMOBILIZED AMINOSILANE-GRAFTED SiO_2/SiO_2-TiO_2 COMPOSITE HOLLOW FIBER AS A HETEROGENEOUS CONTINUOUS-FLOW REACTION IN THE DEGRADATION OF 4-NITROPHENOL

Yingxin He,[‡] Fateme Rezaei,[‡] Ali A. Rownaghi*,[‡]

[‡] Department of Chemical & Biochemical Engineering, Missouri University of Science and Technology, 1101 N. State Street, Rolla, Missouri 65409, United States

* E-mail: rownaghia@mst.edu

ABSTRACT

The Pd-immobilized aminosilane (APS)-grafted variety SiO_2-TiO_2 composite hollow fiber (Pd-immobilized PAI-grafted PAI-HFs) is recently creatively being used in the degradation reaction of 4-nitrophenol (4-NP) to generate 4-aminophenol (4-AP) which is a very important reaction in water treatment process. The hollow fibers will first be grafted by APS which functioned them with bifunctional group for cooperative interactions, as well as increasing the mechanical strength, and then modified by covalent post-modification with salicylic aldehyde for binding catalytically active Pd(II) ions, to formed the Pd(0)-immobilized aminosilane-grafted SiO_2-TiO_2 composite hollow fibers under reacting with the $NaBH_4$. After that, being treated with $NaBH_4$ to synthesis the Pd-loaded APS-grafted SiO_2-TiO_2 hollow fibers catalysts. The catalytic activity of the active Pd(0) ion can be obtained by tested via the 4-NP reduction reaction to convert to 4-aminophenol.

Keywords:

Degradation of 4-nitrophenol, Hollow fiber catalysts, Heterogeneous catalysts, Continues-flow reaction system

1. INTRODUCTION

4-nitrophenol (4-NP), a typical byproduct from the production of drugs, pesticides, herbicides, to darken leather, and synthetic dyes, is one of major pollutant listed by the US EPA in water system[1,2]. When exposed under excess concentration level of 4-NP, it may cause blood disorders, eye, skin irritation, kidney, and liver damage as well as the poisoning of the central nervous system in individual humans and animals[3,4]. Therefore, removing 4-NP from the water system keep stays as a popular topic in both environmental and water system protection. On the other hand, 4-aminophenol (4-AP), one of the pathway products of the 4-NP reduction reaction, is an important intermediate for fine chemicals synthesis process, such as dyes, pharmaceuticals, and pesticides[5]. 4-AP is one of the intermediates for the manufacture of azo dyes, Sulphur dyes, acid dyes, and fur dyes[6]. The 4-AP is used by the pharmaceutical industry to manufacture drugs such as paracetamol and clofibrate. In addition, it is also applied as an analytical reagent, assay gold, and measures copper, iron, magnesium, vanadium, nitrite, and cyanate[7]. Besides, the 4-AP also used in the preparation of developer N-methyl-p-aminophenol, antioxidants and petroleum additives, synthetic polymeric stabilizers 4-hydroxydiphenylamine, N,N'-diphenyl-1,4-phenylenediamine, N-(4-hydroxyphenyl)-2-naphthylamine, etc[8]. Therefore, the reduction

of 4-NP to 4-AP is one of the popular pathway being a study for the 4-NP removal in these decades[5].

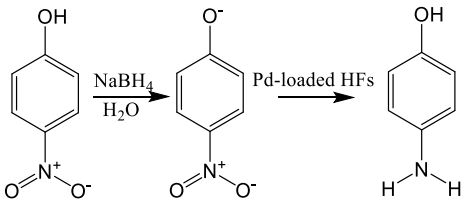

Scheme 1. Reaction scheme of the 4-nitrophenol reduction reaction.

According to the previous researches, the oxidation-reduction reaction between 4-nitrophenol (4-NP) and 4-aminophenol (4-AP) have been investigated under a fairly wide range of conditions by several research groups. Also, $NaBH_4$ was investigated for the efficient production on the 4-AP. It is clearly shown in the previous research that $NaBH_4$ have efficiently assisted in with the reduction of 4-NP, however, it also proved that no reduction of 4-NP was observed without the catalysts. In other words, It is easily reduced by the $NaBH_4$ in the presence of metals in solution[9]. Experimentally, the reaction scheme shown as scheme 1, under the exist of $NaBH_4$ in the 4-NP aqueous, an intense yellow color was observed owing to the formation of 4-nitrophenolate intermediate, the 4-nitrophenolate ion, having a strong absorption at 400 nm, which allows for an easy and reliable means to measure reaction rates by UV−vis spectroscopy[10]. It has also been revealed that the $NaBH_4$ works as a reducing agent to a reduce the o-quinone units in the PDA structure. The overall reaction rate is pseudo-first-order when both the metal catalyst and $NaBH_4$ are in excess. Reduction of 4-NP on Pd nanoparticles has been demonstrated to follow

Langmuir−Hinshelwood mechanism statistics. In this mechanism, both molecules adsorb onto a surface before undergoing the bimolecular reaction. When $NaBH_4$ is in excess, the rate is controlled by the adsorption of 4-NP. Au, Ag, and Pd is the most comment mental nanoparticles (MNPs) that applied as catalysts for the 4-NP reduction reaction in the previous studies. Usually, after reaction under the catalysts, there was a continuous decrease in the intensity of color until it finally turned colorless, which indicated the generate of 4-AP[9,10,11].

As we mentioned above, the MNPs, such as Au, Ag, and Pd, are the most popular catalysts that apply to the 4-NP reduction reaction. Except for the above MNPs catalysts, the photocatalysts is also one of the hot topics for the study of the 4-NP reduction reaction. TiO_2, one of the comment photocatalysts for the 4-NP reduction reaction, Saraschandra et al. also reported that by doping metals on TiO_2, can increase the visible light sensitive for the photocatalysts[12]. However, by using photocatalysts, like TiO_2, for catalysts and heterogeneous support, lacks flexibility and increasing the difficulty for the scale-up process. Besides, compared to the stability of the photocatalysts, the MNPs immobilized catalysts show higher efficiency and catalytical stability[12,13]. There was a variety of traditional modification method that has been developed for the combination of the MNPs with the material supporters, such as ion doping, noble metal deposition, and surface sensitization. Organic ligands, high porous polymers, and surfactants are all popular material for the MNPs supporters[12].

Carbon porous materials (CPMs) is another popular supporting material that attracting research interest in this decades, due to its special physicochemical properties and low cost. Pitchainmani et al. reported a biomass-derived activated carbon supported

magnetite nanoparticles recyclable catalysts for the 4-NP reduction reaction, which also comes with high catalytic efficiency[13]. However, the extra separation step may also need for the reaction, as well as consumption of packing and recycle process.

On the other hand, in the previous researches, it is obvious that the leaking of MNPs is a serious problem for the traditional surface modification methods. Membrane surface modification method is a newly developed method which used commonly in these decades to form the metal nanoparticle immobilized catalysts. Inert membrane reactor (IMRCF) and the catalytic membrane reactor (CMR) are the two main kinds of membrane reactors. As the CMR usually refer to them to the membrane that coated with or made of the material that contains catalysts, reaction always happened during the reactant pass through the membrane and the separation process can also occur in the same time. Due to the immobilization way formed between the MNPs and the membrane, the structure of the membrane intended to be extremely stable and solving the MNP leaking problem caused by the traditional surface modification method.

Here, we are going to report the novel Pd-immobilized membrane hollow fiber microporous reactor and its application the 4-NP reduction reaction. The MNPs were immobilized onto the high porous hollow fiber through cross-linking with the membrane formed between the HFs with the APS-grafted and post-treatment, which shows higher stability and catalytic efficiency[14].

In our novel Pd-immobilized HFs membrane catalysts, under the exist of $NaBH_4$, the Pd(II) will convert to Pd(0) loaded on the HFs catalysts, and the Pd-MNPs will work for the reduction of 4-NP to regenerate the catechol group, and contributed to stabilizing metallic MNPs within the pore arrays, which makes the HFs more stable, so that except for

the continues reaction, the HFs catalysts can also achieve recycled used in the 4-NP reduction reaction with higher conversion and selectivity. Depending on the physical, catalytical, and thermos test results, we believe this kind of Pd-immobilized membrane HFs is much stable compared with those previous Pd-membranes catalysts.

The membrane hollow-fiber catalyst is a class of artificial membranes containing a semi-permeable barrier in the form of a hollow fiber, and we functionalized the hollow-fiber catalyst by doing the toluene-exchanged process and after that via a series of solvent exchanged and Pd(0) ion loaded to provide the hollow fiber functionalization with 3-aminopropyl trimethoxy silane (APS). These kinds of functionalized hollow fiber with the amino and hydroxide functional group have bifunctional cooperative characteristics which can help enhance the catalytic performance.

This report also studies the performance of the metalized hollow-fiber catalysts in heterogeneous 4-NP reduction reactions, as well as investigating the effect of the existence of $NaBH_4$ and its concentration in the 4-NP reaction. We synthesized Pd-NPs immobilized PAI HFs catalysts that which applied in the Heck coupling reaction in the previous research, in the current study, we seek further applications of this metal nanoparticles immobilized APS-grafted PAI hollow fiber catalysts. We try to apply this kind of catalysts in the water treatment filed, such as 4-NP reduction reaction. Firstly, we apply this catalyst in the batch reaction system to prove its catalysts efficiency, After that, continued-flow system test will be explored to investigate the yield and selectivity of this catalysts. Besides, the HFs we applied in this report is the highly hydrophilic and solvent/mechanical-stable porous polyamide-imide (PAI) Hollow fiber, with high-cost efficiency and easy to scale up for the continues reaction by increasing the length[15].

In recent decades, catalytic membrane and membrane reactors have recently driving extremely hot attention among the different research groups[16]. As an inherently multidisciplinary concept combining chemical reaction engineering separation technology, materials science, and mathematical modeling aspects, the catalytic membrane and membrane reactors are being provided a more compact and less capital intensive system design, but also often improved performance in terms of enhanced selectivity for the reactions. Generally speaking, the catalytic membranes are formed by immobilizing the metallic nanocatalysts in the membranes. And the metal nanoparticles (MNPs) binding with membranes, such as the Au, Ag, Pd and so on, appear having higher catalytic activity compared with those other homogeneous and heterogeneous catalysts, during with its higher stability and loading ratio. These kinds of catalytic NMP-membranes have been studying in different areas, such as the CO_2 absorption[17], and some other chemical reactions, like Heck coupling reaction in the previous studies[18]. Except for the reaction mention above, catalytic membrane and membrane reactors become a potential study direction for the water treatment area, such as the 4-nitrophenol (4-NP) reduction reaction.

2. EXPERIMENTAL SECTION

2.1. CHEMICALS AND MATERIALS

Titania and silica (average particle size 100 nm, Sigma Aldrich), Torlon 4000T-HV, a commercially available polyamide-imide (PAI) (Solvay Advanced Polymers, Alpharetta, GA), poly (vinylpyrrolidone) (PVP) (average MW≈1300 K, Sigma Aldrich), n-methyl-2-pyrrolidone (NMP) and ethanol (ACS Reagent, >98.5 %, VWR) were used for polymer dope preparation and formation of the composite hollow fiber catalysts.

The aminopropyltriethoxysilane (APS) (95 %) was purchased from Gelest and the $PdCl_2(CH_3CN)_2$ (99 %) was purchased from Sigma-Aldrich, which used as the grafting agent for functionalizing SiO_2- and SiO_2-TiO_2 /PAI hollow fiber catalysts, and $NaBH_4$ (98%) was purchased from Sigma-Aldrich, which is used to reducing Pd(II) to form the Pd(0) metal nanoparticles (NMPs). 4-nitrophenol (4-NP, 98%) and 4-aminophenol (4-AP, 98%) were also purchased in Sigma-Aldrich as reactant and standard.

2.2. SiO_2- AND SiO_2-TiO_2/PAI-HFs REACTOR FORMATION, APS-GRAFTED, AND PALLADIUM-LOADED HFs FUNCTIONALIZATION

The polymer dope composition was determined by the clod-point technique and fibers were produced via co-extrusion of the polymer dope and a bore fluid solution through a spinneret using an important variation of the well-known non-solvent phase inversion technique commonly referred to as “dry-jet, wet quench spinning”. The polymer dope composition and SiO_2- and SiO_2-TiO_2/PAI hollow fiber formation approach taken in this work has been already described in our previous works in detail. The SiO_2- and SiO_2-TiO_2/PAI-HFs sample contains titania-silica nanoparticles.

Silica and titania were chosen on the basis of previous studies, as noted above, demonstrating that more effective amine-stabilizing sites can be created upon titania/silica addition. Scheme 2 and 3 shows the mechanism of the produce of fiber modification from bare fiber to Pd-immobilized HFs catalysts. The post-infusion graft in of hollow fibers was carried out under nitrogen pressure at 80 ℃ for 2 h. the amine grafting was performed in a mixture of toluene and water. The water content of the mixture was kept within the range of 0.01-2.00 wt%. Hollow fibers were then washed, filtered with 100 mL each of toluene and ethanol, and dried under vacuum at 80 ℃ for 4 h.

After the APS-grafting process, APS-grafting fibers was solvent exchange with toluene over a 2-h period. The salicyclic aldehyde was added into the toluene solvent and keep the reaction at 50 ℃ for 5 days. After five days, the fiber was exchanged with fresh toluene to remove unreacted salicylic aldehyde to obtain the Toluene-exchanged sample. Next, solvent exchanged with CH_2Cl_2 about a 2-h period. Next, $PdCl_2$ $(CH_3CN)_2$ was dissolved in CH_2Cl_2 to keep at room temperature in two days to form the Pd(II)-binding APS-grafted SiO_2- and SiO_2-TiO_2/PAI-HFs fiber catalysts. Finally, the Pd(II)-fiber catalysts treated with the $NaBH_4$ solvent for a 2-h period, and later washed by CH_2Cl_2. The solvent was removed from the pores of the framework by vacuum for 12h at 85 ℃ to obtain the Pd(0)-loaded APS-grafted SiO_2- and SiO_2-TiO_2/PAI composite hollow fiber, shown as **Scheme 3**.

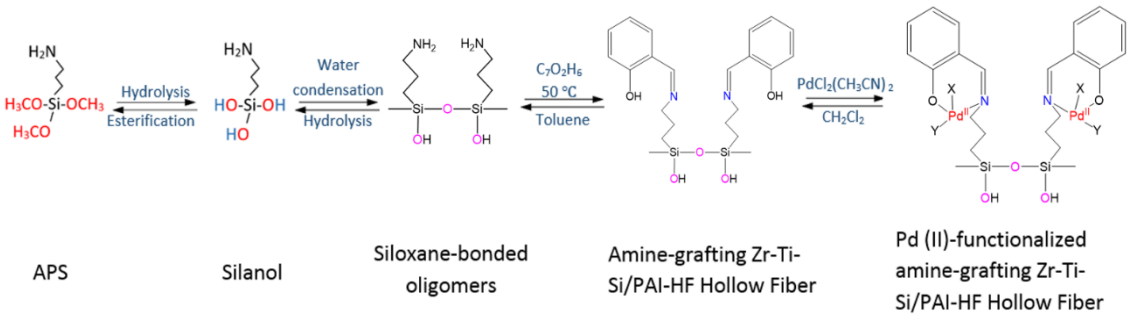

* X and Y is Cl and CH3CN, respectively

Scheme 2. Proposed reaction mechanism between Si/Ti/PAI-fiber catalysts and primary aminosilanes and Pd (II) during Pd (II)-functionalized amine-grafting.

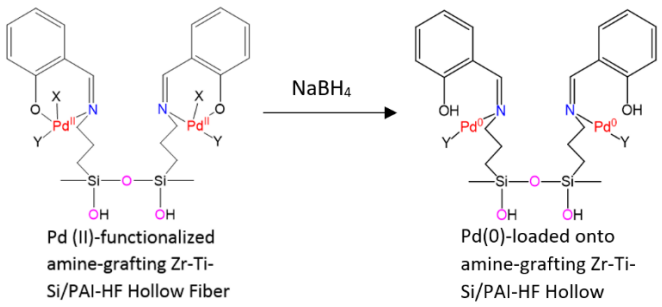

Scheme 3. Reduction of Pd (II) to form the Pd(0)-loaded onto hollow fiber via a $NaBH_4$ solvent.

2.3. FIBER CATALYSTS CHARACTERIZATION

A higher resolution scanning electron microscope (Hitachi S-4700 FE-SEM) was used to assess the morphology of the hollow fibers before and after grafting. The cross-section and surface of the fiber catalysts were examined and Pd-immobilization onto aminosilane-grafting within the Torlon fiber catalyst, as well as onto the zirconia, titania and silica nanoparticles was confirmed by Fourier Transform Infrared Spectroscopy (FTIR) at room temperature over a scanning range of 400-4000 cm^{-1} with a resolution of 4.0 cm^{-1}, using Bruker Tenser spectrophotometer. Bulk elemental analysis (EA) was used to determine the amine loading and zirconia, titania and silica nanoparticles content of the hollow fiber. Nitrogen adsorption isotherms were measured with a Micromeritics 3Flex Surface Characterization Analyzer apparatus at 77 K. Pd-immobilized amine-grafted SiO_2-TiO_2/PAI hollow fiber sorbents were degassed at 110 ℃ under vacuum for 24 h prior to analysis. Surface area and pore volume were calculated from the isotherm data using the Brunauer-Emmett-Teller (BET) and Barrett-Joyner Halenda (BJH) methods, respectively.

2.4. CATALYTIC TEST FOR THE DEGRADATION OF 4-NITROPHENOL

2.4.1. Batch Reaction Test for the 4-NP Reduction Reaction. 1 mM 4-NP solution was made with Millipore water, take about 10 mL, add variety amount of $NaBH_4$ to make the different $NaBH_4$ concentration (0, 1, 10, 100, 500, 1000 PPM) in the aqueous solution reactant system under 30 or 50 ^oC about 3 h. To this mixture, about 25 mg of 5 mol% Pd(II)/APS/PAI-HFs was added as a heterogeneous catalyst. Eventually, the final concentrations of 4-NP and $NaBH_4$ concentration in 10 mL Millipore water were 1mM and various $NaBH_4$ concentration. The reaction progress was monitored and analyzed by the Hitachi UV-Visible spectrophotometry instrument after diluted by Millipore water in the wavelength range 200-500 nm.

2.4.2. Recycle Reaction Test for the 4-NP Reduction Reaction. The Pd-immobilized HFs were collected by a filter to separate from the reaction system. After being washed by DI water and ethanol for three times, the collected catalysts will be being tested as a recycle catalysts to follow the same procedure for the rerun the reaction in 1 mM 4-NP with 500 PPM $NaBH_4$ under 30 or 50 ^oC about 3 h. The same procedure will produce about 3 times to test the recycle-ability.

2.4.3. Continuous-flow Reaction Test for the 4-NP Reduction Reaction. To test the bifunctional catalytic activity of hollow fiber in the continuous flow system, we carried out a set of proof-of-concept studies.

The reaction was conducted in a stainless steel module containing five hollow fibers (Fibers inner diameter 0.1 μm, length 15 cm, total volume 10 mL) at room temperature. Pd-immobilized SiO_2- and SiO_2-TiO_2 /PAI-HFs with APS-grafted were investigated systematically. The reactants were then continuously run through the hollow fiber reactor

at 0.02 cm^3min^{-1} flow rates in room temperature. A syringe pump equipped with two syringes was used to feed the hollow fiber reactor with the reagents through a T-Junction. A solution of mixtures for the 1mM 4-NP aqueous solution and 1000 PPM $NaBH_4$ were introduced at one inlet (hollow fiber shell side) Total outlet flow was 4.8-24 cm^3min^{-1} (various residence time). The schematic diagram of the system is illustrated in Figure 1. The product was then collected from the gore side of hollow fiber reactor.

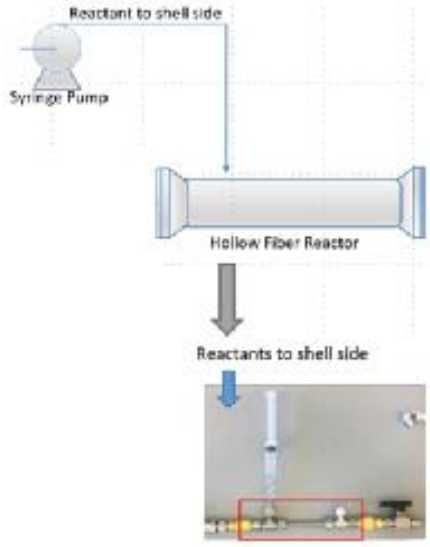

Figure 1. Design of the continuous-flow reaction system.

In the hollow fiber reactor, the palladium NMPs are immobilized and resides within the porous wall while the reagents are passed through the fiber shell and products are collected from the bore side, so in principle, no separation of the product from the catalyst is required. Also, by operating under a condition to achieve high conversion, minimal separation of unreacted products are required. Furthermore, through this configuration, the

hollow fiber catalysts can be easily regenerated and reused. These advantages render the hollow fiber catalyst system as the most convenient configuration to perform a reaction under continuous flow conditions.3. Results and discussion.

3. RESULTS AND DISCUSSION SECTION

3.1. Pd-IMMOBILIZED MEMBRANES PAI HOLLOW FIBER CHARACTERIZATION

Pd-immobilized membrane SiO_2 and SiO_2-TiO_2 PAI-HFs were successfully formed on the APS-grafted hollow fiber catalysts which consisted of Torlon fiber with a series of heteroatoms (such as Si and Ti). In order to verify the influence of post-modification and Pd-immobilization on the fiber structure and performance, the N_2 adsorption-desorption isotherms experiments were conducted both the bare, APS-grafted HFs and the Pd-immobilization HFs for before and after the reaction. Table 1 shows the textural properties and permeability results of the membrane PAI-HFs before and after post-modification, Pd (II) and Pd (0) immobilized with membrane states were also being analyzed by the N_2 physisorption and N_2 permeation.

Depend on the data from Table1, it can easy to found out that by following by different surface modification steps the BET surface area and pore volume have a different decreasing tendency. After the APS-grafting procedure, the BET surface area shows a decrease about 50~60%, and the pore volume also drops for about 60~75%, this situation causing by the cross-linking grafted of APS on the HFs. The further decreasing of BET surface area and the pore volume after the Pd-immobilization process, also supported the successfully loading of Pd-MNPs. The results of ICP and XPS analysts also prove the successfully of the Pd-MNPs.

Table 1. Textual properties and palladium loading of the bare and post-modified PAI hollow fibers.

Catalysts	S_{BET}[a] (m^2/g)	V_{PORE}[b] (cm^3/g)	Pd loading (mmol/g fiber)	
			ICP[d]	XPS
Bare SiO_2 /PAI-HFs	40	0.14	-	-
Bare SiO_2-TiO_2 /PAI-HFs	41	0.16	-	-
SiO_2 /APS-PAI-HFs	15	0.08	-	-
SiO_2-TiO_2/APS-PAI-HFs	20	0.04	-	-
Pd(II)/SiO_2 /APS-PAI-HFs	-	-	-	-
Pd(II)/SiO_2-TiO_2/APS-PAI-HFs	13	0.03	0.40	0.40
Pd(0)/SiO_2/APS-PAI-HFs	-	-	-	-
Pd(0)/SiO_2-TiO_2/APS-PAI-HFs	12	0.03	0.39	0.39
Used Pd/SiO_2/APS-PAI-HFs	-	-	-	-
Used Pd/SiO_2-TiO_2/APS-PAI-HFs	11	0.03	0.38	0.38

Besides, the used HFs after the reaction is also being tested by the BET, ICP, and XPS. It this observed that only slightly change of BET surface area, pore volume, and the Pd-loading results tested by the ICP and XPS, which agree with the previous results from the Heck coupling reaction that after the reaction, the loading of palladium should be strongly stable. It also shows that in the reduction process of Pd(II) to Pd(0) and after the reaction only shows about 2.5~5% leaking from the ICP and XPS results. Therefore, this HFs catalysts should be set for potential recycle catalysts for the reaction.

FTIR is shown in the previous research also prove the successfully post-modifications and the PD- immobilization[15]. SEM images are shown in Figure 2 also support the higher porous structure of the Si/Ti/HFs catalysts before and after modification, as well as reaction and prove the success of APS-grafted and Pd-immobilized. In Figure 2, it shows that (a) the cross-section of a single-layer bare Si/Ti/ PAI hollow fiber catalysts, (b) cross-section of bare Si/Ti/PAI-HF, (c) cross-section of APS-grafted Si/Ti/PAI-HF, (d)

outer surface of bare Si/Ti/PAI-HF, (e) outer surface of APS-grafted Si/Ti/PAI hollow fiber catalysts, (f) outer surface of Pd(0)-loaded APS-grafted Si/Ti/PAI-HF, (g) the same fiber catalysts of (f) after reaction, from these SEM spectra, it is obvious that the bare fiber shows highly porous state from the (a) and (b). However, it seems like the HFs did not maintain the highly porous state after the post-modification and the Pd-immobilization depend on the (c), (e), and (f) which also meets the BET results, the post-modification and MNPs immobilization process did affect the surface area and pore volume, but it can also confirm the success of APS-grafting and MNPs immobilization.

Besides, compared with the (f) before and after the reaction (with blue outline) we can see the HFs still maintain a porous structure which indicated the stabilizer of the HFs even after three times of recycling test, which also proved the HFs have high mechanical strength. This high mechanical strength also indicated that this novel membrane HFs catalysts is an ideal support and microreactor for the scale-up continues flow water treatment process.

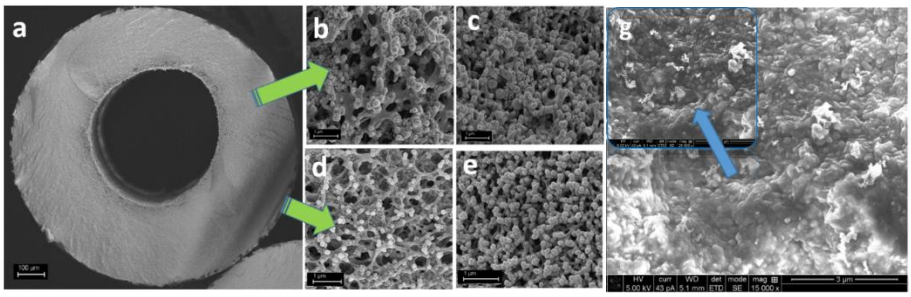

Figure 2. SEM images of (a) the cross-section of a single-layer bare Si/Ti/ PAI hollow fiber catalysts, (b) cross-section of bare Si/Ti/PAI-HF, (c) cross-section of APS-grafted Si/Ti/PAI-HF, (d) outer surface of bare Si/Ti/PAI-HF, (e) outer surface of APS-grafted Si/Ti/PAI hollow fiber catalysts, (f) outer surface of Pd(0)-loaded APS-grafted Si/Ti/PAI-HFs before the reaction and after reaction (in blue outline).

In order to confirm the mechanical strength and evaluate the swelling properties of the Pb-immobilized HFs, the diameter and length of the Pd/APS/PAI-HFs were measured before and after the reaction, and the most interesting thing is it shows no significant difference after the reaction. This indicated, under the 4-NP reduction reaction, the Pd/APS/PAI-HFs shows high potential as recycling catalysts and continues flow membrane microreactor.

3.2 CATALYTIC EFFICIENCY TEST RESULTS

The catalytic performance of the Pd-immobilized APS-grafted membranes was demonstrated, as mentioned, by performing the reduction of 4-NP to 4-AP in water at different temperature. To prove the concept of Pd-immobilized HFs membrane microreactor working for the 4-NP reduction reaction, both batch, and continues-flow system were investigated flowing the modification of the other previous published works[18, 19, 20].

3.2.1 Batch Reaction Test for the 4-NP Reduction Reaction. To confirm the canalization ability, a series of batch reaction sets is being conducted as comparison groups. The controlling reactions were conducted by only Pd(II)/APS/PAI-HFs and only $NaBH_4$ with different concentration, which shows no 4-NP conversion and 4-AP selectivity in the UV-Vis results, and also not observable color change in the reaction mixture. Table 2 shows all the batch results of the batch reactions under different reaction conditions. And the reaction condition which was investigated by the batch reaction system is involved with $NaBH_4$ and various reaction temperatures. All the results were estimated from the UV-Vis

Spectroscopy analyzer, a popular analytical instrument being used by other previous research.

Table 2. Reaction results of the batch reaction test.

Cat./25mg	$NaBH_4$	Temp/^oC	Time/h	Conversion (%)	Selectivity (%)
Pd(II) APS-grafted Si/Ti/PAI-HFs	-	30	3	-	-
-	1mM	30	3	-	-
-	10mM	30	3	-	-
Pd(0) APS-grafted Si/Ti/PAI-HFs	10mM	30	3	10	5
Pd(0) APS-grafted Si/Ti/PAI-HFs	-	50	3	-	-
Pd(0) APS-grafted Si/Ti/PAI-HFs	10mM	50	3	45	30
Pd(0) APS-grafted Si/Ti/PAI-HFs	100mM	50	3	75	40
Pd(0) APS-grafted Si/Ti/PAI-HFs	1000mM	50	3	100	100
Pd(0) APS-grafted Si/Ti/PAI-HFs	500mM	50	3	100	100
Pd(0) APS-grafted Si/PAI-HFs	500mM	50	3	100	100

* Reaction results being analyzed by UV-Vis spectroscopy.

Depend on the results we obtained from UV-Vis, we found that, when under only $NaBH_4$, the reaction of did not happen, 4-NP also remains the same without convert to 4-AP, the same situation happened without the existence of $NaBH_4$, the similar reaction

results happened, either under the involved of catalysts for both Pd(II) and Pd(0)-immobilized APS-grafted Si/Zr/Ti/PAI-HFs. These results also support the previous research conclusion, the existence of $NaBH_4$ can achieve to convert the 4-NP aqueous solution to the 4-nitrophnate ion aqueous solution and help the access to the 4-NP reduction reaction. However, in the reaction only with $NaBH_4$ involved, shows no conversion and selectivity of the 4-AP, this reaction result also proves that the reduction reaction could happen in the absence of catalysts.

According to the previous research, a UV-visible instrument is being used in the monitoring of the 4-NP reduction reaction process. A typical UV-Vis spectra result showing in Figure 3 is the samples analyzed before and after under 500mM $NaBH_4$ at 50^oC reaction catalytic by Pd(0)/SiO_2-TiO_2/PAI-HFs. During the reaction, after adding the $NaBH_4$ into the 4-NP aqueous system the intense yellow color can be observed to form the 4-nitrophnate ion with high stability, which can be confirmed by the strong absorption in the UV-Vis spectra at 400 nm with two slightly absorptions around. After adding 25mg HFs into the system, under reaction at about 50^oC, as the results shown in Figure 3, the peak around 230 appeared after the reaction. The disappear of absorption peak around 400 nm and the new generated appear around 230 nm indicated the convert from 4-NP to 4-AP.

Figure 3-(b) shows the photographs of samples before and after 4-NP reduction reaction it shows clearly that after the reaction the intense yellow color turned to become colorless finally, which also being proved by the UV-Vis results that the generation of 4-AP from 4-NP. Besides, based on the compared batch reaction results, the composition results between the Pd(0)/SiO_2 and Pd(0)/SiO_2-TiO_2/PAI-HFs did not shows strong

difference under the same reaction condition. Therefore, a set of samples were collected during the recycle reaction test.

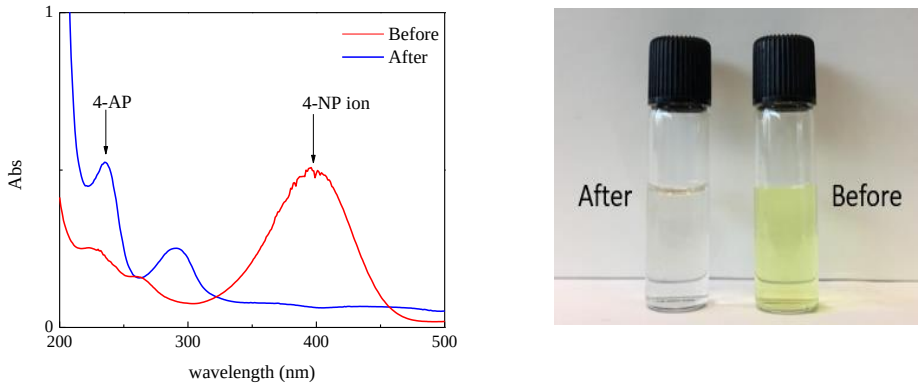

Figure 3. (a) UV-Vis Spectra result; (b) the digital photo of aqueous solutions shows before and after the reaction.

Furthermore, depending on the results from Table 2, without the existence of $NaBH_4$, the catalysts could not catalyze the reaction to generate the 4-AP, this meets the previous research, $NaBH_4$ can help to generate the 4-NP ion and also assist the MNPs on catalyzing the reduction reaction. Besides, with 25 mg Pd-MNPs HFs, increasing the concentration of $NaBH_4$ and reaction temperature can also increase the catalytic efficiency on the 4-NP reduction reaction.

3.2.2 Recycling Test for the 4-NP Reduction Reaction. The stability and repeatability of catalytic properties of the Pd-immobilized HFs membrane catalysts were being investigated by three times of recycling tests.

These three times of recycling test have been produced for the 4-NP reduction reaction of both the Pd(0)/SiO_2 and Pd(0)/SiO_2-TiO_2/PAI-HFs. During the recycling test, a set of samples collected at different reaction time, 5, 10, 20, 40, 60, 120, 180 min, the conversion of 4-NP and the selectivity of 4-AP were shown in the Figure 4. It can be observed that the reaction was equilibrated and completed at the first 60 min under the Pd(0)/SiO_2/PAI-HFs, while the catalytical efficiency show lower than the Pd(0)/SiO_2-TiO_2/PAI-HFs. From the Figure 4-(b), the reaction became stabilized and finished at the first 20 min, which means the Pd(0)/SiO_2-TiO_2/PAI-HFs catalysts show higher catalytic efficiency in the 4-NP reaction. Both of the HFs membrane catalysts show a stable and high conversion percentage at 50^oC.

Depend on the BET surface area and the pore volume results from Table 1, the Pd(0)/SiO_2-TiO_2/PAI-HFs shows higher BET surface area and pore volume before and after different surface modification steps, which leads to higher palladium MNPs loading ratio. This situation may be caused by the doping of TiO_2 is not only increase the strength of the HFs but also increasing the BET surface area and the pore volume.

From Table.3, after conducted the recycle test for about three times, the reaction still showing high conversion and selectivity, and as mentioned above, by measuring about the length and diameter of HFs and the data of ICP and XPS analysis before and after the reaction, this Pd-immobilized/APS/PAI-HFs shows extremely high stability and catalytic efficiency for the 4-NP reduction reaction. Besides, the low leaching level of Pd-MNPs, this HFs membrane catalysts is an ideal supporting material for the Pd-NMPs immobilization. Combining of all the BET, ICP, XPS, and catalytic test results, it can be confirmed that the fine immobilized stability of Pd-MNPs on the HFs membrane catalysts

by the membrane post-modification and it does not need to confirm the stability of the proposed system by running any further experimental cycles.

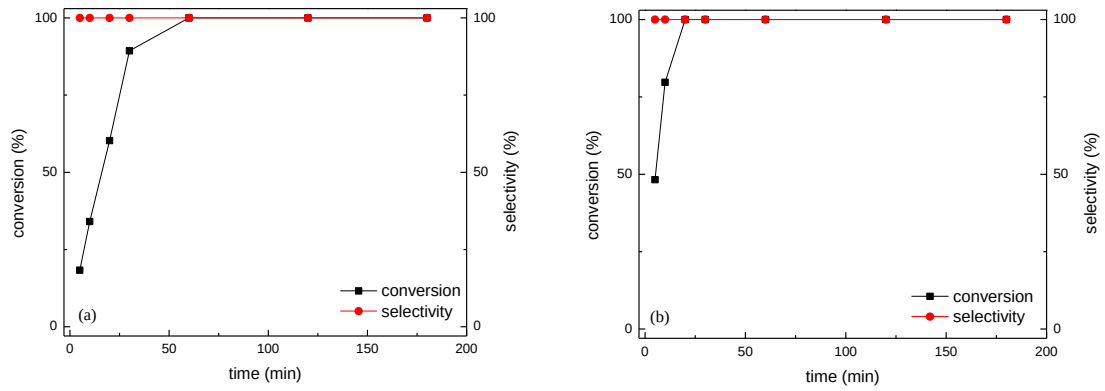

Figure 4. Conversion and selectivity results of the first recycle test monitoring by Uv-Vis spectroscopy of 4-NP reduction batch reaction with (a) Pd(0)-immobilized SiO_2/PAI-HF_S; (b) Pd(0)-immobilized SiO_2-TiO_2/PAI-HF_S.

Table 3. Reaction results of the batch reaction recycling test.

Recycle	Cat./25mg	$NaBH_4$	Temp /^oC	Time /h	Conversion (%)	Selectivity (%)
1st	Pd(0) APS-grafted Si/PAI-HFs	500mM	50	3	100	100
2nd	Pd(0) APS-grafted Si/PAI-HFs	500mM	50	3	100	100
3rd	Pd(0) APS-grafted Si/PAI-HFs	500mM	50	3	100	100
1st	Pd(0) APS-grafted Si/Ti/PAI-HFs	500mM	50	3	100	100
2nd	Pd(0) APS-grafted Si/Ti/PAI-HFs	500mM	50	3	100	100

Table 3. Reaction results of the batch reaction recycling test. (cont.)

3rd	Pd(0) APS-grafted Si/Ti/PAI-HFs	500mM	50	3	100	100

* Reaction results being analyzed by UV-Vis spectroscopy.

Therefore, the results confirmed that the Pd-immobilized HFs membrane catalysts can provide a stable and repeatable catalytic characteristic for the 4-NP reduction reaction.

3.2.3 Continues-flow Reaction Test for the 4-NP Reduction Reaction. According to the concept of the membrane reactor, this kind of HFs which worked as the Pd-immobilized membrane reactor is a potential membrane micro-reactor to scale up and apply in the 4-NP reduction reaction. Based on the above results of both the batch and recycle rest, both of the Pd(0)/SiO_2 and Pd(0)/SiO_2-TiO_2/PAI-HFs shown high stability and catalytic efficiency in the 4-NP reduction reaction.

In order to confirm the catalytic efficiency and stability of the Pd-immobilized HFs membrane catalysts for the 4-NP reduction reaction in the scale-up continues flow system, a continues-flow reaction test was conducted by following reaction condition.

The reactants and reaction condition were the same followed by the above batch reaction condition, but the length of the HFs catalysts was fixable to selected and during the continues reaction test. Since in the continues flow system, the length and number of HFs catalysts will increase up to five HFs, and length up to 15 cm to each, the reaction temperature considered to set at room temperature to run the reaction first. Figure 5 (a) and (b) shown the relationship between the reaction performed with the reaction time in the continuous hollow fiber module for the 4-NP reduction reaction.

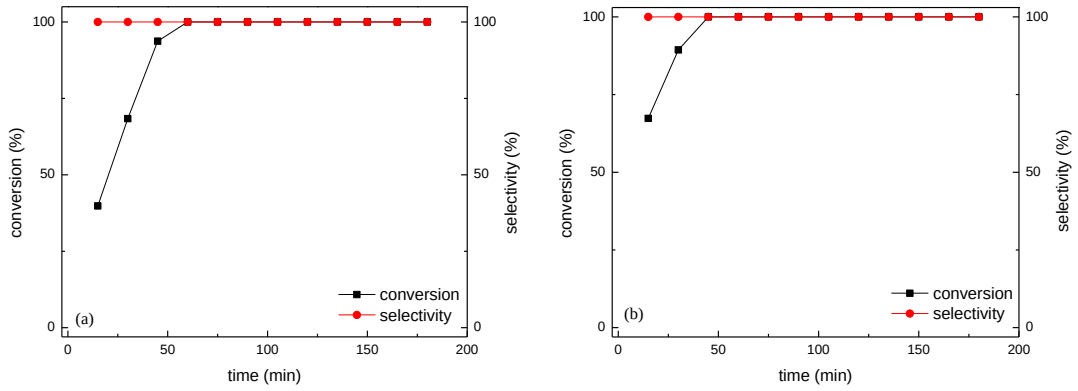

Figure 5. Conversion and selectivity results monitoring by Uv-Vis spectroscopy of 4-NP reduction continues reaction with (a) Pd(0)-immobilized SiO_2/PAI-HFS; (b) Pd(0)-immobilized SiO_2-TiO_2/PAI-HFS.

From the results of the continues-flow test, the most interesting points are the results of continues-flow test pretty close to the results of the batch reaction test even under different reaction temperature. This situation may be caused by the increasing length of HFs in the module, the reactant mixture has to go through the wall of the membranes on HFs and pass through the whole HFs length which increases the contact between the reactant mixture and the catalysts to promote the catalytic efficiency of the catalysts. And the similar reaction results also indicated that the palladium loading efficiency contributed to higher BET surface area and pore volume the Pd(0)/SiO_2-TiO_2/PAI-HFs have by doping the titanic oxide. The increasing the amount used in the continuous-flow reaction system leading to the increased contacting time and causing the sharp interaction between the 4-NP and Pd-MNPs.

Owing to the higher interactions between the reactant and membrane micro-reactor, the thermos influence can be overcome to have met the similar reaction results to the batch reaction. Compared to the existing heterogeneous Pd catalysts continuous-flow reaction

system, this membrane micro-reactor shows higher stability and flexibility. Therefore, this Pd-immobilized membrane HFs mic-reactor is a potential scale-up catalyst for the 4-NP reduction reaction. Besides, as the reaction catalytic results were close to the one in the batch reaction with room temperature, it is indicated that the scale-up system was more energy economy compared to the batch reaction system.

4. CONCLUSION

From the previous research, we report the concept-proved test of the novel HFs catalysts with successfully Pd-MNPs immobilized modification that has been proved applied to the Heck coupling reaction. In this report, we improve the concept study of the Pd-MNPs immobilized HFs catalysts and develop the new application. This Pd-MNPs immobilized HFs membrane catalysts have been proved to apply in the nitrophenol reduction reaction successfully with strong stability, which related to the stable membrane structure formed on the HFs catalysts. Besides, it has been proved that to promote the 4-NP reduction reaction, the efficient catalysts is the loading of Pd-MNPS, which also indicated the composition changing of the HFs, such as the adding of metal oxides which change the acidic sites, like Titania did not shows strong affection in this reaction, but increasing the strengthen of the HFs. However, by adding the titania to change the composition of the HFs can strengthen the stability of the HFs and provide the idea supporter for the palladium immobilized recycle and continues reactor. The investigation results provide valuable guidance for developing membranes HFs catalysts with highly efficient catalytic performance in the continuous-reaction system.

ACKNOWLEDGMENT

We thank the University of Missouri Research Board (UMRB) for supporting this work. We acknowledge Professor William J. Koros from the School of Chemical and Biomolecular Engineering at Georgia Institute of Technology for giving us access to his fiber-spinning facilities.

REFERENCE

1. W.B. Zhang, X.M. Xiao, T.C. An, Z.G. Song, J.M. Fu, G.Y. Sheng, M.C. Cui, J. Chem. Technol. Biotechnol. 78 (2003) 788–794.

2. O. Gazi, R. Ananthakrishnan, Metal-free-photocatalytic reduction of4-nitrophenol by resin-supported dye under the visible irradiation, Appl.Catal. B 105 (2011) 317–325.

3. M.B. Gholivand, M. Khodadadian, G. Bahrami, Molecularly imprinted polymerpreconcentration and flow injection amperometric determination of4-nitrophenol in water, Anal. Lett. 48 (2015) 2856–2869.

4. S. Harish, J. Mathiyarasu, K.L.N. Phani, V. Yegnaraman, Catal. Lett. 128 (2009) 197–202.

5. Aditya, T.; Pal, A.; Pal, T. Nitroarene reduction: A trusted model reaction to test nanoparticle catalysts. Chem. Commun. 2015, 51, 9410−9431.

6. S. Praharaj, S. Nath, S.K. Ghosh, S. Kundu, T. Pal, Langmuir 20 (2004) 9889–9892.

7. S. Arora, P. Kapoor, M.L. Singla, React. Kinet. Mech. Catal. 99 (2010) 157–165.

8. Z.M. El-Bahy, K.H. Mahmoud, Spectrochim. Acta A 92 (2012) 105–112.

9. K. Rajan, D. Thangaraju, N. Prakash, Y. Hayakawa. Cryst. Eng. Comm. 17(2015).

10. R. Seoude, F. A. Al-Marhaby. WJNSE. 128(2017) 120-128.

11. M. A. Bhosale, D. R. Chenna, J. P. Ahire, B. M. Bhanage. RSC Adv. 5(2015) 52817-52823.

12. S. Naraginti, P. L. Kumari, R. K. Das, A. Sivakumar, S. J. Patil, V. V. Andhalkar. Materials Sci. & Eng: C 62(2016) 293-300.

13. P. Veerakumar, I. P. Muthuselvam, C.-T. Hung, K.-C. Lin, F-C Chou, S-B Liu. ACS Sustainable Chem. Eng. 4(2016) 6772-6782.

14. F. Rezaei, R. Lively, Y. Labreche, G. Chen, Y. Fan, W.J. Woros, C.W. Jone, A.C.S. Appl. Mater. Interfaces 5(2013)3921-3931.

15. Y. He, A. Jawad, X. Li, M. Atanga, F. Rezaei, A. A. Rownaghi. J. Catal. 341(2016)149-159.

16. A. A. Ismall, A. Hakki, D. W. Bahnemann, J. Molecular Catal. 358(2012) 145-151.

17. A. A. Rownaghi, F. Rezaei, Y. Labrechem P.J. Brennan, J.R.Johnson, S. Li, W. J. Koros, ChemSusChem 8(2015)3439-3450.

18. Y. He, F. Rezaei, S. Kapila, A. A. Rownaghi. ACS Appl. Mater. Interfaces 9(2017) 16288-16295.

19. Y. Liu, K. Zhang, W. Li, J. Ma, G. J. Vancso. J. Mater. Chem. A. 6(2018) 7741-7748.

20. R. Xie, F. Luo, L. Zhang, S.-F. Guo, Z. Liu, x.-J. Ju, W. Wang, L.-Y. Chu. Small. 14(2018) 1703650.

SECTION

2. CONCLUSIONS AND FUTURE WORK

2.1. CONCLUSION

In this dissertation, the composite porous polymeric hollow fiber microfluidic reactor was worked as the heterogeneous membrane reactor in the organocatalytic and metal-catalytic reaction. It has been demonstrated that the porous polymeric hollow fiber catalysts were can be employed as an ideal and flexible supporting platform for the loading the catalytic efficiency composition, which can be applied into developing the laboratory-scale continuous-flow reactor system.

The HFs were proved to be successful being the surface modification to load various catalytic efficiency composite on the inner wall of the fiber shell, and employed into various organic synthesis reactions. Meanwhile, the different doping of the metal oxide not only help to improve the mechanical strength of the HFs catalysts but also providing various acidic sites to help to increase the cooperation of the acidic sites when working as the bifunctional catalysts. Besides, depend on the BET surface area and pore size measurement analysis, the polymeric hollow fiber appeared having highly porous and surface to volume ratio, which can improve the contact between the reactant residential time with the catalytic area, provide excellent mass transfer properties, and lower resistance to flow during the pass-thought the shell of the hollow fiber inner-wall.

The dissertation mainly focused on describe two different modification way for the various surface functionalization. The first objective of the functionalization is the aminosilane-grafted composite hollow fiber bifunctional membrane reactor, the grafted step with the aminosilanes can providing bifunctional acid-base character and catalyst

activity. Meanwhile, during the catalytic reaction, a good distribution and accessibility of bother amine and weakly acidic silanol sites can be offered by the APS-grafting. Besides, the APS-grafted modification could not only provide the cooperated acid-base site but also improve the mechanical strength of the polymer matrix of the HFs. The HFs appear to have long-term stability in the reaction system.

It has been demonstrated that the APS-grafted hollow fiber reactor could also be further post-modification and provide the ideal supporting platform for the Pd-MNPs immobilization and from the Pd-immobilized membrane reactor. The palladium catalytic efficiency site immobilized within porous PAI-HFs and offered a powerful catalytic system which has to prove that the Pd-immobilized membrane reactor can provide a serious of advantages of nano-catalyst in continuous-flow reaction with significant palladium leaching.

By applying the novel polymeric hollow fiber membrane reactor catalysts into the laboratory-scale continuous-flow reaction system, the various parameter, such as the contact time and reaction temperature can be achieved to be controlled in a simple process. Herein, with the multifunctional catalysis ability, the continuous-flow reactor module can be applied to meet a various demand to catalyzing a different reaction.

2.2. FUTURE WORK

In this dissertation, the proof-of-concept study of the continuous-flow polymeric hollow fiber membrane reactor has been successfully conducted for sustainable chemical transformation reactions. However, in order to the insight view of the novel hollow fiber continuous-flow reaction system, further optimization and study should be focused on the reactor design. Meanwhile, this novel reactor was provided a special model for further

simulation investigations to have a further understanding of how to have a better controllable of various parameter to improve the catalytic performance

For the surface modification process, further study should be focused on the control of the loading of catalytic efficiency composition. In order to improve the distribution of the catalytic efficiency embedded on the inner-wall on the fiber shell, further investigation should be emphasized on seeking for suitable surface modification method and simulation model.

BIBLIOGRAPHY

1. Jin, Z.; Liu, C.; Qi, K.; Cui, X. Photo-Reduced Cu/CuO Nanoclusters on TiO 2 Nanotube Arrays as Highly Efficient and Reusable Catalyst. *Sci. Rep.* **2017**, *7* (November 2016), 1–9.

2. Coppens, M. O.; Tsotsis, T. T. Editorial Overview: Reaction and Catalysis Engineering: Back to Fundamentals. *Curr. Opin. Chem. Eng.* **2016**, *13*, ix–xi.

3. Doornkamp, C.; Ponec, V. The Universal Character of the Mars and Van Krevelen Mechanism. *J. Mol. Catal. A Chem.* **2000**, *162* (1–2), 19–32.

4. Powell, J. B. Application of Multiphase Reaction Engineering and Process Intensification to the Challenges of Sustainable Future Energy and Chemicals. *Chem. Eng. Sci.* **2017**, *157*, 15–25.

5. Yoo, C. J.; Rackl, D.; Liu, W.; Hoyt, C. B.; Pimentel, B.; Lively, R. P.; Davies, H. M. L.; Jones, C. W. An Immobilized-Dirhodium Hollow-Fiber Flow Reactor for Scalable and Sustainable C−H Functionalization in Continuous Flow. *Angew. Chemie - Int. Ed.* **2018**, *57* (34), 10923–10927.

6. Antonetti, C.; Licursi, D.; Fulignati, S.; Valentini, G.; Raspolli Galletti, A. New Frontiers in the Catalytic Synthesis of Levulinic Acid: From Sugars to Raw and Waste Biomass as Starting Feedstock. *Catalysts* **2016**, *6* (12), 196.

7. Yue, H.; Ma, X.; Gong, J. An Alternative Synthetic Approach for Efficient Catalytic Conversion of Syngas to Ethanol. *Acc. Chem. Res.* **2014**, *47* (5), 1483–1492.

8. Taarning, E. Development of Green and Sustainable Chemical Reactions Development of Green and Sustainable Chemical Reactions. **2008**, No. December 2008.

9. Chapter Submitted to Sustainable Engineering Principles Book. 1. 1–24.

10. Collier, V. E.; Ellebracht, N. C.; Lindy, G. I.; Moschetta, E. G.; Jones, C. W. Kinetic and Mechanistic Examination of Acid-Base Bifunctional Aminosilica Catalysts in Aldol and Nitroaldol Condensations. *ACS Catal.* **2016**, *6* (1), 460–468.

11. Brown, J. W.; Jarenwattananon, N. N.; Otto, T.; Wang, J. L.; Glöggler, S.; Bouchard, L. S. Heterogeneous Heck Coupling in Multivariate Metal-Organic Frameworks for Enhanced Selectivity. *Catal. Commun.* **2015**, *65*, 105–107.

12. Zhang, Z.; Liu, B.; Zhao, Z. Conversion of Fructose into 5-HMF Catalyzed by GeCl4in DMSO and [Bmim]Cl System at Room Temperature. *Carbohydr. Polym.* **2012**, *88* (3), 891–895.

13. Zhou, X.; Zhu, X.; Huang, J.; Li, X.; Fu, P.; Jiao, L.; Huo, H.; Li, R. Programmed Synthesis of Pd@hTiO $_2$ Hollow Core–shell Nanospheres as an Efficient and Reusable Catalyst for the Reduction of p-Nitrophenol. *RSC Adv.* **2014**, *4* (62), 33055.

14. Mak, X. Y.; Laurino, P.; Seeberger, P. H. Asymmetric Reactions in Continuous Flow. *Beilstein J. Org. Chem.* **2009**, *5*, 1–11.

15. Crouch, R. D.; Richardson, A.; Howard, J. L.; Harker, R. L.; Barker, K. H. The Aldol Addition and Condensation: The Effect of Conditions on Reaction Pathway. *J. Chem. Educ.* **2007**, *84* (3), 475.

16. Nikbin, N.; Ladlow, M.; Ley, S. V. Continuous Glow Ligand-Free Heck Reactions Using Monolithic Pd(0) Nanoparticles. *Org. Proc. Res. Dev.* **2007**, *11* (5), 458–462.

17. He, Y.; Jawad, A.; Li, X.; Atanga, M.; Rezaei, F.; Rownaghi, A. A. Direct Aldol and Nitroaldol Condensation in an Aminosilane-Grafted Si/Zr/Ti Composite Hollow Fiber as a Heterogeneous Catalyst and Continuous-Flow Reactor. *J. Catal.* **2016**, *341*, 149–159.

18. He, Y.; Rezaei, F.; Kapila, S.; Rownaghi, A. A. Engineering Porous Polymer Hollow Fiber Micro Fl Uidic Reactors for Sustainable C − H Functionalization. **2017**.

19. Rezaei, F.; Lively, R. P.; Labreche, Y.; Chen, G.; Fan, Y.; Koros, W. J.; Jones, C. W. Aminosilane-Grafted Polymer/Silica Hollow Fiber Adsorbents for CO $_2$ Capture from Flue Gas. *ACS Appl. Mater. Interfaces* **2013**, *5* (9), 3921–3931.

20. Rownaghi, A. A.; Bhandari, D.; Burgess, S. K.; Mikkilineni, D. S. Effects of Coating Solvent and Thermal Treatment on Transport and Morphological Characteristics of PDMS/Torlon Composite Hollow Fiber Membrane. *J. Appl. Polym. Sci.* **2017**, *134* (42), 1–10.

21. Brennan, P. J.; Thakkar, H.; Li, X.; Rownaghi, A. A.; Koros, W. J.; Rezaei, F. Effect of Post-Functionalization Conditions on the Carbon Dioxide Adsorption Properties of Aminosilane-Grafted Zirconia/Titania/Silica-Poly(Amide-Imide) Composite Hollow Fiber Sorbents. *Energy Technol.* **2017**, *5* (2), 327–337.

22. Moschetta, E. G.; Negretti, S.; Chepiga, K. M.; Brunelli, N. A.; Labreche, Y.; Feng, Y.; Rezaei, F.; Lively, R. P.; Koros, W. J.; Davies, H. M. L.; et al. Composite Polymer/Oxide Hollow Fiber Contactors: Versatile and Scalable Flow Reactors for Heterogeneous Catalytic Reactions in Organic Synthesis. *Angew. Chemie - Int. Ed.* **2015**, *54* (22), 6470–6474.

23. Rownaghi, A. A.; Kant, A.; Li, X.; Thakkar, H.; Hajari, A.; He, Y.; Brennan, P. J.; Hosseini, H.; Koros, W. J.; Rezaei, F. Aminosilane-Grafted Zirconia-Titiania-Silica Nanoparticles/Torlon Hollow Fiber Composites for CO2Capture. *ChemSusChem* **2016**, *9* (10), 1166–1177.

24. Glasnov, T. N.; Findenig, S.; Kappe, C. O. Heterogeneous versus Homogeneous Palladium Catalysts for Ligandless Mizoroki-Heck Reactions: A Comparison of Batch/Microwave and Continuous-Flow Processing. *Chem. - A Eur. J.* **2009**, *15* (4), 1001–1010.

25. Lewandowski, M.; Babu, G. S.; Vezzoli, M.; Jones, M. D.; Owen, R. E.; Mattia, D.; Plucinski, P.; Mikolajska, E.; Ochenduszko, A.; Apperley, D. C. Investigations into the Conversion of Ethanol to 1,3-Butadiene Using MgO:SiO2supported Catalysts. *Catal. Commun.* **2014**, *49*, 25–28.

26. Masuda, K.; Ichitsuka, T.; Koumura, N.; Sato, K. Flow Fi Ne Synthesis with Heterogeneous Catalysts. **2018**, *74*.

27. Oger, N.; Le Grognec, E.; Felpin, F. X. Continuous-Flow Heck - Matsuda Reaction: Homogeneous versus Heterogeneous Palladium Catalysts. *J. Org. Chem.* **2014**, *79* (17), 8255–8262.

28. Zhao, D.; Ding, K. Recent Advances in Asymmetric Catalysis in Flow. *ACS Catal.* **2013**, *3* (5), 928–944.

29. Elmekawy, A. A.; Shiju, N. R.; Rothenberg, G.; Brown, D. R. Environmentally Benign Bifunctional Solid Acid and Base Catalysts. *Ind. Eng. Chem. Res.* **2014**, *53* (49), 18722–18728.

30. Hanspal, S.; Young, Z. D.; Shou, H.; Davis, R. J. Multiproduct Steady-State Isotopic Transient Kinetic Analysis of the Ethanol Coupling Reaction over Hydroxyapatite and Magnesia. *ACS Catal.* **2015**, *5* (3), 1737–1746.

31. Brand, S. K.; Josephson, T. R.; Labinger, J. A.; Caratzoulas, S.; Vlachos, D. G.; Davis, M. E. Methyl-Ligated Tin Silsesquioxane Catalyzed Reactions of Glucose. *J. Catal.* **2016**, *341*, 62–71.

32. Hill, I. M.; Hanspal, S.; Young, Z. D.; Davis, R. J. DRIFTS of Probe Molecules Adsorbed on Magnesia, Zirconia, and Hydroxyapatite Catalysts. *J. Phys. Chem. C* **2015**, *119* (17), 9186–9197.

33. Moschetta, E. G.; Brunelli, N. A.; Jones, C. W. Reaction-Dependent Heteroatom Modification of Acid-Base Catalytic Cooperativity in Aminosilica Materials. *Appl. Catal. A Gen.* **2015**, *504*, 429–439.

34. Dixon, D. J. Bifunctional Catalysis. *Beilstein J. Org. Chem.* **2016**, *12* (April), 1079–1080.

35. Allen, A. E.; MacMillan, D. W. C. Synergistic Catalysis: A Powerful Synthetic Strategy for New Reaction Development. *Chem. Sci.* **2012**, *3* (3), 633–658.

36. Zuo, Y.; Song, J.; Niu, H.; Mao, C.; Zhang, S. Synthesis of TiO 2 -Loaded Co 0 . 85 Se Thin Fi Lms with Heterostructure and Their Enhanced Catalytic Activity for p-Nitrophenol Reduction and Hydrazine Hydrate Decomposition. *Nanotechnology* **2016**, *27* (14), 145701.

37. Xiong, Z.-C.; Yang, Z.-Y.; Zhu, Y.-J.; Chen, F.-F.; Yang, R.-L.; Qin, D.-D. Ultralong Hydroxyapatite Nanowire-Based Layered Catalytic Paper for Highly Efficient Continuous Flow Reactions. *J. Mater. Chem. A* **2018**, *6* (14), 5762–5773.

38. Silva, L. P. C.; Terra, L. E.; Coutinho, A. C. S. L. S.; Passos, F. B. Sour Water–gas Shift Reaction over Pt/CeZrO2catalysts. *J. Catal.* **2016**, *341*, 1–12.

39. Patel, A. D.; Telalović, S.; Bitter, J. H.; Worrell, E.; Patel, M. K. Analysis of Sustainability Metrics and Application to the Catalytic Production of Higher Alcohols from Ethanol. *Catal. Today* **2015**, *239*, 56–79.

40. Chen, X.; Cai, Z.; Chen, X.; Oyama, M. AuPd Bimetallic Nanoparticles Decorated on Graphene Nanosheets: Their Green Synthesis, Growth Mechanism and High Catalytic Ability in 4-Nitrophenol Reduction. *J. Mater. Chem. A* **2014**, *2* (16), 5668–5674.

41. Lin, T.; Li, Z.; Song, Z.; Chen, H.; Guo, L.; Fu, F.; Wu, Z. Visual and Colorimetric Detection of P-Aminophenol in Environmental Water and Human Urine Samples Based on Anisotropic Growth of Ag Nanoshells on Au Nanorods. *Talanta* **2016**, *148*, 62–68.

42. Wang, L.; Zhang, J.; Yi, X.; Zheng, A.; Deng, F.; Chen, C.; Ji, Y.; Liu, F.; Meng, X.; Xiao, F. S. Mesoporous ZSM-5 Zeolite-Supported Ru Nanoparticles as Highly Efficient Catalysts for Upgrading Phenolic Biomolecules. *ACS Catal.* **2015**, *5* (5), 2727–2734.

43. Yew, M.; Ren, Y.; Koh, K. S.; Sun, C.; Snape, C. A Review of State-of-the-Art Microfluidic Technologies for Environmental Applications: Detection and Remediation. *Glob. Challenges* **2018**, *1800060*, 1800060.

44. Finelli, F. G.; Miranda, L. S. M.; De Souza, R. O. M. A. Expanding the Toolbox of Asymmetric Organocatalysis by Continuous-Flow Process. *Chem. Commun.* **2015**, *51* (18), 3708–3722.

45. Mendes, P. S. F.; Lapisardi, G.; Bouchy, C.; Rivallan, M.; Silva, J. M.; Ribeiro, M. F. Hydrogenating Activity of Pt/Zeolite Catalysts Focusing Acid Support and Metal Dispersion Influence. *Appl. Catal. A Gen.* **2015**, *504*, 17–28.

46. Gupta, N.; Singh, H. P.; Sharma, R. K. Metal Nanoparticles with High Catalytic Activity in Degradation of Methyl Orange: An Electron Relay Effect. *J. Mol. Catal. A Chem.* **2011**, *335* (1–2), 248–252.

47. Zeng, Z.; Wen, M.; Yu, B.; Ye, G.; Huo, X.; Lu, Y.; Chen, J. Polydopamine Induced In-Situ Formation of Metallic Nanoparticles in Confined Microchannels of Porous Membrane as Flexible Catalytic Reactor. *ACS Appl. Mater. Interfaces* **2018**, *10* (17), 14735–14743.

48. Kattel, S.; Yu, W.; Yang, X.; Yan, B.; Huang, Y.; Wan, W.; Liu, P.; Chen, J. G. CO2Hydrogenation over Oxide-Supported PtCo Catalysts: The Role of the Oxide Support in Determining the Product Selectivity. *Angew. Chemie - Int. Ed.* **2016**, *55* (28), 7968–7973.

49. Belskaya, O. B.; Stepanova, L. N.; Gulyaeva, T. I.; Erenburg, S. B.; Trubina, S. V.; Kvashnina, K.; Nizovskii, A. I.; Kalinkin, A. V.; Zaikovskii, V. I.; Bukhtiyarov, V. I.; et al. Zinc Influence on the Formation and Properties of Pt/Mg(Zn)AlOxcatalysts Synthesized from Layered Hydroxides. *J. Catal.* **2016**, *341*, 13–23.

50. Ouyang, W.; Yepez, A.; Romero, A. A.; Luque, R. Towards Industrial Furfural Conversion : Selectivity and Stability of Palladium and Platinum Catalysts under Continuous Fl Ow Regime. *Catal. Today* **2018**, *308* (May 2017), 32–37.

51. Li, J.; Wu, F.; Lin, L.; Guo, Y.; Liu, H.; Zhang, X. Flow Fabrication of a Highly Efficient Pd/UiO-66-NH2film Capillary Microreactor for 4-Nitrophenol Reduction. *Chem. Eng. J.* **2018**, *333* (September 2017), 146–152.

52. Ponce-ortega, J. M.; Al-thubaiti, M. M.; El-halwagi, M. M. Chemical Engineering and Processing : Process Intensification Process Intensification : New Understanding and Systematic Approach. *Chem. Eng. Process. Process Intensif.* **2012**, *53*, 63–75.

53. Peng, W. chao; Chen, Y.; Li, X. yan. MoS2/Reduced Graphene Oxide Hybrid with CdS Nanoparticles as a Visible Light-Driven Photocatalyst for the Reduction of 4-Nitrophenol. *J. Hazard. Mater.* **2016**, *309*, 173–179.

54. Bond, J. Q.; Upadhye, A. a.; Olcay, H.; Tompsett, G. a.; Jae, J.; Xing, R.; Alonso, D. M.; Wang, D.; Zhang, T.; Kumar, R.; et al. Production of Renewable Jet Fuel Range Alkanes and Commodity Chemicals from Integrated Catalytic Processing of Biomass. *Energy Environ. Sci.* **2014**, *7* (4), 1500.

55. Nahreen, S.; Gupta, R. B. Conversion of the Acetone-Butanol-Ethanol (ABE) Mixture to Hydrocarbons by Catalytic Dehydration. *Energy and Fuels* **2013**, *27* (4), 2116–2125.

56. Hartman, R. L.; McMullen, J. P.; Jensen, K. F. Deciding Whether to Go with the Flow: Evaluating the Merits of Flow Reactors for Synthesis. *Angew. Chemie - Int. Ed.* **2011**, *50* (33), 7502–7519.

57. Atodiresei, I.; Vila, C.; Rueping, M. Asymmetric Organocatalysis in Continuous Flow: Opportunities for Impacting Industrial Catalysis. *ACS Catal.* **2015**, *5* (3), 1972–1985.

58. Liu, H.; Cheng, S. Power Generation in Fed-Batch Microbial Fuel Cells as a Function of Ionic Strength , Temperature , and Reactor Configuration. **2005**, *39* (14), 5488–5493.

59. Anaya, F.; Zhang, L.; Tan, Q.; Resasco, D. E. Tuning the Acid – Metal Balance in Pd / and Pt / Zeolite Catalysts for the Hydroalkylation of m-Cresol. *J. Catal.* **2015**, *328*, 173–185.

60. Bollini, P.; Choi, S.; Drese, J. H.; Jones, C. W. Oxidative Degradation of Aminosilica Adsorbents Relevant to Postcombustion CO2 Capture. *Energy and Fuels* **2011**, *25* (5), 2416–2425.

61. Marin Flores, O. G.; Ha, S. Activity and Stability Studies of MoO2 Catalyst for the Partial Oxidation of Gasoline. *Appl. Catal. A Gen.* **2009**, *352* (1–2), 124–132.

62. Valera, F. E.; Quaranta, M.; Moran, A.; Blacker, J.; Armstrong, A.; Cabral, J. T.; Blackmond, D. G. The Flow s the Thing … Or Is It ? Assessing the Merits of Homogeneous Reactions in Flask and Flow **. **2010**, 2478–2485.

63. Boudart, M. Turnover Rates in Heterogeneous Catalysis. *Chem. Rev.* **1995**, *95* (3), 661–666.

64. Kozlowski, J. T.; Davis, R. J. Heterogeneous Catalysts for the Guerbet Coupling of Alcohols. *ACS Catal.* **2013**, *3* (7), 1588–1600.

65. Scalbert, J.; Thibault-Starzyk, F.; Jacquot, R.; Morvan, D.; Meunier, F. Ethanol Condensation to Butanol at High Temperatures over a Basic Heterogeneous Catalyst: How Relevant Is Acetaldehyde Self-Aldolization? *J. Catal.* **2014**, *311*, 28–32.

66. Kreituss, I.; Bode, J. W. Parallel Kinetic Resolution of Chiral Saturated. *Nat. Chem.* **2016**, *9* (5), 446–452.

67. Bourne, S. L.; O'Brien, M.; Kasinathan, S.; Koos, P.; Tolstoy, P.; Hu, D. X.; Bates, R. W.; Martin, B.; Schenkel, B.; Ley, S. V. Flow Chemistry Syntheses of Styrenes, Unsymmetrical Stilbenes and Branched Aldehydes. *ChemCatChem* **2013**, *5* (1), 159–172.

68. Fitzpatrick, D. E.; Ley, S. V. Engineering Chemistry for the Future of Chemical Synthesis. *Tetrahedron* **2018**, *74* (25), 3087–3100.

69. Faigl, F.; Wirth, T. Bioorganic & Medicinal Chemistry. *Bioorg. Med. Chem.* **2017**, *25* (23), 6180–6189.

70. Riittonen, T.; Toukoniitty, E.; Madnani, D. K.; Leino, A.-R.; Kordas, K.; Szabo, M.; Sapi, A.; Arve, K.; Wärnå, J.; Mikkola, J.-P. One-Pot Liquid-Phase Catalytic Conversion of Ethanol to 1-Butanol over Aluminium Oxide—The Effect of the Active Metal on the Selectivity. *Catalysts* **2012**, *2* (4), 68–84.

71. Yoon, S. B.; Won, J. C. Determination of Molecular Weight Distribution and Average Molecular Weights of Oligosaccharides by HPLC with a Common C18 Phase and a Mobile Phase with High Water Content. *Bull. Korean Chem. Soc.* **2007**, *28* (5), 847–850.

72. Zhang, M.; Yu, Y. Dehydration of Ethanol to Ethylene. *Ind. Eng. Chem. Res.* **2013**, *52* (28), 9505–9514.

73. Puglisi, A.; Benaglia, M.; Chiroli, V. Green Chemistry. **2013**, 1790–1813.

74. Lively, R. P.; Koros, W. J.; Johnson, J. R. Enhanced Cryogenic CO2capture Using Dynamically Operated Low-Cost Fiber Beds. *Chem. Eng. Sci.* **2012**, *71*, 97–103.

75. Phillips, T. W.; Bannock, J. H.; Nightingale, A. M.; Mello, J. C. De. Droplet Reactor. *Nat. Commun.* **2014**, *5* (May), 1–8.

76. Zhang, J.; Gong, C.; Zeng, X.; Xie, J. Continuous Flow Chemistry: New Strategies for Preparative Inorganic Chemistry. *Coord. Chem. Rev.* **2016**, *324*, 39–53.

77. Organic Pollutants and Monitoring Techniques.

78. Liu, Z.; Dong, W.; Cheng, S.; Guo, S.; Shang, N.; Gao, S.; Feng, C.; Wang, C.; Wang, Z. Pd9Ag1-N-Doped-MOF-C: An Efficient Catalyst for Catalytic Transfer Hydrogenation of Nitro-Compounds. *Catal. Commun.* **2017**, *95*, 50–53.

79. Torkkeli, A. Droplet Microfluidics on a Planar Surface. *VTT Publ.* **2003**, *62* (504), 3–194.

80. Tanimu, A.; Jaenicke, S.; Alhooshani, K. Heterogeneous Catalysis in Continuous Flow Microreactors : A Review of Methods and Applications. *Chem. Eng. J.* **2017**, *327*, 792–821.

81. Lively, R. P.; Chance, R. R.; Mysona, J. A.; Babu, V. P.; Deckman, H. W.; Leta, D. P.; Thomann, H.; Koros, W. J. CO 2 Sorption and Desorption Performance of Thermally Cycled Hollow Fiber Sorbents. *Int. J. Greenh. Gas Control* **2012**, *10*, 285–294.

82. Mederos, S.; Ancheyta, J.; Chen, J. Applied Catalysis A : General Review on Criteria to Ensure Ideal Behaviors in Trickle-Bed Reactors. **2009**, *355*, 1–19.

83. Albalá-Hurtado, S.; Veciana-Nogués, M. T.; Izquierdo-Pulido, M.; Vidal-Carou, M. C. Determination of Free and Total Furfural Compounds in Infant Milk Formulas by High-Performance Liquid Chromatography. *J. Agric. Food Chem.* **1997**, *45* (6), 2128–2133.

84. Linares, N.; Silvestre-Albero, A. M.; Serrano, E.; Silvestre-Albero, J.; García-Martínez, J. Mesoporous Materials for Clean Energy Technologies. *Chem. Soc. Rev.* **2014**, *43* (22), 7681–7717.

85. Porta, R.; Benaglia, M.; Puglisi, A. Flow Chemistry: Recent Developments in the Synthesis of Pharmaceutical Products. *Org. Process Res. Dev.* **2016**, *20* (1), 2–25.

86. Niederberger, M. Aqueous and Nonaqueous Sol-Gel. *Met. Oxide Nanoparticles Org. Solvents* **2009**, 7–19.

87. Thakkar, H.; Eastman, S.; Hajari, A.; Rownaghi, A. A.; Knox, J. C.; Rezaei, F. 3D-Printed Zeolite Monoliths for CO2Removal from Enclosed Environments. *ACS Appl. Mater. Interfaces* **2016**, *8* (41), 27753–27761.

88. Thakkar, H.; Issa, A.; Rownaghi, A. A.; Rezaei, F. CO2Capture from Air Using Amine-Functionalized Kaolin-Based Zeolites. *Chem. Eng. Technol.* **2017**, *40* (11), 1999–2007.

89. Li, F. S.; Qiu, W.; Lively, R. P.; Lee, J. S.; Rownaghi, A. A.; Koros, W. J. Polyethyleneimine-Functionalized Polyamide Imide (Torlon) Hollow-Fiber Sorbents for Post-Combustion CO2capture. *ChemSusChem* **2013**, *6* (7), 1216–1223.

90. Li, X.; Kant, A.; He, Y.; Thakkar, H. V.; Atanga, M. A.; Rezaei, F.; Ludlow, D. K.; Rownaghi, A. A. Light Olefins from Renewable Resources: Selective Catalytic Dehydration of Bioethanol to Propylene over Zeolite and Transition Metal Oxide Catalysts. *Catal. Today* **2016**, *276*, 62–77.

VITA

The author, Yingxin He was born in Foshan, Guangdong, China. She entered The Guangdong University of Science and Technology, China in 2009. She received her B.E degree with a major in Chemical Engineering and Technology from The Guangdong University of Science and Technology in June 2013. In August 2014, she came to the USA and attended Missouri University of Science & Technology. She received a Doctor of Philosophy degree in Chemical Engineering from Missouri University of Science and Technology in December 2018.